

**Editor-in-Chief B.E.Paton**

**Editorial board:**

Yu. S. Borisov	V. F. Grabin
A. Ya. Ishchenko	V. F. Khorunov
B. V. Khitrovskaya	I. V. Krivtsun
S. I. Kuchuk-Yatsenko	
Yu. N. Lankin	V. K. Lebedev
V. N. Lipodaev	L. M. Lobanov
V. I. Makhnenko	A. A. Mazur
O. K. Nazarenko	I. K. Pokhodnya
I. A. Ryabtsev	K. A. Yushchenko
N. M. Voropai	A. T. Zelnichenko

**International editorial council:**

N. P. Alyoshin	(Russia)
U. Diltey	(Germany)
Guan Qiao	(China)
D. von Hofe	(Germany)
V. I. Lysak	(Russia)
N. I. Nikiforov	(Russia)
B. E. Paton	(Ukraine)
Ya. Pilarczyk	(Poland)
P. Seyffarth	(Germany)
G. A. Turichin	(Russia)
Zhang Yanmin	(China)
A. S. Zubchenko	(Russia)

**Promotion group:**

V. N. Lipodaev, V. I. Lokteva  
A. T. Zelnichenko (exec. director)

**Translators:**

I. N. Kutianova, V. F. Orets,  
T. K. Vasilenko, N. V. Yalanskaya

**Editor**

N. A. Dmitrieva  
*Electron galley:*  
I. S. Batasheva, T. Yu. Snegiryova

**Address:**

E.O. Paton Electric Welding Institute,  
International Association «Welding»,  
11, Bozhenko str., 03680, Kyiv, Ukraine  
Tel.: (38044) 287 67 57  
Fax: (38044) 528 04 86  
E-mail: journal@paton.kiev.ua  
http://www.nas.gov.ua/pwj

State Registration Certificate  
KV 4790 of 09.01.2001

**Subscriptions:**

**\$324**, 12 issues per year,  
postage and packaging included.  
Back issues available.

All rights reserved.

This publication and each of the articles  
contained herein are protected by copyright.  
Permission to reproduce material contained in  
this journal must be obtained in writing from  
the Publisher.

Copies of individual articles may be obtained  
from the Publisher.

**CONTENTS**

SCIENTIFIC AND TECHNICAL

*Kuchuk-Yatsenko S.I., Grigorenko G.M., Novikova D.P., Zagadarchuk V.F., Kharchenko G.K., Grigorenko S.G. and Alekseenko I.I.* Effect of energy input on ductile properties of flash butt welded joints in steel X70 ..... 2

*Lobanov L.M., Pashchin N.A., Loginov V.P. and Smilenko V.N.* Change of the stress-strain state of welded joints of aluminium alloy AMg6 after electrodynamic treatment ..... 7

*Moravetsky S.I., Parshenkov N.A. and Sokirko V.A.* Features of electromagnetic impacts on the metals and their welded joints (Review) ..... 14

*Kharchenko G.K., Ishchenko A.Ya., Falchenko Yu.V., Muravejnik A.N. and Gordan G.N.* Pressure welding of AMg5/23 % SiC composite ..... 20

*Razmyshlyayev A.D., Deli A.A. and Mironova M.V.* Effect of longitudinal magnetic field on the efficiency of wire melting in submerged-arc surfacing ..... 23

INDUSTRIAL

*Nikiforchin G.N., Student O.Z., Stepanyuk S.M. and Markov A.D.* Evaluation of technical state of welded joints on HPS steam lines allowing for hydrogen-induced degradation of metal in operation ..... 28

*Emelianov O.A., Slavinsky R.L. and Yaremenko D.V.* Secondary stresses in welded gantry cranes ..... 33

*Bolotov G.P.* Effect of the state of surface of electrodes on stability of glow discharge under welding conditions ..... 36

*Tsybulkin G.A.* Automation of training procedures of PUMA family robots ..... 39

*Kolyada V.A. and Shapovalov E.V.* Stereoscopic measurement of spatial coordinates of joints in welding production ..... 41

BRIEF INFORMATION

*Lankin Yu.N. and Bajshtruk E.N.* Sensor of molten metal pool level in ESW ..... 44

News ..... 46

NEWS

Exhibition «Welding. Allied Technologies-2007» in Kiev ..... 48

Prof. V.K. Lebedev is 85 ..... 50

Developed at PWI ..... 27, 38, 40, 47, 51



# EFFECT OF ENERGY INPUT ON DUCTILE PROPERTIES OF FLASH BUTT WELDED JOINTS IN STEEL X70

S.I. KUCHUK-YATSENKO, G.M. GRIGORENKO, D.P. NOVIKOVA, V.F. ZAGADARCHUK,  
G.K. KHARCHENKO, S.G. GRIGORENKO and I.I. ALEKSEENKO  
E.O. Paton Electric Welding Institute, NASU, Kiev, Ukraine

The effect of energy input in flash butt welding of pipes of steel 10G2FB on ductile properties of welded joints was investigated. It is shown that impact toughness of metal of the welded joints is determined by its structural state and grain size. It is recommended to reduce the energy input of the welding process to achieve consistently high ductile properties of the welded joints, as this provides formation of fine-grained two-phase structure in the weld metal, consisting of the MAC-phase in the ferritic matrix.

*Keywords:* flash butt welding, energy input, low-alloy steel, microstructure, grain, MAC-phase, impact toughness

Flash butt welding (FBW) has found wide application in different industries, including construction of pipelines in the gas industry. Increased interest in FBW is explained, first of all, by a high and consistent quality of the welded joints, combined with high productivity of the welding process [1]. Quality of the flash butt welded joints on pipes meets requirements of the corresponding international standard in force [2].

Construction of a new generation of pipelines designed for increased gas pressure has been started lately in the territory of the CIS countries. The pipelines are built from thick-walled pipes made from high-strength steels of the X70 and X80 grades. Considerable part of these pipelines will be constructed in the north regions of Russia. Therefore, the new standards specify increased requirements to quality of the welded joints, and to impact toughness in particular [3].

The E.O. Paton Electric Welding Institute conducted research aimed at finding the ways of improving ductile properties of flash butt welded joints on pipes made from steel of the X70 grade. One of the main factors determining formation of structure of the flash butt weld metal is a thermal cycle caused by the welding energy input.

As shown in study [4], sound flash butt welded joints in different low-alloy steels can be produced by varying the thermal cycles over a wide range. In this case, decrease in the energy input to ensure the required properties of the joints should be combined with intensive flashing in a period that precedes up-setting, which is accompanied by increase in power consumption. However, the trend in welding of pipes (especially of a large cross section) under field conditions is to decrease power of mobile power units. Therefore, in the majority of cases the welding parameters of choice are those that feature a low specific power (10–14 V·A/mm<sup>2</sup>) and high energy input.

The purpose of this study was to investigate the effect of structure in the flash butt weld metal on pipe

steel 10G2FB of the X70 grade using different energy input on values of impact toughness of the welded joints.

Investigations were conducted on plates of steel 10G2FB produced by the Khartsyzsk Works. The plates had width of 300 mm, and were cut from pipes with a wall thickness of 8 and 18 mm. As found in the earlier studies [5], welding of plates of the above width provides a sufficiently accurate simulation of the conditions of heating and formation of the joints in the process of welding large-diameter pipes. The pipe steel used had the following chemistry, wt. %: 0.078 C, 0.258 Si, 1.67 Mn, 0.05 Nb, 0.01 Ti, 0.017 Mo, 0.003 S, 0.007 P, 0.0026 O, and 0.0061 N. The hydrogen concentration was 1.64 cm<sup>3</sup>/100 g. Steel 10G2FB is characterised by the following mechanical properties:  $\sigma_y = 516.8$  MPa,  $\sigma_t = 620$  MPa,  $\delta = 19$  %, and  $KCV_{20} = 218.2$  J/cm<sup>2</sup>.

The joining technology is based on the continuous flash butt welding method with programmed variation of the main process parameters, which provides for three flashing periods [4]. Duration of the second period and the final rate of flashing in the third period were varied during the welding process.

The welding thermal cycles investigated are characterised by a family of the temperature field curves, which were plotted for the joints made at a different duration and final rate of flashing (Figure 1). The maximal possible heating can be provided in mode A of FBW (Figure 1, curve 1). The time of flashing in this case is 180 s, and the maximal specific power consumption in the final period of welding is 12 V·A/mm<sup>2</sup> (Figure 2). Increasing the heating temperature above the given values leads to decrease in mechanical properties of the joints because of formation of structure defects (porosity, delaminations, etc.). FBW performed in mode B (Figure 1, curve 4) provides the absence of defects within the joining zone (oxide films, lacks of fusion) and formation of a joint with a minimal length of HAZ. Such joints were produced on plates of a smaller cross section with 8 mm thickness at a limited power of the laboratory unit.

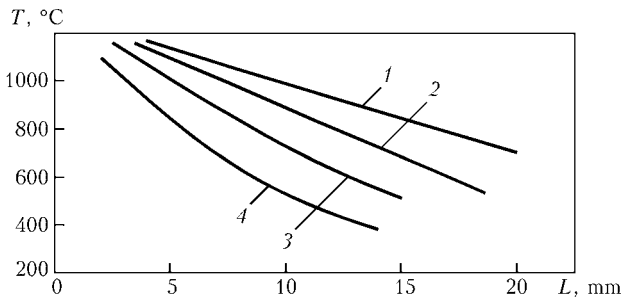


**Figure 1.** Distribution of temperatures in HAZ of flash butt welded joints at different duration and rate of flashing: 1 —  $\tau = 180$  s (mode A); 2 — 120 s; 3 — 60 s; 4 — 30 s (mode B); L — distance from joining line

The flashing duration in this case was 30 s, and the maximal specific power consumption in the final period of welding was  $40 \text{ V}\cdot\text{A}/\text{mm}^2$  (Figure 2, curve 2).

Intermediate welding modes (Figure 1, curves 2 and 3) are characterised by a prolonged flashing and maximal power consumption. They provide the level of mechanical properties that satisfy requirements of the standards, except for impact toughness KCV.

Mechanical properties of the joints produced in modes A and B are given in the Table. It can be seen from the Table data that the difference in heating has a substantial effect on impact toughness of the joints. The main cause of decrease in impact toughness of the joints produced in mode A of FBW was formation of unfavourable structures, as fractures of impact test specimens contained no defects.

Comparative metallographic analysis was conducted to study the effect of welding modes A and B on the character of structures formed in the weld metal and HAZ of the joints.

To determine size of austenite grain, microstructure of specimens was examined with the «Neophot-32» microscope at  $\times 100$  magnification by visual comparison with reference scales according to GOST 5639–82 after etching in nital. Identification of structural components after etching in sodium picrate [6] and counting of volume content of the second phase by the procedure described in [7] were carried out at  $\times 1000$  magnification.

Initial structure of the steel in the as-controlled rolling state consists of pearlite precipitates extending along the rolling direction in the ferritic matrix (Figure 3). Ferrite grain has size 7–8 and hardness — 2530–2540 MPa. Integrated hardness of the test specimens was measured using the Vickers hardness meter under a load of 50 N (HV5).

Mechanical properties of flash butt welded joints

Welding mode	$\sigma_y$ , MPa	$\sigma_t$ , MPa	$\delta$ , %	$\alpha$ , deg	KCV <sub>20</sub> , J/cm <sup>2</sup>
A	471.1	606.4	21.3	180	18.4
B	515.3	619.4	19.2	180	208.3

Notes. 1. Specimens were tested according to requirements of standard API 1104. 2. Cross section of impact test specimen without notch was  $5 \times 10$  mm.

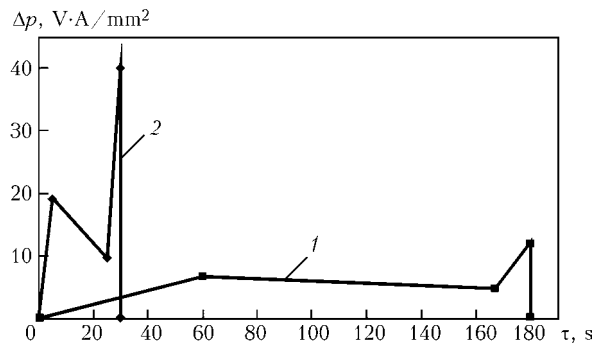


**Figure 2.** Variation in specific power consumption,  $\Delta p$ , in FBW modes A (1) and B (2) at different flashing moments of welded joints

Characteristic feature of a macrostructure (Figure 4) is the presence of a light band with fine dark-etching inclusions of the second phase and HAZ symmetrically located on its both sides.

Analysis of a microstructure allows distinguishing the most characteristic regions in the joints made in modes A and B to conduct comparative metallographic examinations. Peculiarities of structural components were examined in metal of the joining zone and HAZ in coarse-grained and normalised regions, which differ markedly from each other in structure and length.

In a sample made in mode A, metal of the joining zone 0.5 mm wide is cast, containing no porosity and no oxide films. Characteristic structure in this region is coarse-grained ferrite mostly with size 4, as well as insignificant dispersed precipitates of the second phase. Metal hardness is 2500 MPa. This region borders on each side with the HAZ regions, about 2 mm long, of the ferritic matrix of the same grain size (size 4) and particles of the second phase located in it, the volume content of the latter in the structure being 3.72 %. These precipitates were identified by etching in sodium picrate as a MAC-phase [6]. In addition to the latter, the structure also comprises lamellae of polygonal ferrite formed along the austenite grain boundaries, and elements of the structure with particles of the MAC-phase arranged parallel to each other and oriented along the ferrite boundaries. According to the IIW document, this structural component is classified as ferrite with the ordered second phase (OSP) [8]. Hardness in a region of the coarse-grained structure amounts to 2800 MPa.

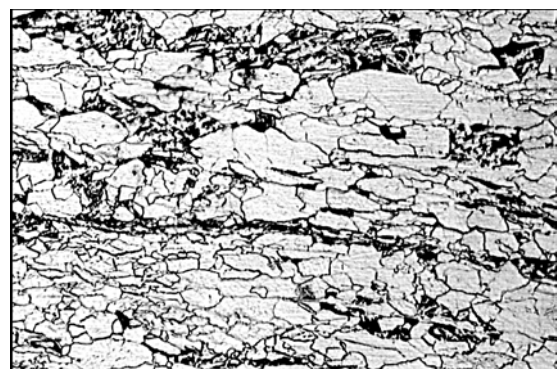


**Figure 3.** Microstructure of steel 10G2FB in as-received state ( $\times 500$ )

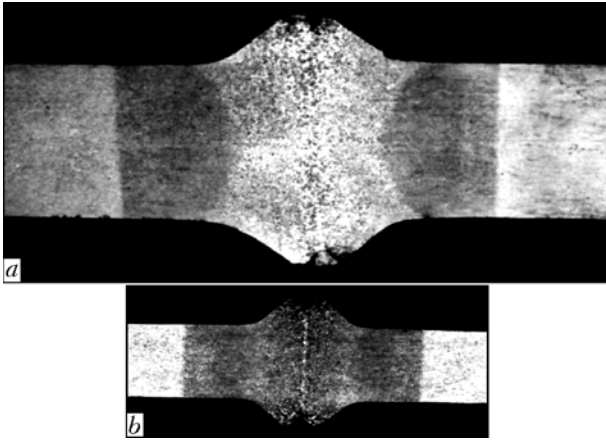


**Figure 4.** Macrosection of welded joints made by FBW in modes A (a) and B (b) ( $\times 1.68$ )

Within the regions examined, i.e. joining zone and coarse-grained region of HAZ, the temperature of metal heating amounts to 1200–1300 °C (see Figure 1). Microstructure of the welded joint made in mode A is shown in Figures 5 and 6.

The normalised HAZ region about 11 mm long, where metal is heated from a temperature a bit higher than point  $A_{c3}$  to 1100 °C, is characterised by a homogeneous structure with grain size 7–8, comprising the MAC-phase particles in the ferritic matrix, which are more dispersed than in the previous regions. Hardness of the normalised region is 2010–2020 MPa.

As found by examination of the structural state of a sample welded in mode B (Figure 7), the joining zone 0.2 mm wide contains no cast metal and no oxide

films. The structure comprises ferrite mostly with grain size 6 and occasional precipitates of the MAC-phase. Hardness of this region is 2010 MPa. Length of the coarse-grained region in the HAZ metal is 0.8 mm. Its structure comprises the MAC-phase particles (2.55 %) chaotically distributed in the ferritic matrix. Hardness of metal in this region is 2400 MPa, and grain size is 6.

Length of the next structural HAZ region, i.e. normalised region, is 4.5 mm. Grain size in this region is 7–10. The two-phase structure, i.e. MAC-phase in ferrite, changes but insignificantly. Comparison with the joining zone and coarse-grained region shows refining of the second phase.

The character of distribution of hardness in metal of the joining zone and HAZ of the welded joints made in modes A and B is shown in Figure 8. It can be seen that hardness of metal in the joining zone is equal to 2500 and 2010 MPa, respectively. Hardness in the regions of coarse-grained HAZ amounts to 2800 and 2400 MPa. Metal hardness in normalised regions of the joints investigated is 2010–2020 MPa. Increase in hardness observed in the coarse-grained structure regions is indicative of the process of metal hardening developing in them, which may have a negative effect on impact toughness [9, 10].

Lower values of impact toughness were fixed in metal of the joining zone and coarse-grained HAZ structure of a sample welded in mode A. In the normalised region, toughness of metal grows with distance from the coarse-grained region, and at a distance

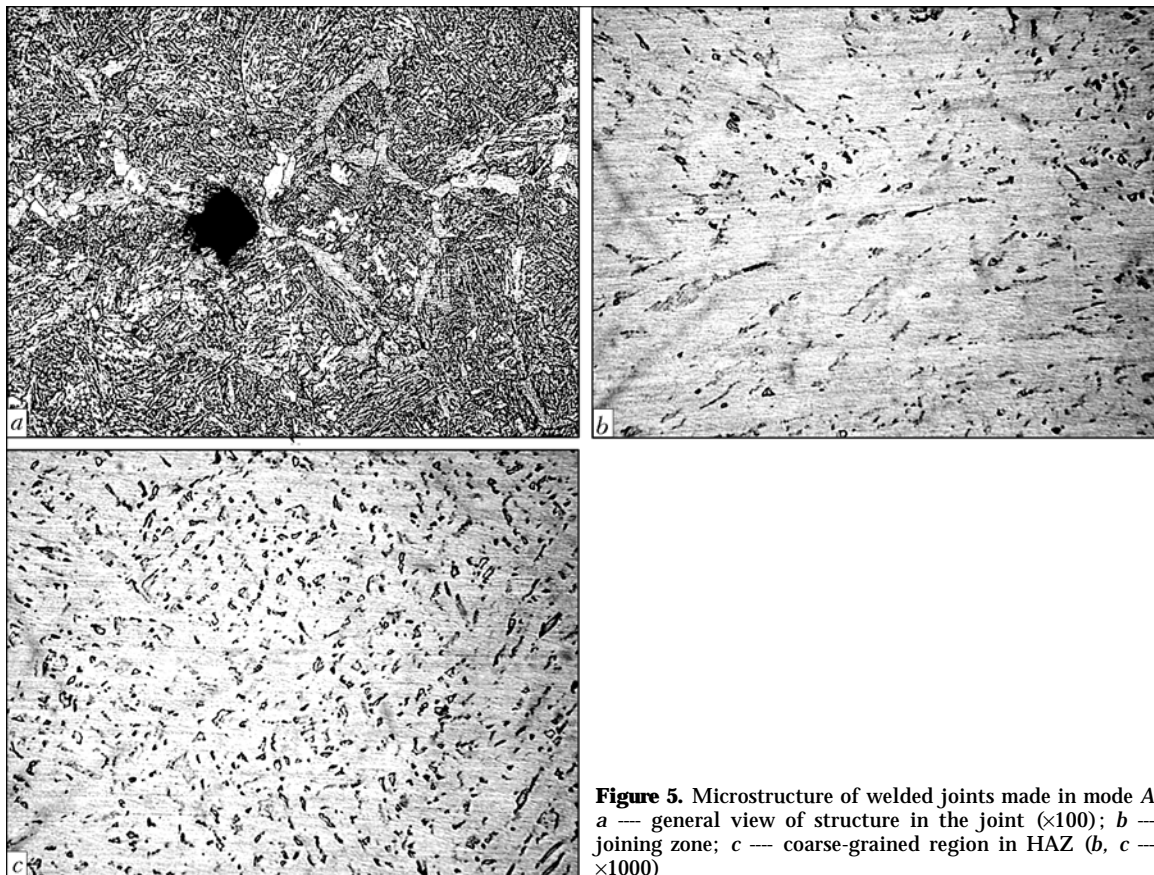


**Figure 5.** Microstructure of welded joints made in mode A: a — general view of structure in the joint ( $\times 100$ ); b — joining zone; c — coarse-grained region in HAZ (b, c —  $\times 1000$ )



of 3 mm from this region it amounts to the values close to those of the base metal (Figure 9, curve 1). All of the examined structural regions in the welded sample made in mode B are characterised by high impact toughness (Figure 9, curve 2).

It can be concluded from analysis of the above data that the substantial differences observed in values of impact toughness of the welded joints made with different energy input are attributable, first of all, to changes in such structural factors as size of austenite grain, structure of the joining zone and coarse-grained HAZ regions. According to modern notions, impact toughness of the welded joints in low-alloy low-carbon steels is determined to a considerable degree by grain size. Coarsening of grains has a negative effect on impact toughness of the joints [8]. Polygonal ferrite [11, 12] and regions of ferrite with OSP [13] present in structure of the welded joints also have a negative effect on impact toughness of the joints. The FBW thermal cycles accepted in this study initiate formation of the MAC-phase in structure of the joints welded in modes A and B. In studies [9, 14], the MAC-phase is classed with the factors that cause decrease in ductility and impact toughness of the weld metal on steels of the above grade. Considering the above-said, it can be concluded that welding performed in mode A promotes, first of all, coarsening of grain in the joining zone and HAZ region to size 4, formation of polygonal ferrite and regions of ferrite with OSP, as well as formation of up to 3.72 vol.% MAC-phase in their structure.

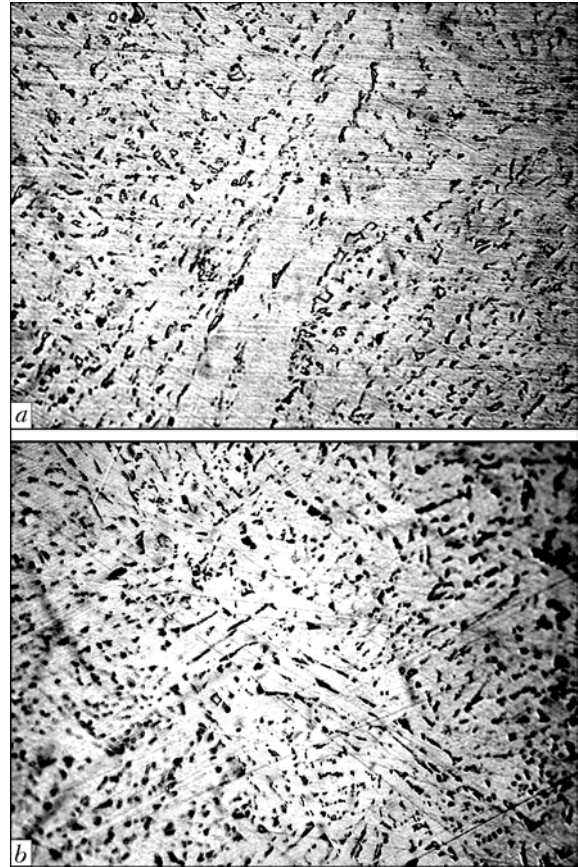


Figure 6. Polygonal ferrite (a) and ferrite with OSP (b) in welded joint made in mode A (a, b —  $\times 1000$ )

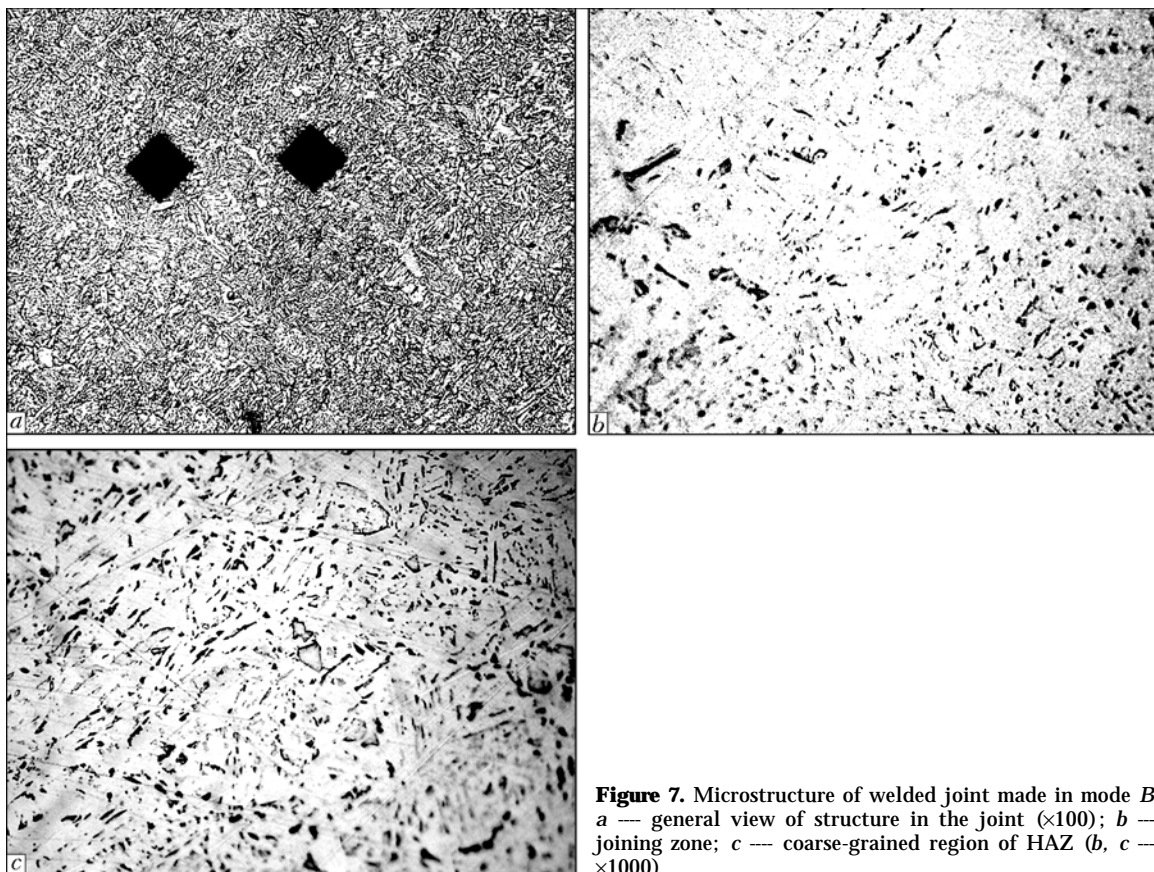
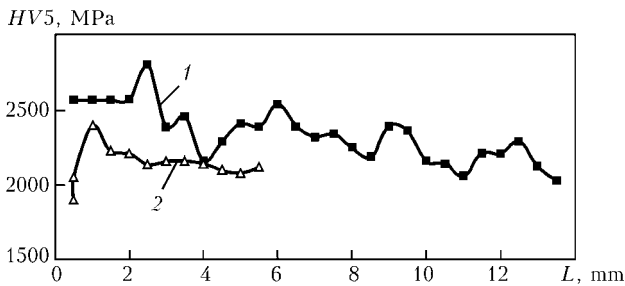


Figure 7. Microstructure of welded joint made in mode B: a — general view of structure in the joint ( $\times 100$ ); b — joining zone; c — coarse-grained region of HAZ (b, c —  $\times 1000$ )



**Figure 8.** Distribution of hardness in the zone of FB welded joints made in modes A (1) and B (2)

In welding in mode B, structure of the joining zone and coarse-grained region differs greatly from the above one: grain has size 6, structure comprises no polygonal ferrite and ferrite with OSP, and volume content of the MAC-phase is no more than 2.55 %.

The coarse-grained structure of the weld, which is characteristic of mode A, as well as polygonal ferrite and ferrite regions with OSP present in HAZ are the key factors that determine low values of impact toughness KCV. The MAC-phase present in the structure may also play a negative role. Additional investigations are required to determine the degree of its effect on values of impact toughness of the FB welded joints.

Impact tests of the joints investigated show that the preferable structural state is that formed in welding mode B with a low energy input. This guarantees the high and consistent properties of the welded joints on pipes in low-alloy steels of the X70 grade.

## CONCLUSIONS

1. The effect of energy input was investigated in flash butt welding of low-alloy steels 10G2FB. It was established that sound joints meeting requirements of standards can be produced at an energy input decreased 3–4 times, compared with the accepted technologies. In this case, mechanical properties ( $\sigma_y$ ,  $\sigma_t$ ,  $\delta$ ,  $\alpha$ ) differ but insignificantly, whereas impact toughness KCV strongly depends upon the thermal cycles used in welding.

2. When welding is performed in modes that provide heating close to the maximal one, which can be achieved in continuous flashing, impact toughness of the joining zone and adjoining regions substantially decreases. It is considered that the main causes of decrease in KCV are formation of the coarse-grained structure (grain with size 4), presence of polygonal ferrite, ferrite with OSP and, probably, MAC-phase. Hardening of metal developing in the coarse-grained region also leads to decrease in ductility of the welded joints.

3. The 4-fold decrease in energy input (energy consumption), accompanied by acceleration of flashing, allows decreasing the KCV values to the level of the base metal. Improvement of ductile properties is attributable, first of all, to refining of the metal structure (grain size 6), as well as to absence of polygonal ferrite and ferrite with OSP. In this case, the volume content of the MAC-phase decreases by 1.17 %.

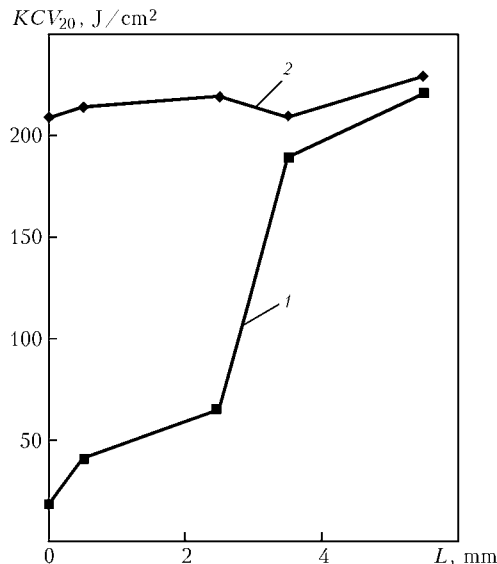


**Figure 9.** Distribution of impact toughness KCV<sub>20</sub> in FB welded joints made in modes A (1) and B (2)

4. In FBW of steels of the X70 grade, to provide high values of impact toughness KCV it is necessary to use the welding parameters with decreased energy input and increased concentration of heating within the narrow adjoining layer. This recommendation is not always feasible, as it is associated with increase in the installed capacity of power units. In such cases, welding should be followed by heat treatment, i.e. normalising.

1. Mazur, I.I., Serafin, O.M., Karpenko, M.P. (1988) Flash butt welding of pipelines: ways of improvement. *Stroitelstvo Truboprovodov*, **4**, 8–11.
2. *API Standard 1104: Welding of pipelines and related facilities*. Publ. Sept. 1999.
3. *SP 105-34-96: Codes for construction of main gas pipelines*. Introd. 11.09.96.
4. Kuchuk-Yatsenko, S.I., Lebedev, V.K. (1976) *Flash butt welding*. Kiev: Naukova Dumka.
5. Kuchuk-Yatsenko, S.I., Zhemchuzhnikov, G.V., Kazymov, B.I. (1980) Influence of defects of flash butt welding on strength of joints at low temperatures. *Avtomatich. Svarka*, **12**, 1–3.
6. (1972) *Atlas on metallography of iron*. Ed. by F.N. Tavazde. Vol. 2. Moscow: Metallurgiya.
7. Grigorenko, G.M., Grabin, V.F., Golovko, V.V. et al. (2003) Procedure of determination of sizes of ultradispersed non-metallic inclusions in metal of low-alloy steel welds. *The Paton Welding J.*, **4**, 26–28.
8. (1986) Guidelines for the classification of ferritic steel weld metal microstructural constituents using the light microscope. *Welding in the World*, **24(7/8)**, 144–148.
9. Hrivnyak, I. (1998) Weldability of current high-strength steels. In: *Proc. of Int. Conf. on Welding and Related Technologies into 21st Century* (Kiev, November, 1998). Kiev: PWI, 41–55.
10. (1986) *Static strength and fracture mechanics of steel*. Ed. by V. Dal, V. Anton. Moscow: Metallurgiya.
11. Novikova, D.P., Bogachek, Yu.L., Mandelberg, S.L. et al. (1973) Relationship between microstructure and impact toughness of welds on pipe low-alloy steel. *Avtomatich. Svarka*, **8**, 6–9.
12. Pokhodnya, I.K., Makarenko, V.D., Korsun, A.O. et al. (1986) Effect of nickel on structure and mechanical properties of weld made with basic electrodes. *Ibid.*, **2**, 1–5.
13. Grabin, V.F., Golovko, V.V., Kostin, V.A. et al. (2004) Morphological peculiarities of microstructure of weld metal from low-alloy steels with ultralow content of carbon. *The Paton Welding J.*, **7**, 15–20.
14. Hrivnyak, I., Matsuda, F. (1994) Metallographic examinations of martensite-austenite constituent (MAC) in HAZ of high-strength low-alloy steels. *Avtomatich. Svarka*, **3**, 22–30.



# CHANGE OF THE STRESS-STRAIN STATE OF WELDED JOINTS OF ALUMINIUM ALLOY AMg6 AFTER ELECTRODYNAMIC TREATMENT

L.M. LOBANOV, N.A. PASHCHIN, V.P. LOGINOV and V.N. SMILENKO

E.O. Paton Electric Welding Institute, NASU, Kiev, Ukraine

The effect of electrodynamic treatment (EDT) on the stress-strain state of flat specimens of AMg6 alloy at different diagrams of preliminary loading was studied. The measurement procedure based on ultrasonic NDT method was developed, and residual stresses in butt welded joints were measured. As established, EDT allows residual stresses in AMg6 alloy welded joints to be decreased by 50–65 %.

*Keywords:* arc welding, welded joint, residual stresses, electrodynamic treatment, current pulse, aluminium alloys, prestress, plastic deformation

Progress in development of modern equipment is due to application of welded structures with high specified technological and service properties. Use of such traditional treatments for welded joints as roll treatment, forging, heat treatment, etc. does not always promote an extension of the residual service life of structures under hard operating conditions. In this connection the problem of external energy impacts on mechanical properties of metals and alloys, as well as their welded joints, has become particularly urgent. Experimental studies of high-density electric currents, high-energy fields, plasma currents, ion implantation, laser radiation, as well as their combined impact on the structural materials, have formed the basis for creation of a new class of high-efficient technological processes of welded joint treatment.

In the last decade of the XX century there was a significant increase of the number of studies related to investigation of different variants of the electromechanical effect (change of properties under the impact of electric fields and currents) for semi-conductor, dielectric materials, and, primarily, for metals and alloys applied in mechanical engineering.

It is established that the impact of current pulses on the metals and alloys leads to an increase of their static and fatigue strength, as well as relaxation of the stress-strain state [1].

Electrodynamic treatment (EDT) is one of the new methods of current impact on the metals and alloys. It is based on initiation of electrodynamic forces in the material, which arise at transient processes and accompany the current discharge running in the material [2]. At summing up of the electrodynamic forces with static loading the material of the treated structure can develop structural changes, which are favourable for its residual life. The impact of current pulses on the metal, which is subjected to tension in the elastic and plastic loading fields [3, 4], results in a change of the metal stressed state.

Now, one of the causes for lowering of welded structure performance are residual welding stresses (furtheron referred to as RS), which are unfavourable for the strength properties and cause the residual distortion of the items. As tensile stresses close to the material yield point are found in the weld and near-weld zone, EDT of welded joints can initiate processes lowering the overall level of welded joint RS. While for titanium alloys [3] and thermally stable steels [4] investigations of the mechanism of stressed state variation in pre-loaded samples of welded joints under the impact of current pulses were conducted, no such data are available for aluminium alloys.

This study is aimed at investigation of EDT influence on lowering of the stress-strain state of welded joints of AMg6 aluminium alloy. For preliminary evaluation of EDT influence on RS in the above material the treatment was conducted under the conditions of tension of blade-type flat samples. A laboratory unit, based on a capacitor-type machine [4], was used for initiation of individual current pulses in the metal. A discharge of the capacitor bank was transmitted to the sample through contact of a copper electrode with the metal surface in EDT zone. Schematic of EDT of a sample at uniaxial tension is shown in Figure 1. Base metal samples were cut out along the rolling direction from sheet blanks of non-cold-worked aluminium alloy AMg6 4 mm thick. At the initial stage of the experiments EDT was performed on samples of the base metal pre-loaded by longitudinal uniaxial tension in the elastic, elasto-plastic and plastic deformation fields. Samples of butt welded joints of AMg6 alloy 4 mm thick (see Figure 1), which were cut out across the weld from plates of  $500 \times 500 \times 4$  mm size, were also subjected to EDT. Butt joints were made by automatic single-pass nonconsumable-electrode argon-arc welding in AS-TV-2M unit in the following mode: welding current of 220 A; arc voltage of 18 V; welding speed of 14 m/h; filler wire of SvAMg6 grade of 2.0 mm diameter. The above mode ensured a guaranteed penetration and satisfactory formation of the welded joint.

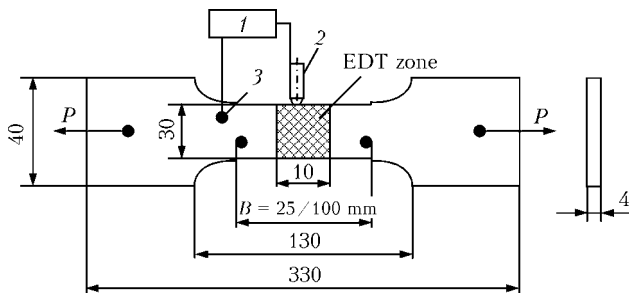


**Figure 1.** Schematic of EDT of samples of base metal and welded joint on AMg6 alloy for testing by uniaxial tension: 1 --- unit for EDT; 2 --- electrode; 3 --- fastening of return wire; P --- tensile force

EDT of welded joint samples was conducted along the near-weld zone. Its selection as the treatment zone was dictated by the presence of longitudinal compressive plastic deformations  $\epsilon_{pl}$  in it. Summing up of  $\epsilon_{pl}$  values with those of plastic deformations, initiated by current pulses, triggers off relaxation processes in AMg6 alloy, which may result in lowering of RS level.

Testing of samples of AMg6 alloy was performed in TsDM-10 rupture testing machine with the maximum tensile force of 10 t at the deformation rate of 6 mm/min. Change of the tensile force up to the above material reaching the required stressed state was recorded during the entire cycle of sample loading.

The purpose of these experiments was studying the peaks of electrodynamic effect, which appear at an abrupt lowering of deformation resistance of AMg6 alloy under the impact of a current discharge. The effect was manifested in the form of a characteristic lowering of the deforming force in the tensile diagrams (Figure 2).

The sample fastened in the grips of the testing machine was stretched up to the specified value, and a discharge was performed with registering of the deforming force drop by a data recorder (incorporated into TsDM-10 machine) and mechanical strain gauge (with measurement base  $B = 25$  and 100 mm). Three diagrams of sample loading were studied:

- first --- tension was performed discretely with pauses for EDT by isolated current pulses and recording of the deforming force drop;
- second --- similar to the first schematic, but with compensation of the deforming force with the tensioning rate  $v = 6$  mm/min;
- third --- at continuous loading the material was treated by current discharges during increase of the tensile force up to sample fracture.

The first diagram of sample loading represented the mechanism of the stressed state of butt welded joints at EDT. In this case the elastic tensile stresses in the near-weld zone were simulated by uniaxial tension of the sample.

When studying the nature of variation of the deforming force in a broad range of pre-loading, special attention was given to investigation of the electrodynamic effect at pre-stresses close in magnitude to RS in welded joints of AMg6 alloy. EDT was performed in the following mode: electrode current  $I_{el} = 3500$  A; electrode voltage  $U_{el} = 450$  V; current pulse duration  $\tau_p = 0.5$   $\mu$ s; capacitance of capacitor bank  $C_{cap} = 1400$ – $2800$   $\mu$ F. Values of pre-loading  $\sigma_{pr}$  of samples of the base metal and welded joints of AMg6 alloy, as well as parameters characterizing its change as a result of EDT, are shown in Table 1.

Based on the data of Table 1, we can conclude that EDT of AMg6 alloy by the first treatment diagram (series 1–3) causes a discrete drop of the deforming force in the material in the studied loading range. Unlike the conclusions of works [3, 5], where it says that the current pulses do not influence the lowering of the tensile load in the elastic field of material loading, a discrete lowering of the loading force (15–30 % of the initial value) was observed on samples of series 1 and 2 loaded by tension in the load range below the limit of proportionality, which is equal to 130 MPa in AMg6 alloy. The maximum values of the total relative drop of tensile stresses after EDT cycle  $\Sigma\Delta\sigma\%$  (up to 30 %) were recorded at  $\sigma_{pr} = 116.7$  MPa (see Table 1, sample series 2), which is close to the real values of longitudinal tensile stresses  $\sigma_x$  in welded joints of AMg6 alloy.

At loading of samples of series 4 above the proof stress (samples of series 3) lowering of the deforming load did not exceed 15 %. The closer were the values of  $\sigma_{pr}$  and yield point, the lower the values of  $\Sigma\Delta\sigma\%$  determining the treatment effectiveness.

For each pulse series the current relative drop of tensile stresses was analyzed after each discharge  $\Delta\sigma\%$  (see Table 1), which reflects the current change of the isolated jump of the deforming force at EDT in samples in each test series. It is noted that at sample treatment by the first diagram, the maximum drop of the tensile forces in the treatment cycle (50 % of the total value of  $\Sigma\Delta\sigma\%$ ) is observed during the first current discharge in the pulse series. At subsequent current impacts the effectiveness of this process decreases, which is attributable to «depletion» of the dislocation

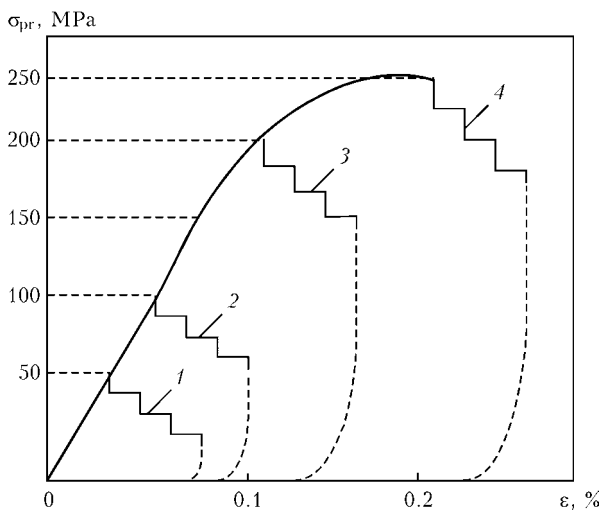


**Figure 2.** Change of elastic tension (1, 2) and tension in the elasto-plastic field (3, 4) of samples of AMg6 alloy at EDT:  $\sigma_{pr}$  --- pre-stress;  $\epsilon$  --- relative deformation



**Table 1.** Change of deforming force of samples of base metal and welded joints on AMg6 alloy at EDT under pre-tension

Sample series No.	<i>n</i>	$\sigma_{pr}$ , MPa	$\sigma_n$ , MPa	$\Delta\sigma_n$ , MPa	$\Delta\sigma\%$ , %	$\Sigma\Delta\sigma\%$ , %	$C_{cap}$ , $\mu F$
<i>Base metal</i>							
1	--	52.9	--	--	--	~21	1400
	1		45.80	7.10	13.50		
	2		43.30	2.50	4.70		
	3		41.70	1.60	3.00		
2	--	116.7	--	--	--	~30	1400
	1		104.10	12.60	11.00		
	2		99.10	5.00	4.30		
	3		92.50	6.60	5.70		
	4		86.60	5.90	5.00		
	5		83.30	3.30	3.00		
3	--	258.0	--	--	--	~14	1400
	1		229	29.00	11.20		
	2		224	5.00	2.00		
	3		222	2.00	0.80		
4	--	52.9	--	--	--	~32	2800
	1		40.40	12.50	23.60		
	2		36.25	4.15	7.90		
5	--	116.7	--	--	--	~50	2800
	1		88.34	20.36	24.30		
	2		77.50	10.84	9.30		
	3		70.00	7.50	6.43		
	4		62.90	7.10	6.10		
	5		59.50	3.40	3.00		
<i>Welded joint</i>							
6	--	100.0	--	--	--	~57	2800
	1		70.00	30.00	30.00		
	2		56.67	13.33	13.33		
	3		50.00	6.67	6.67		
	4		45.40	4.60	4.60		
	5		43.50	1.90	1.90		
7	--	80.5	--	--	--	~28	2800
	1		58.20	22.30	27.70		
	--	80.5	--	--	--	~17	
	1		66.60	13.90	17.30		
	--	80.5	--	--	--	~14	
	1		69.30	11.20	13.90		
	--	161.0	--	--	--	~22	
	1		125.00	36.00	22.36		
	--	161.0	--	--	--	~17	
	1		133.00	28.00	17.39		
	--	161.0	--	--	--	~19	
	1		130.00	31.00	19.25		
	--	161.0	--	--	--	~19	
1	130.00		31.00	19.25			



Sample series No.	$n$	$\sigma_{pr}$ , MPa	$\sigma_n$ , MPa	$\Delta\sigma_n$ , MPa	$\Delta\sigma\%$ , %	$\Sigma\Delta\sigma\%$ , %	$C_{cap}$ , $\mu F$	
7	--	247.0	--	--	--			
	1		194.00	53.00	21.45	~21		
	--	247.0	--	--	--			
	1		200.00	47.00	19.20	~19		
	--	247.0	--	--	--			
	1		205.00	42.00	17.00	~17		
	--	288.6	--	--	--			
	1		238.65	49.95	17.30	~17		
	--	288.6	--	--	--			
	1		241.42	47.18	16.34	~16		
	--	288.6	--	--	--			
	1		249.75	38.85	13.46	~13		
	--	330.0 (before fracture)	--	--	--			
	1		277.50	52.50	15.90	~16		
--	291.0	--	--	--				
8	--	110.0	--	--	--		2800	
	1		72.00	38.00	34.54	~35		
	--	138.7	--	--	--			
	1		80.47	58.23	41.98	~42		
	--	163.7	--	--	--			
	--	80.47	83.23	50.84	~51			
	--	0	--	--	--			
	--	47.0	--	--	--			
	1		47.00	0	0	0		
	--	83.25	--	--	--			
	1		83.25	0	0	0		
	--	133.2	--	--	--			
	1		133.20	0	0	0		
	--	138.75	--	--	--			
	1		138.75	0	0	0		
	--	194.25	--	--	--			
	1		97.10	97.15	50.01	~50		
	--	0	--	--	--			
	--	61.0	--	--	--			
	1		61.00	0	0	0		
	--	111.0	--	--	--			
	1		111.00	0	0	0		
	--	174.8	--	--	--			
	1		174.80	0	0	0		
	--	202.5	--	--	--	0		
	--		127.65	74.85	36.96	--		
	--	219.22	--	--	--	~37		
1		122.26	96.96	44.22				
--	241.42	--	--	--	44			



Sample series No.	$n$	$\sigma_{pr}$ , MPa	$\sigma_n$ , MPa	$\Delta\sigma_n$ , MPa	$\Delta\sigma\%$ , %	$\Sigma\Delta\sigma\%$ , %	$C_{cap}$ , $\mu\text{F}$
8	1		149.85	91.57	37.92	--	
	--	0	--	--	--	~38	
		290 (fracture)					

Note.  $\sigma_{pr}$  --- current tensile stress after discharge;  $\Delta\sigma_n = \sigma_n - \sigma_{n+1}$  --- current drop of tensile stresses after each discharge; dash --- absence of current pulses.

structure of the material at loading of its crystalline lattice [1].

The influence of increasing EDT efficiency by increasing the capacitance of the capacitor bank  $C_{cap}$  up to 2800  $\mu\text{F}$  (see Table 1, samples of series 4 and 5) was also studied. From the tabulated data it is seen that with increase of  $C_{cap}$  both at small values of  $\sigma_{pr}$  (samples of series 4) and at those close to the welding values,  $\Sigma\Delta\sigma\%$  values increased 1.5–1.7 times. Results of investigations of the features of EDT of the welded joint are given for samples of series 6–8. Value of  $\sigma_{pr}$  in samples of series 6 (similar to series 2 and 5) was selected close to RS in alloy AMg6 --- 100 MPa. It is established that similar to the previous test series at the first impact of current on the material  $\sigma_{pr}$  drops to 50 %.

The features of development of plastic yield of the material under the impact of a series of current pulses were studied on samples of alloy AMg6 using a mechanical deformer. The obtained data lead to the conclusion that the values of preloading of welded joint samples (series 6) are comparable with the load values accepted for the base metal (samples of series 5). If we compare  $\Delta\sigma\%$  values in samples of series 5 and 6, the deformation processes are more pronounced in welded joints, which are determined by a drop of the pre-tension force during the time of impact of the first two current pulses. At comparison of  $\Sigma\Delta\sigma\%$  values in the base metal and welded joint, it is seen that the values of the above parameter are 10 % higher in the latter, which is attributable to a higher ductility of the near-weld zone metal. This proves that EDT of welded joints of AMg6 alloy is more effective compared to the base metal.

A mechanical deformer was used to determine on the base metal samples the features of development of plastic deformation directly in the treatment zone, i.e. in the section of electrode contact (see Figure 1) with the metal surface. First a compressive plastic deformation equal to about 0.1 % was induced in the material of the sample working part, which was followed by stretching the samples up to  $\sigma_{pr} = 110$  MPa. This loading diagram induces in the material a stress-strain state, similar to that observed in the near-weld zone of welded joints of alloy AMg6 [5]. Loaded samples were subjected to EDT by the mode given in Table 1, at the bank capacitance  $C_{cap} = 1400$   $\mu\text{F}$ . After EDT a mechanical deformer ( $B = 25$  mm) was used to determine a discrete drop of the load force  $\sigma_{pr}$  and lowering of the values of relative deformation  $\varepsilon$  oc-

curing after the impact of the current discharge, respectively. Figure 1 shows the arrangement of the instrument contact bases on the sample surface. Figure 3 shows the diagrams of the dependence  $\sigma_{pr} = f(n)$  and  $\varepsilon = f(n)$  (here  $n$  is the number of current discharges in EDT cycle). From the Figure it is seen that already after the first ( $n = 1$ ) current pulse, the metal loses its elastic properties at tension below the elasticity limit  $\sigma_e$ , and at further treatment ( $n > 2$ ) it is in the elasto-plastic state. After completion of EDT cycle and unloading, the metal develops the residual plastic tensile deformation  $\varepsilon = 0.1$  %.

Comparison of Figure 3, *a* and *b* leads to the conclusion that plastic pre-deformation of AMg6 alloy in

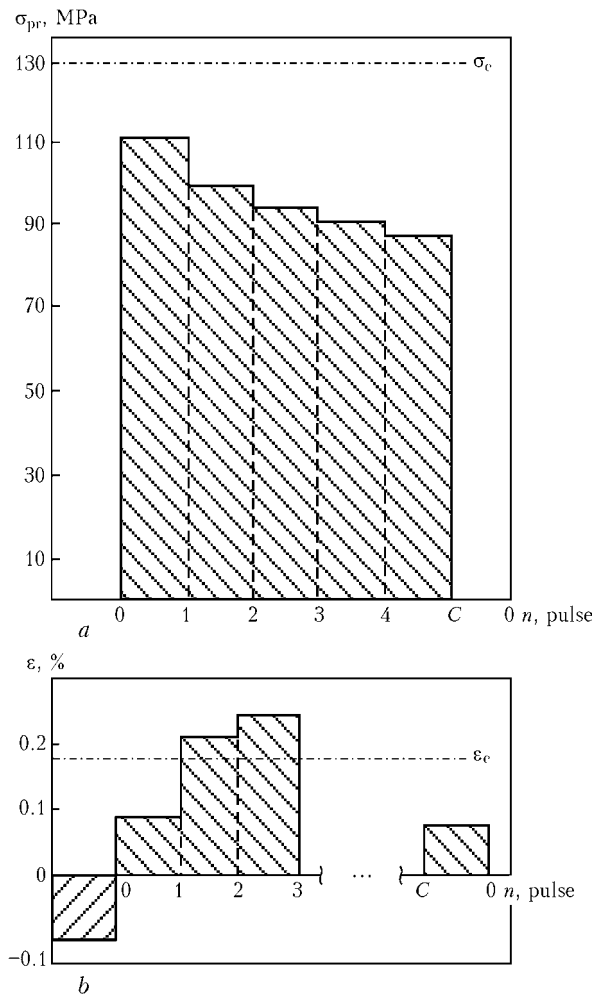


Figure 3. Drop of pre-deforming force  $\sigma_{pr}$  (*a*) and change of relative deformation  $\varepsilon$  (*b*) on samples of alloy AMg6 at EDT: C --- unloading after EDT cycle;  $\sigma_e$  --- limit of elasticity;  $\varepsilon_e$  --- elastic deformation of AMg6 alloy; ... --- no data



combination with subsequent elastic loading and EDT can form the fields of elasto-plastic deformations in this material. On the other hand, the stress-strain state of the near-weld zone of AMg6 alloy welded joints is characterized by the presence of compressive plastic deformations in combination with elastic tensile stresses. Thus, the test results presented in Figure 3, simulate with a sufficient degree of validity, the relaxation processes occurring in the «active» zone of the joint at its treatment by current pulses. Formation of the fields of tensile plastic deformations, «reverse» relative to the welding ones, during EDT, can be positive for lowering the overall level of the stressed state of welded joints.

Lowering of the effectiveness of electrodynamic impact on the material at a greater distance from the treatment zone was measured. With this purpose, the discrete drop of  $\sigma_{pr}$  value was measured using a strain gauge with the variable measurement base ---  $B = 25$  and  $100$  mm.

Current changes of the values of relative deformations  $\varepsilon$  at EDT were studied in the assumption that if EDT is of a local nature, then at each current discharge a discrete drop of tensile load  $\Delta\sigma_{pr}$  will correspond to different  $\varepsilon$  values ( $B = 25$  and  $100$  mm).

EDT of the samples was conducted in the mode given in Table 1 at  $C_{cap} = 2800 \mu F$ . The sample was subjected to pretension up to  $180$  MPa, which corresponded to elasto-plastic region of deformation of AMg6 alloy. Investigation results are given in Table 2. From the Table data it is seen that decrease of  $\varepsilon$  values at EDT is of a damping nature, which is in agreement with the data of Table 1 on discrete lowering of  $\sigma_{pr}$  values. The electrodynamic action is localized in EDT zone (see Figure 1), the surface of which was treated. So, the sample material in the zone of measurement base  $B = 25$  mm after the first current pulse was in the condition of a developed plastic flow, and in the zone of measurement base  $B = 100$  mm it experienced deformations, only slightly higher than the limit of elasticity of AMg6 alloy. At subsequent current pulses the change of  $\varepsilon$  values is of a damping nature, and the difference of deformer readings at  $B = 25$  and  $100$  mm is indicative of lowering of the influence of the electrodynamic effect on the material properties at greater distance from EDT zone.

**Table 2.** Relative tensile deformation  $\varepsilon$  of AMg6 alloy samples at EDT at  $\sigma_{pr} = 180$  MPa

n	$\Delta\sigma_{pr}$ , MPa	$\varepsilon$ , %	
		$\hat{A} = 25$ mm	$\hat{A} = 100$ mm
–	–	0.26	0.27
1	50	0.51	0.16
2	22	0.29	0.07
3	11	0.12	0.05
4	13	0.07	0.06
5	8	–	0.01

To study the features of EDT mechanism material treatment was conducted at loading by the second diagram. For this purpose, samples of the butt welded joint of AMg6 alloy were used (see Figure 1). After elastic pre-tension of the metal in the elastoplastic tension region and impact of current pulses, the drop of the tensile load was compensated using tightening of the moving grip of the tensile testing machine to the level of  $\sigma_{pr}$ . The nature of variation of tensile load  $\Delta\sigma_n$  under the influence of EDT of the welded joint on AMg6 alloy at compensation of its current drop  $\Delta\sigma_n$  caused by electrodynamic impact, is shown in Table 1 (sample of series 7). The data of this Table was used to evaluate the variation of a unit jump of the deforming force after restoration of the initial load  $\sigma_{pr}$  in different pre-tension ranges. Assuming that lowering of the unit jump of  $\sigma_{pr}$  values in the previous series is associated mainly with the conditions of fastening by the first diagram, i.e. absence of the possibility of realization of displacements along the sample longitudinal axis, compensation of  $\sigma_{pr}$  drop by repeated tightening should promote stabilization of  $\sigma_n$  after each subsequent impact of current pulses. On the other hand, having analyzed the data (sample of series 7, Table 1) one can see that  $\Sigma\Delta\sigma\%$  values in each range of tensile loads differ from each other. Difference in values  $\Delta\sigma_{pr}$  at the first ( $n = 1$ ) and last ( $n = 4$ ) current discharges at  $\sigma_{pr} \approx 161$  MPa, i.e. at loads close in their values to the maximums of longitudinal RS for AMg6 alloy, is equal to  $25\%$ . Thus, in aluminium alloys EDT enables creating zones of elasto-plastic deformation of the material, this allowing adjustment of the stressed state of welded structure elements which are under the impact of operating loads. Fabrication of metal structures by the method of elastic pre-tension in combination with EDT appears to be effective for improving the accuracy of their manufacture.

In order to study the influence of the mode of continuous loading of the material on the electrodynamic effect at treatment of aluminium alloy AMg6 a flat sample of base metal  $4$  mm thick was subjected to a force impact by the third loading diagram at the rate of material deformation  $v = 6$  mm/min (Figure 4). The data of [3] lead to the conclusion that treatment of the sample material by current pulses at its continuous tension leads to an increase of the values of the deforming force drop compared to samples subjected to EDT under the conditions of discrete loading by the first diagram.

In order to study EDT in the mode of loading by the third diagram, the samples were subjected to continuous tension. At the first loading stage  $\sigma_{pr} = 110, 139$  and  $164$  MPa an isolated current pulse was initiated in the above mode ( $C_{cap} = 2800 \mu F$ ) on the sample working surface, with recording of the jump of the deforming force (Figure 4, a). After completion of a series of current pulses complete unloading of the sample was performed. At repeated loading (second stage, Figure 4, b) the sample was subjected to tension up



to 200 MPa, conducting EDT by individual current pulses until  $\sigma_{pr} = 85, 130$  and 200 MPa has been reached. Then in the third loading stage (Figure 4, c) EDT was performed until  $\sigma_{pr} = 61, 111, 175, 202, 220$  and 242 MPa have been reached with nulling and subsequent tension of the sample to fracture which occurred at  $\sigma_{pr} = 290$  MPa. Values of drop of the deforming force as a result of EDT at continuous tension of the samples are given in Table 1 (samples of series 8).

Having analyzed the data in Table 1, one can see significant differences in the nature of a discrete drop of the force of deforming AMg6 alloy by the third loading diagram.

Comparing values  $\Delta\sigma\%$  after the impact of the first pulse in samples of series 5 ( $\sigma_{pr} = 116.7$  MPa) produced without compensation of tension, where  $\Delta\sigma\% = 24.30\%$ , with samples of series 8 ( $\sigma_{pr} = 110$  MPa), where  $\Delta\sigma\% = 34.54\%$ , one can see an increase of the effectiveness of an isolated impact of the pulse current at continuous tension of the sample. At increase of the load to 163.7 MPa further increase of the values of deforming jump to  $\Delta\sigma\% = 50.84\%$  was observed. At comparison of these data with those obtained for samples of series 7 for the first current impact at  $\sigma_{pr} = 161$  MPa, it is seen that they have lower values of  $\Delta\sigma\% = 22.36\%$ . This is attributable to the fact [1] that at continuous deformation of polycrystalline structures under the conditions of current impact a large number of incomplete shear dislocations form along the slip bands (compared to discrete tension), which are exposed to current pulse impact.

The influence of EDT on the features of the drop of the deforming force after  $\sigma_{pr}$  recovery was studied at continuous loading of samples of series 8. It should be noted that at achievement of  $\sigma_{pr} = 163.7$  MPa and load drop to zero and subsequent tension of the sample, the jump of the deforming force was recorded only after exceeding the initial load (163.7 MPa) and achievement of  $\sigma_{pr} = 194.25$  MPa. At subsequent loading and nulling of  $\sigma_{pr}$  values the presence of a discrete drop of the deforming force was recorded only at  $\sigma_{pr} \geq 202.5$  MPa.

Absence of the jump after repeated loading can be explained by analogy with the phenomena observed at investigation of the process of electric pulse treatment of titanium alloys [3]. The impact of the current discharge on the deformed sample results in transformation of the material structure, namely shifting of part of the dislocations to a new position with a higher level of the energy of dislocation pinning on the stoppers. The higher the energy of stripping from the stoppers (activation energy), the higher the external tensile stress, at which the dislocations will separate from the stoppers. Thus, according to [3], the activation energy is determined by summing of the constant component of the current pulse energy and the variable component related to the continuously increasing sample deformation. At re-loading up to  $\sigma_{pr}$  value lower than the initial value, the activation energy does not

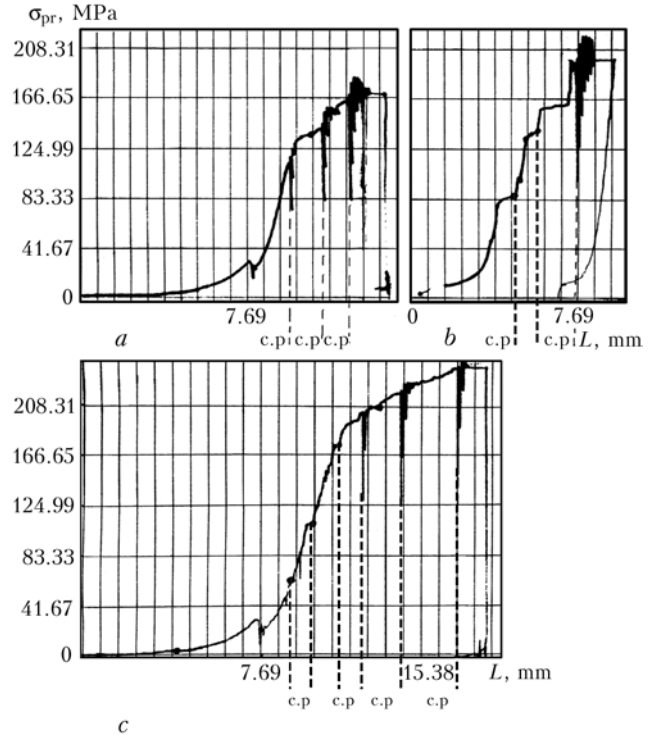


**Figure 4.** Curves of relaxation of deforming force  $\sigma_{pr}$  on sample of AMg6 alloy in the third loading diagram: a — first loading stage; b — second; c — third; c.p. — current pulse; L — spacing of rupture machine grips

allow initiating the dislocation separation from the stoppers, this preventing the realization of the deforming force jump.

To study the change of the residual stressed state of welded joints of thin-walled structural elements as a result of electrodynamic impact on full-scale samples, flat samples were prepared from aluminium alloy AMg6 of  $450 \times 400 \times 4$  and  $500 \times 500 \times 3$  mm dimensions. The plates were welded along the longitudinal axis of symmetry by the above-described technology and mode. RS were determined by non-destructive ultrasonic (US) technique, which is based on the dependence of the velocity of ultrasonic wave propagation on stresses in the metal [6]. This method allows evaluation of uni- and bi-axial stressed state without disturbance of the integrity of the studied object.

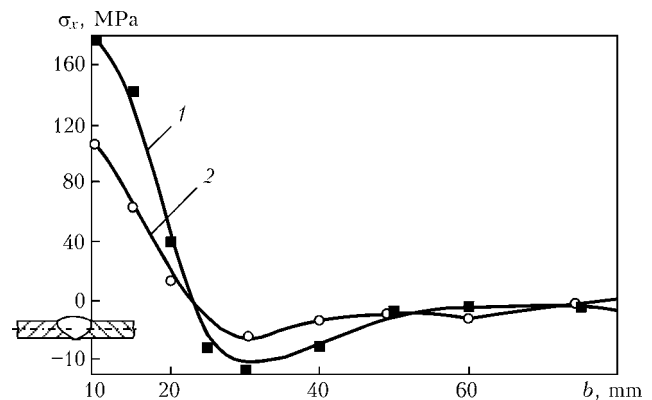


**Figure 5.** Distribution of longitudinal residual stresses  $\sigma_x$  in samples of butt welded joints of AMg6 alloy without treatment (1) and after EDT (2): b — weld width



A feature of US method is the possibility of determination of RS in full-scale structures in the unloaded and loaded conditions. In these studies loading was the impact of electrodynamic forces on the metal initiated by isolated current pulses.

US method allowed conducting multiple measurements of the current RS values after each impact of the current pulse in EDT cycle. The above method was used to evaluate the effectiveness of current impact on sample material by lowering RS level, depending on the quantity of current pulses.

Measurement of RS values was conducted in the plate central cross-section. Longitudinal  $\sigma_x$  and transverse  $\sigma_y$  components of the plane stressed state of the sample material before and after EDT were determined. Treatment along the fusion line was performed along the entire weld length. Butt joint sample during EDT was in the free state without application of static loads to it, this allowing EDT influence on welding stress relaxation to be evaluated.

Determination of longitudinal RS after welding in the treated and untreated samples of AMg6 alloy is shown in Figure 5, from which it is seen that EDT of

the welded joint promotes lowering of longitudinal RS  $\sigma_x$  by 45–50 %. Lowering of transverse RS  $\sigma_y$  by 60–65 % after EDT was found in the near-weld zone. Thus, the data given in this work are indicative of the effectiveness of EDT application for adjustment of the stressed state of AMg6 aluminium alloys and their welded joints.

1. Lobanov, L.M., Pashchin, N.A., Loginov, V.P. et al. (2005) Application of electric pulse treatment of structural elements to extend their service life (Review). *The Paton Welding J.*, **11**, 19–23.
2. Aleksandrov, G.N., Borisov, V.V., Ivanov, V.L. et al. (1985) *Theory of electric apparatuses*. Moscow: Vysshaya Shkola.
3. Semashko, N.A., Krupsky, R.F., Kupov, A.V. et al. (2004) Acoustic emission in electric pulse deformation of titanium alloys. *Materialovedenie*, **7** (special issue), 29–33.
4. Lobanov, L.M., Pashchin, N.A., Skulsky, V.Yu. et al. (2006) Influence of electrodynamic treatment on the stress-strain state of heat-resistant steels. *The Paton Welding J.*, **5**, 8–11.
5. Lobanov, L.M., Pavlovsky, V.I., Loginov, V.P. et al. (1990) Control of thermodynamic cycles in welding of sheet structures using the heat absorbers. *Avtomatich. Svarka*, **9**, 39–49.
6. Guz, A.N., Makhort, F.G., Gushcha, O.N. et al. (1974) *Fundamentals of ultrasonic nondestructive method for determination of stresses in solids*. Kiev: Naukova Dumka.

## FEATURES OF ELECTROMAGNETIC IMPACTS ON THE METALS AND THEIR WELDED JOINTS (REVIEW)

S.I. MORAVETSKY<sup>1</sup>, N.A. PARSHENKOV<sup>1</sup> and V.A. SOKIRKO<sup>2</sup>

<sup>1</sup>E.O. Paton Electric Welding Institute, NASU, Kiev, Ukraine

<sup>2</sup>DS Company, Nikolaev, Ukraine

Published data on the main features and mechanisms of electromagnetic impact on the structure of the base metal and welded joints are described.

*Keywords:* metallic materials, welded joints, treatment, electromagnetic impacts, plastic deformation, mechanical properties, residual welding stresses

In fabrication of critical welded structures requirements are made of improvement of ductile properties of the weld metal and HAZ which have been exposed to the thermodeformational welding cycle (TDWC), as well as relieving the residual welding stresses (RWS). The essence of any process of post-weld treatment to meet these requirements is reduced to a method of energy transfer into the metal volume, its kind and role. Under the impact of post-weld heat treatment the elastic energy accumulated during TDWC is relaxed through running of plastic deformation at different scale levels of the metal. The latter running on the level of the macroscopic metal body, enables lowering RWS of the 1st kind, and on the level of grains, subgrains and crystalline lattice of the metal it is one of the key factors affecting the residual mechanical properties of welded joint metal. The metal treatment

methods known so far use such kinds of energy as thermal, chemical and mechanical (energy of explosion).

In view of the objective and subjective circumstances, the influence of electromagnetic impact (EMI) on the physicomechanical properties of welded joint metal and RWS level is still practically unstudied. On the other hand, numerous works in the field of engineering physics show that the energy of electromagnetic origin can have a quite significant influence on running of plastic deformation, and stressed state of the metal body, and can noticeably change its mechanical characteristics. In this connection, research of this kind conducted for the first time in the middle of XIX century, starting from 1950–1960s [1], has become systematic. At present, change of the properties and mechanical behaviour in a wide range of metallic materials and non-metals, both unloaded and under active loading, is studied, as well as the process of creep or stress relaxation under the impact of pulsed and constant electric (EF) and magnetic (MF) fields,



and electric current (EC) of a broad range of values in the temperature interval from 4.2 to  $1 \cdot 10^3$  K. Theories of the mechanisms of EMI influence are being developed in parallel with obtaining test data, and knowledge gained in this field has been presented in many monographs and reviews [1–6]. Results of some of this work have gained applied importance; they enabled development of various industrial processes of metal treatment using EMI, which have become widely accepted in practice.

Right now among the publications on the above-mentioned subjects there are quite few works on investigation of EMI on welded joint metal. It is known that during TDWC the processes of thermomechanical excitation and the concurrent, but not compensating them, processes of relaxation run in the metal of the parts being welded. In this case the elastic, diffusion and plastic deformations occur. A high non-uniformity of spatial distribution of the latter is found both in the macro- and microvolumes of the metal leading to appearance of fracture sites. After welding the joint is a non-equilibrium structure with a high level of the accumulated elastic energy, up to 98 % of which are inner stresses of the 3rd kind.

The authors do not pretend to a completeness of the review or exhaustive depth of understanding the physical essence of EMI. Nonetheless, it appears to be necessary to provide a general description of EMI as a potential tool for influencing the welding processes, and processes underlying various post-weld treatments, and possible development of new independent and combined methods of welded joint treatment. Quite interesting, probably, also are the already formed concepts of the mechanisms of the above influence. Practical usefulness of such a review is not so much in analysis of the fundamental physical generalizations, as in consideration and understanding of the applied importance of the facts obtained by researchers in different field of metal physics and set forth in the published sources. Further on a brief description is given of the main features of EMI influence on the mechanical properties of materials and their behaviour under load proceeding from the known investigation results.

**Influence of electromagnetic impacts on mechanical behaviour and properties of materials.** MF classification given in [1] can be taken as the criteria for evaluation of EMI level. According to this classification, MF based on intensity  $H$  are divided into superweak ( $1 \cdot 10^{-5}$ – $1 \cdot 10^2$ ), weak ( $1 \cdot 10^2$ – $1 \cdot 10^5$ ), medium ( $1 \cdot 10^5$ – $5 \cdot 10^6$ ), strong ( $5 \cdot 10^6$ – $80 \cdot 10^6$ ) and super-strong (more than  $80 \cdot 10^6$  A/m). EC can be evaluated under the same classification by the intensity of MF induced by it, the maximum of which in the case of a rectilinear infinite conductor of a round section falls on its surface and is simple to calculate.

In numerous works by V.I. Spitsin, O.A. Troitsky, V.I. Stashenko and other researchers, EC pulses of density  $j \sim 1 \cdot 10^2$ – $1 \cdot 10^3$  A/mm<sup>2</sup> and duration  $\tau \sim 1 \cdot 10^{-4}$  s led to a multiple increase of deformation accumulated

by a zinc sample of the cross-section of approximately 1 mm<sup>2</sup> during the time of testing in the creep mode at the temperature of 78 K. Under the impact of a pulsed MF ( $H \sim 1 \cdot 10^5$  A/m), as well as alternating, direct and pulsed EC at equal effective density of  $10^2$ – $10^3$  A/mm<sup>2</sup> a noticeable (5–130 %) increase of sample deformation rate is found in samples from indium, lead, tin and zinc loaded in the creep mode [7]. Under the impact of pulses, synchronous drops of the tensile force are observed in the diagrams of sample tension [1, 2], which in the opinion of the researchers [2], is indicative of metal softening at the moment of the pulse.

Using strong EMI in some cases it is possible to achieve an intensive plastic deformation of the metal samples without application of mechanical load to them. MF pulses were applied to induce residual deformation of samples from copper alloys [1, 8] and aluminium [9], and EC pulses ( $500$ – $7000$  A/mm<sup>2</sup>) essentially changed the relief of the polished surface of foils from copper due to dislocations exiting from it and regrouping of the initial unevenness [10].

Weak EMI also have a marked influence on the mechanical behaviour of materials. At creep testing of such metals as aluminium, cobalt, copper, iron, nickel and titanium, as well as D16, KhN77TYu, Kh18N10T and other alloys at  $T = 20$ – $1150$  °C, a multiple increase of creep rate was noted at superposition of EF (electric filed intensity  $E = 10$  W/mm), MF ( $H = 1.6$ – $40$  kA/m) and flowing of constant EC ( $j = 0.15$  A/mm<sup>2</sup>). The degree of manifestation of the effect of the above impacts was maximum in the first several minutes after their start, it decreased with time, and approximately 0.5 h after deformation under EMI conditions the creep rate dropped approximately to its initial value [11–14].

Exposure of materials (LiF, NaCl, Si and Al) to a weak MF or EC ( $j < 0.3$  A/mm<sup>2</sup>) flowing through conducting solids under certain conditions allows increasing the dislocation path from several tens up to several hundred percent during the fixed time of sample loading [6, 15–17]. Effect of increase of dislocation mobility is observed not only at combining EMI with loading, but also after completion of 5-hour exposure of silicon in a weak MF it was preserved practically unchanged for the first 150 h and decreased almost two times after 400 h [16]. Post-effects were observed also at strong EMI [2].

Application of X-ray and electron methods of investigation allows revealing a wide range of changes caused by EMI in the material microstructure [2]. Influence of treatment by current pulses of alternating polarity ( $j = 6.0$ – $16.4$  A/mm<sup>2</sup>;  $\tau = 2.0$ – $2.5$  s at the pause of 4–10 s) of samples from high-strength steel AK-25 simulating the joints produced by electron beam welding was studied. X-ray microprobe analysis revealed a lowering of the density of dislocations and stresses of the 2nd kind in the metal of samples produced by electron beam welding after treatment [18]. Noticeable changes of structurally-dependent mag-



netic characteristics of the material were also observed. On the whole, microstructural changes caused by EMI are quite diverse, and their study could be the subject of a separate paper. For us it is more rational to consider the change of structurally-dependent mechanical properties of materials subjected to EMI.

Mechanical properties are evaluated both after completion of EMI (residual) and during EMI. In the second case, EMI are observed during the entire testing time or at its individual stages, for instance, after achievement of a certain value of deformation or stress, at the stage of unsteady creep, etc.

Electromagnetic treatment by several current pulses ( $\tau \sim 10^{-2}$ – $10^{-1}$  s,  $j \sim 10^2$  A/mm<sup>2</sup>), which do not eliminate the thermal impact, provides high residual plastic properties of titanium and aluminium alloys [19, 20]. The authors of these studies report an increase of the residual relative elongation by 30–60 %, impact toughness by 20–50 % and lowering of the yield point by 30–50 %, compared to the initial condition of the alloys with the specified work hardening. Impact toughness and crack resistance characteristics of aluminium alloys are 10–15 % higher than the level ensured by the traditional tempering of these alloys for 1 h, and the ultimate strength  $\sigma_t$  can both rise by 5–30 % and drop considerably.

EMI have an influence at cyclic loading of the materials. Electromagnetic treatment (including by direct EC,  $j \sim 0.1$  A/mm<sup>2</sup>, combined with fatigue testing) increased the fatigue life of Armco-iron, steel and titanium alloys 2–3 times [21–23].

Change of mechanical properties of the materials at EMI combination with the testing process is highly diverse, but not always favourable in terms of practical needs and depends on many factors (nature and initial condition of the material, kind and parameters of electromagnetic impact, environment, temperature, deformation rate, etc.). It was studied mainly for corrosion-resistant steels, alloys of titanium, aluminium and copper [1], but there are also data on high-purity and commercial-purity iron [11].

In the works by M.L. Bernshtejn, V.N. Pustovojt [4] and other authors the high effectiveness of combining the operations of heat treatment and EMI is demonstrated, which is manifested in development of practically useful stable changes in the structure, phase composition and mechanical properties of steels of different classes under the impact of weak and strong MF.

MF impact allows a more complete realization of the mechanisms of strengthening of carbon and alloyed structural steels at marquenching. For 45Kh and 30KhGSA steel quenched with superposition of MF ( $H \sim 10^6$  A/m)  $\sigma_t$  turned out to be 1.5 times higher than after quenching without MF. Studying the fracture characteristics and tensile diagrams showed that at quenching in MF presence of plastic deformation preceding fracture, was what allowed determination of the proof stress, which would have been impossible at quenching without MF.

MF superposition on the process of bainite transformation of low-alloyed steels can lead both to softening of steels (1–3 % for 30KhGSA and 45Kh steel), and to their strengthening (3–8 % for 65G and 14Kh2GMR), but increase of impact toughness *KCU* by 11–87 % was found in all the cases. MF superposition on pearlite transformation of hypereutectoid carbon steels leads to strengthening with a certain lowering of ductility and impact toughness. Hypoeutectoid steels subjected to pearlite transformation in MF are significantly softened and have a noticeably increased residual relative elongation at somewhat smaller relative residual reduction compared to steels, which experienced transformations without MF [4].

Impact of constant MF ( $H = 66$  kA/m) during tempering of 40Kh steel at the temperature of 550 °C allowed avoiding temper embrittlement caused by diffusion of sulphur and phosphorus to grain boundaries. In this case, steel after the above treatment has the impact toughness 3 times higher than after tempering without MF at the same hardness [24].

**Concepts of the mechanisms of electromagnetic impacts.** A considerable data file has been accumulated, which is indicative of the fact that a particular change of the mechanical properties of materials which is also easy to determine, is associated with application of different kinds of EMI with readily measured or calculated parameters. However, the intermediate links of this cause-effect chain still are out-of-sight of the researchers, in view of the complexity of direct observation of the processes on the material microlevel. On the other hand, physical science knows a variety of manifestations of interaction of the magnetic field and the substance.

Such a situation has not so far allowed providing an explanation for the experimentally observed effects from the viewpoint of one of versatile theory. Instead of that individual researchers and physical schools discuss as EMI mechanisms the concepts and hypothesis of the connection between phenomena on little studied structural levels of the solid and a visible change of its mechanical characteristics [1–6, 25].

When interpreting the influence of a powerful pulsed EC on mechanical behaviour of highly-pure single-crystals and commercial alloys, the key role is quite often given to the phenomenon of electron-dislocation interaction (EDI) [1, 3, 26]. The works by V.Ya. Kravchenko, who analytically predicted this phenomenon, as well as by a number of other researchers [27–29], are devoted to quantum-mechanical description of EMI. EMI are characterized using the analogy between the dynamic impact of simple wind on stationary objects and impact of conductivity electrons forming the EC «electron wind», on dislocations, assuming that the electron gas, similar to any other gas features a certain viscosity [26]. In view of the above impact of electron gas, acceleration of sliding dislocations and facilitating of tearing the pinned dislocations from the stoppers are found, which is exactly the cause



for intensification of plastic deformation and lowering of metal resistance to deformation.

Stress  $\sigma(j)$  characterizing the mechanical equivalent of electron wind impact on sliding and stationary dislocations has been calculated, which depends on current density and quantum-mechanical characteristics of the metal lattice. The order of current density ( $1 \cdot 10^3$ – $1 \cdot 10^5$  A/mm<sup>2</sup>), at which dislocation multiplication will occur as a result of functioning of Frank–Reed sources without any external mechanical load, has also been calculated.

The discussed interaction is reversible: directed flow of any structural defects leads to disturbance of the electronic subsystem of the crystal, and appearance of the electric field or current [27, 28, 30], which is exactly confirmed during observation of pressure welding [31].

Results of numerous experimental and theoretical studies by Yu.I. Golovin, V.M. Frenkel, A.A. Sletkov and other scientists showed that the tips of macro- and microcracks, non-metallic inclusions and other inhomogeneities of the metal structure are concentrators of the electromagnetic and temperature fields at passage of high-density EC pulse through the metal.

Depending on EC parameters and kind of inhomogeneity, the temperature, to which small local volumes of metal adjacent to these defects are heated, can reach the values of the temperature of its recrystallization and even melting. The temperature beyond these volumes does not exceed its values, noticeably influencing the initial structure. These phenomena influence the growth of the propagating crack, accelerating and inhibiting it [32].

In study [19] the statement substantiated by the results of experiments and tests by Yu.I. Golovin with associates was accepted, namely that if specific energy, which is equal to approximately  $1 \cdot 10^8$ – $1 \cdot 10^{10}$  J/m<sup>3</sup>, is applied to the metal, during time  $\tau$  smaller than the time  $\tau^*$  of the temperature field reaching the steady-state mode ( $\tau^* \sim \rho c \lambda^{-1} l^2$ , where  $\rho$  is the density;  $c$  is the specific heat capacity;  $\lambda$  is the material heat conductivity;  $l$  is the characteristic structural dimension of the material taken to be approximately  $1 \cdot 10^{-4}$  m), the applied energy will be dissipated predominantly in the metal microvolumes with the electric conductivity below the matrix value (structural inhomogeneities, micro- and submicrodefects) causing a considerable heating there. For metals,  $\tau^*$  calculation gives the order of  $1 \cdot 10^{-4}$  s. At  $t < \tau^*$  the concept of overall heating of the metal macrovolume loses its meaning, as the temperature field during time  $\tau$  does not manage to equalize between the zones of predominant heat evolution and the rest of the metal volume, i.e. it is of a locally-inhomogeneous (mosaic) nature. Increase of residual plastic properties of the metals treated by powerful electric pulses, is attributed by the authors of the above work to the action of electromagnetic and thermoelastic forces in the local volumes causing microplastic deformation, promoting the processes of recrystallization and «healing» of struc-

tural microdefects. Now lowering of the metal resistance to deformation at the moment of the pulse, according to this scientific school, is due to reaching the «state of dynamic (high-speed) superplasticity» [19].

Specific processes in ferromagnets under the impact of external MF influence the structure, phase composition and microplastic deformation of the respective steels. They promote refinement of the products of  $\gamma \rightarrow \alpha$  transformation, as well as its earlier and more complete running. As follows from [4], the following factors have the main influence: change of the magnetic state of austenite above the Curie point leading to spontaneous appearance of small single-domain ferromagnetic regions, arising and annihilating in the paramagnetic  $\gamma$ -matrix by the statistical laws; lowering of thermodynamic potential of ferromagnetic phases of steels; appearance of magnetostriction local stresses; anisotropy of displacements of the crystalline lattice atoms, disturbing the structural equivalence of octahedral voids and changing the running of diffusion processes.

In particular, shifting of domain boundaries in ferromagnetic crystals at magnetizing promotes dislocation unpinning from the stoppers and causes sliding of unpinned dislocations to distances of approximately  $1 \cdot 10^{-6}$  m [33, 34].

Also considered is such a factor as intensification of plastic deformation using EC and MF as ponderomotive action — electrodynamic action of electric and magnetic fields generating bulk force  $\mathbf{F}$ , compressing the material of the conductor in the radial direction (pinch-effect). In studies [1, 9, 25] it is stated that under the conditions of pulsed MF at a pronounced skin-effect the pinch-effect can make a dominating contribution to plastic deformation of the metals. The degree of its manifestation depends on MF intensity, depth of its penetration into the material and nature of the conductor material. In different studies the contribution of the pinch-effect at EC flowing through a conductor is evaluated by formulas, which are reduced to a known expression:

$$\mathbf{F} = \mathbf{j}\mathbf{B}, \quad (1)$$

where  $\mathbf{j}$  is the vector of current density;  $\mathbf{B}$  is the vector of magnetic inductance created by this current.

Experiments have been conducted [7, 35] on clarifying the role of pinch-effect, in which the latter was induced in isolation from EMI. From experimental results and calculations by (1) it follows that the stresses, caused by pinch-effect, are negligibly small even at a considerable current density. It should be noted, however, that the used procedures [7, 35] are not flawless in terms of correspondence of the nature of MF specially induced in specimen material at EC passage through it. The conclusion about the smallness of the value of bulk force calculated by (1) can be applicable to dia- and paramagnets. However, in the case of ferromagnets, induction  $\mathbf{B}$  inside the material can be presented as  $\mathbf{B} = \mathbf{B}_0 + \mathbf{B}_j$  (here and furtheron  $\mathbf{B}_0$  is the vector of the external MF induction;  $\mathbf{B}_j$  is



the vector of induction due to magnetization of the body proper). At magnetization of the ferromagnet,  $\mathbf{B}_j$  can vary in a broad range, and under certain conditions it can reach values of Weiss stress field [36]. This field is due to the exchange interaction of electrons of unfilled  $d$ - and  $f$ -sublevels of atoms of transient ferro- and antiferromagnetic metals, and occurs inside their domains. Weiss field intensity is equal to  $1 \cdot 10^8$ – $1 \cdot 10^9$  A/m [37], which corresponds to current density of  $1 \cdot 10^4$ – $1 \cdot 10^5$  A/mm<sup>2</sup>, respectively. In addition, variation of magnetic permeability  $\mu$  and density  $\gamma$  of ferromagnets placed into the external MF also influence  $\mathbf{F}$ .

On this basis, the bulk radial force of the pinch-effect for a conductor from a ferromagnetic material should be given by the following expression [38]:

$$\mathbf{F} = j\mathbf{B} - 1/2H^2 \text{ grad } \mu + 1/2 \text{ grad } (H^2 \gamma \partial \mu / \partial \gamma), \quad (2)$$

where the first addend is the force compressing the conductor with current in the MF; the second is the force due to spatial variation of magnetic permeability; the third is the force caused by dependence of magnetic permeability on ferromagnet density.  $\mathbf{F}$  components can vary in broad ranges. So, initial magnetic permeability  $\mu_{in}$  of magnetically soft and magnetically hard materials is equal to 40–35000 units. At a certain value of the external MF,  $\mu_{in}$  drops to a unity, therefore, it can vary  $1 \cdot 10$ – $1 \cdot 10^4$  times.

It can be calculated that the order of EC density, sufficient for plastic deformation of a non-ferromagnetic sample as a result of pinch-effect, is equal to  $1 \cdot 10^5$  A/mm<sup>2</sup> [38, 39]. Here planning and conducting the experiments runs into difficulties both at selection of powerful current sources, and the methods of intensive heat removal, eliminating the thermal impact of current. It is obvious that in the case of a ferromagnetic material the difficulties can be eliminated by using Weiss field, creating bulk forces sufficient for plastic deformation of the sample. It is known [40] that excitation of Weiss field when certain conditions are followed, is possible at passage of current of just 8–12 A/mm<sup>2</sup> density through the ferromagnet.

Influence of weak EMI (magnetic induction  $B \cong 1$  T;  $j \cong 10^{-1}$  A/mm<sup>2</sup>) on the creep rate, and dislocation mobility cannot be explained by their force or energy action by the above mechanisms, as the energy imparted by such EMI to any structural elements is usually lower than the threshold of activation of any changes. In this case plastic flow in the material is presented as a totality of chemical reactions between the interstitial atoms, atoms from the composition of impurity atmospheres — dislocation stoppers — and atoms in the composition of dislocation nuclei.

Then in terms of the theory of spin-dependent manifestations, the mechanism of the influence of weak MF on singlet-triplet transitions (spin conversion) in the atoms making up the complex of the interacting dislocations and stopper, is proposed in chemical physics. The height of the potential barrier to dislocation motion, created by the impurity, is de-

termined by the spin characteristics, radii and charges of ions, their number in the complex. MF changes the state of the electrons providing the covalent bond in the dislocation–stopper complex, removing and imposing spin exclusions for particular reactions possible in thermodynamic terms. In a number of cases it enables reduction of the fraction of the covalent bond in the total energy of interaction of the stopper and dislocation, thus lowering the height of the potential barrier, facilitating dislocation stripping from the stoppers, and decreasing the concentration of impurity centers capable of becoming effective stoppers. In [25] it is assumed that, in addition to the covalent component of the energy of interaction of the stopper and dislocations, MF can lower also the fraction of their electrostatic interaction. The above factors underlie the observed increase of dislocation mobility. Weak MF are ineffective for the ductility of chemically pure, mechanically unloaded materials, as well as at a high frequency of MF variation (approximately  $1 \cdot 10^2$  Hz) [6].

In addition to the main physical processes considered above, also the role of phenomena on the internal and external interfaces [3, 14, 25], macroinhomogeneous temperature fields [1, 25], role of the dynamic non-equilibrium of dislocation clusters [25], Joulean heat are studied and discussed.

**Practical use of electromagnetic impacts.** Results of investigation of EMI on running of plastic deformation in the metals allowed suggesting new methods of pressure treatment of metals (for instance, electroplastic drawing of wires and tubes [2, 41], electrically stimulated rolling of thin strips from vanadium and molybdenum, as well as alloys [26, 42], and methods of achieving high performance of structures.

Data of works by M.A. Krivoglaz, V.D. Sadovsky, M.L. Bernshtejn, V.N. Pustovojt create the prerequisites for highly promising application of heat treatment combined with MF superposition. For instance, quenching and tempering of high-speed steel in MF ensures its phase composition and mechanical properties on the same level, as does the traditional heat treatment, i.e. quenching and triple tempering. On the other hand, drill exposure to MF after traditional treatment is low-efficient (their wear resistance rises noticeably only at low cutting rates) [4] or is completely inefficient [43].

Some of the metal treatment techniques are based on the ability to achieve superfast heating and cooling of a thin surface layer of metal by applying pulsed EMI [44].

In the field of welding fabrication electromagnetic impacts on the welding zone are widely used for controlling mass transfer, solidification and weld shape.

However, individual attempts are known of applying electromagnetic energy for treatment of welded joint metal. In particular, conducting the process of electrosag welding with concurrent electric discharge treatment allowed eliminating normalizing of joints on pearlitic class steel, and improving the corrosion resistance of joints of 10Kh18N10T steel produced by



the process of electrosag welding with electric discharge treatment [45]. It is reported [5] that treatment by current pulses is favourable for strength and ductility properties of dissimilar materials of the type of bimetals produced by explosion welding.

Thus, it is established that application of electromagnetic energy to the metal causes a wide range of sophisticated processes in it, occurring at the macro-, micro- and submicroscopic level. This may have an influence on metal behaviour, as well as its residual mechanical properties. Further studies are rational to evaluate the influence of electromagnetic disturbances on welded joint metal.

1. Strizhalo, V.A., Novogradsky, L.S., Vorobiov, E.V. (1990) *Strength of alloys for cryogenic engineering under electromagnetic actions*. Kiev: Naukova Dumka.
2. Spitsin, V.I., Troitsky, O.A. (1985) *Electroplastic deformation of metals*. Moscow: Nauka.
3. Savenko, V.S. (2000) *Mechanical twinning of metals under the conditions of external energy actions*. Minsk: Tekhnoprint.
4. Bernshhtejn, M.L., Pustovojt, V.N. (1987) *Heat treatment of steel products in magnetic field*. Moscow: Mashinostroenie.
5. Tananov, A.I., Beklemishev, N.N., Zhurkin, B.N. et al. (1983) Methods of evaluation of mechanical properties of metallic materials under electric impacts. *Zavod. Laboratoriya*, 7, 59–66.
6. Golovin, Yu.I. (2004) Magnetoplasticity of solids. *Fizika Tv. Tela*, 46(5), 769–803.
7. Spitsin, V.I., Troitsky, O.A. (1974) Effect of electric current and pulse magnetic field on rate of metal creep. *Doklady AN SSSR*, 216(6), 1266–1269.
8. Strizhalo, V.A., Vorobiov, E.V. (2003) Stepwise deformation of metal under the conditions of pulse magnetic field and cryogenic temperatures. *Problemy Prochnosti*, 1, 137–142.
9. Golovin, Yu.I., Tyalin, Yu.N., Umrikhin, V.M. (1987) Field of mechanical stresses and strength of cylindrical conductors in pinching electromagnetic fields. In: *Abstr. of 1st All-Union Conf. on Action of Electromagnetic Fields on Plasticity and Strength of Metals and Alloys* (Yurmala, Sept. 29–Oct. 1, 1987). Moscow: A.A. Blagonravov IMV, 37.
10. Shcherbakov, I.P., Churaev, D.V., Svetlov, V.N. (2004) Study of submicrorelief variation of copper sample surface at application of high density current pulses to them. *Zhurnal Tekhn. Fiziki*, 74(4), 139–142.
11. Kamenetskaya, D.S., Piletskaya, I.B., Shiryaev, V.I. (1971) About influence of magnetic field on plastic deformation of iron. *Doklady AN SSSR*, 199(6), 1289–1291.
12. Kishkin, S.T., Klypin, A.A. (1973) Effects of electric and magnetic actions on creep of metals and alloys. *Ibid.*, 211(2), 325–327.
13. Klypin, A.A. (1973) About influence of magnetic and electric fields on creep. *Metallovedenie i Term. Obrab. Metallov*, 8, 2–6.
14. Klypin, A.A. (1975) About plastic deformation of metals in the presence of electric action. *Problemy Prochnosti*, 7, 20–25.
15. Datsko, O.I., Abramov, V.S. (2003) Influence of weak magnetic field pulses on processes of microplastic strain and strain ageing. *Fizika i Tekhn. Vys. Davlenij*, 13(1), 84–90.
16. Badylevich, M.V., Iunin, Yu.L., Kveder, V.V. (2003) Influence of magnetic field on start stresses and individual dislocation mobility in silicon. *Zhurnal Eksp. i Teoret. Fiziki*, 124(3), 664–669.
17. Datsko, O.I. (2002) Dislocation internal friction of material with vacancies in pulses of weak magnetic field. *Fizika Tv. Tela*, 44(2), 289–293.
18. Sokirko, V.A., Berezhinskaya, E.Yu., Divak, P.P. et al. (1989) Study of residual stresses in welded joint metal. In: *Abstr. of All-Union Sci.-Techn. Conf. on Electron Beam Welding in Machine-Building* (Nikolaev, Sept. 12–14, 1989). Nikolaev: VNIITSM Sirius, 104.
19. Beklemishev, N.N., Gorbunov, N.M., Koryagin, N.I. et al. (1989) *Plasticity and strength of metallic materials under pulse action of high energy electromagnetic field*. Preprint. Moscow: IPM.
20. Valeev, I.Sh., Barykin, N.P., Trifonov, V.G. (2003) Variation of structure and mechanical properties of aluminium alloy AMg6 under action of powerful current pulses. *Fizika Metallov i Metallovedenie*, 96(4), 85–89.
21. Karpenko, G.V., Kuzin, O.A., Tkachev, V.I. et al. (1976) Influence of electric current on low-cycle fatigue of steel. *Doklady AN SSSR*, 227(1), 85–86.
22. Sosnin, O.V., Ivanov, Yu.F., Gromov, V.E. et al. (2003) Evolution of ferrite-pearlite structure under pulse action of electric current. *Fizika i Khimiya Obrab. Materialov*, 4, 63–69.
23. Loskutov, S.V., Levitin, V.V. (2002) Influence of electric pulse treatment on structure and service life of titanium alloys. *Zhurnal Tekhn. Fiziki*, 72(4), 133–135.
24. Pudov, V.I., Sobolev, A.S. (2004) Optimisation of physico-mechanical properties of polycrystalline multicomponent ferromagnetic materials with the help of thermomagnetic treatment method. Part 2: Thermomagnetic treatment of alloyed steels. *Fizika i Khimiya Obrab. Materialov*, 5, 94–97.
25. Bataronov, I.L. (1999) Mechanisms of electroplasticity. *Sorosovskiy Obrazov. Zhurnal*, 10, 93–99.
26. Klimov, K.M., Shnyrev, G.D., Novikov, I.I. (1974) About «electroplasticity» of metals. *Doklady AN SSSR*, 219(2) 323–324.
27. Fiks, V.B. (1981) Entrainment and retardation of movable defects in metals by conductivity electrons. Role of electron dispersion law. *Zhurnal Eksp. i Teoret. Fiziki*, 80(4), 1539–1542.
28. Fiks, V.B. (1981) On interaction of conductivity electrons with isolated dislocations in metals. *Ibid.*, 80(6), 2313–2316.
29. Natsik, V.D., Makovoz, D.B. (1987) Interaction of plasma oscillations of metal conductivity electrons with dislocations. *Fizika Metallov i Metallovedenie*, 63(4), 645–653.
30. Kravchenko, V.Ya. (1967) About possibility of observation of dislocation motion in conductive crystals by electric effects. *Fizika Tv. Tela*, 9(4), 1050–1056.
31. Kharchenko, G.K., Falchenko, Yu.V., Ignatenko, A.I. (1997) About mechanoelectric effect in pressure welding. *Avtomatich. Svarka*, 1, 50.
32. Sletkov, A.A. (1977) *Crack arrest by electric current pulses*: Syn. of Thesis for Cand. of Techn. Sci. Degree. Voronezh.
33. Chebotkevich, L.A., Urusovskaya, A.A., Veter, V.V. (1965) Dislocation motion under magnetic field action. *Kristallografiya*, 10(5), 688–691.
34. Chebotkevich, L.A., Urusovskaya, A.A., Veter, V.V. et al. (1967) Interaction of Bloch walls with dislocations in weak fields. *Fizika Tv. Tela*, 9(4), 1093–1097.
35. Spitsin, V.I., Troitsky, O.A. (1977) Electroplastic effect in metals. *Vestnik AN SSSR*, 11, 10–15.
36. Parshenkov, N.A. (1991) Evaluation of effect of magnetizing inductive constituent of ferromagnetic structures on welding processes. *Avtomatich. Svarka*, 5, 23–28.
37. Gudenaf, J. (1963) *Magnetics and chemical bond*. Moscow: Metallurgiya.
38. Shimoni, K. (1964) *Theoretical electrical engineering*. Moscow: Mir.
39. Kittel, Ch. (1965) *Elementary physics of solid*. Moscow: Nauka.
40. Latyshev, A.P. (1960) *Theory of demagnetizing*. Leningrad: VMOLA.
41. Troitsky, O.A. (1974) Electroplastic deformation of steel by tension and drawing. *Stal*, 5, 450–453.
42. Klimov, K.M., Novikov, I.I. (2004) On prospects of development of electrostimulated rolling methods of metals. *Metallogy*, 3, 45–51.
43. Bobina, M.M., Majboroda, V.S., Ulianenko, N.V. et al. (2002) Structure and properties of surface layer of R6M5 steel tool after magneto-abrasive treatment. *Fizika i Khimiya Tv. Tila*, 3(4), 577–580.
44. Dudkina, N.G., Zakharov, I.N. (2004) Examination of surface layer microhardness of carbon steels after electromechanical treatment. *Metallogy*, 4, 64–70.
45. Dudko, D.A., Kuzmenko, A.B. (1997) Vibropulsed action on solidifying metal of the weld pool in ESW. *Avtomatich. Svarka*, 11, 32–36.



## PRESSURE WELDING OF AMg5/23 % SiC COMPOSITE

G.K. KHARCHENKO, A.Ya. ISHCHEENKO, Yu.V. FALCHENKO, A.N. MURAVEJNIK and G.N. GORDAN  
E.O. Paton Electric Welding Institute, NASU, Kiev, Ukraine

Technology was developed for vacuum welding of dispersion-strengthened composite material AMg5/23 % SiC. It was established that in welding in the forming matrix with a cyclic application of pressure the interlayer of commercial-purity aluminium is saturated with magnesium and manganese, it is hardened, and shear strength of the welded joint grows.

**Keywords:** pressure welding, welded joints, composite, aluminium-magnesium alloy, strengthening phase, joint strength, forming devices, sublimation

In studies [1–4] it was established that in solid-phase pressure welding of composite materials (CM) having an aluminium-based matrix, formation of a sound welded joint depends on magnesium content in the composite and in the interlayer. In [1] an assumption is made that in diffusion welding magnesium diffuses from the composite (Al–Mg–Cu) to the abutted surfaces, and interacts with aluminium oxide, this leading to fracture of aluminium oxide film (Figure 1). According to [1], magnesium present in the composite reacts with aluminium oxide by the following reaction:



Such a mechanism of magnesium interaction with aluminium in diffusion welding was suggested in [5] long before study [1]. It consists in that during heating (without pressure application) magnesium sublimes and precipitates on the aluminium surface. The sublimation process is determined by the depth of vacuum, heating time and temperature. Then interaction of aluminium oxide with magnesium occurs, and

MgAl<sub>2</sub>O<sub>4</sub> spinel forms, through which the aluminium atoms diffuse faster than the magnesium atoms (diameter of the aluminium atom is smaller than that of magnesium atom).

Strength of the joints of composites of Al–C group with interlayers of Al–Mg alloys was evaluated by shear testing [2, 4]. It is established that with increase of magnesium content in the interlayer from 0.95 to 6 % the shear strength of the welded joint rises. The authors of [2, 4] attribute the increase of strength to that magnesium, probably, binds the graphite particles into stable compounds in the form of carbides, which do not block the process of mass transfer in the contact zone.

The authors of the paper envision another mechanism of the influence of magnesium content in the interlayer metal on its shear strength values. It is known that the joint sections in the form of an intermediate interlayer, the metal of which has the yield point smaller than the metal of the adjacent sections, were named soft interlayers. The role of the latter in the composite welded joints is played by interlayers from commercial aluminium and its alloys with magnesium. In the works of O.A. Bakshi [6] it is shown that unlike tension, at shear the plastic deformation in the soft interlayers is not contained by stronger parts of the joints, so that no contact strengthening is observed in them. Thus, increase of the strength indices of welded joints of composites with interlayers of alloys of aluminium with magnesium in shear testing is due to lowering of the yield point of the interlayer material, in which magnesium content increases.

Analysis of the known publications on studying the solid-phase weldability of dispersion-strengthened aluminium-base CM containing particles of silicon [1] or carbon [2–4], leads to the conclusion on the influence of magnesium on weldability, i.e. in order to improve the welded joint quality, it is necessary to accelerate the processes of its mass transfer.

In study [7] it is shown that cyclic impact of pressure in solid-phase welding leads to a continuous restoration of the high rate of plastic deformation of the metals being joined, initiates development of physical contact, improves the quality of active centers and reduces the activation energy of formation of the chemical (metal) bonds, which in totality increases the rate of chemical interaction (increase of strength).

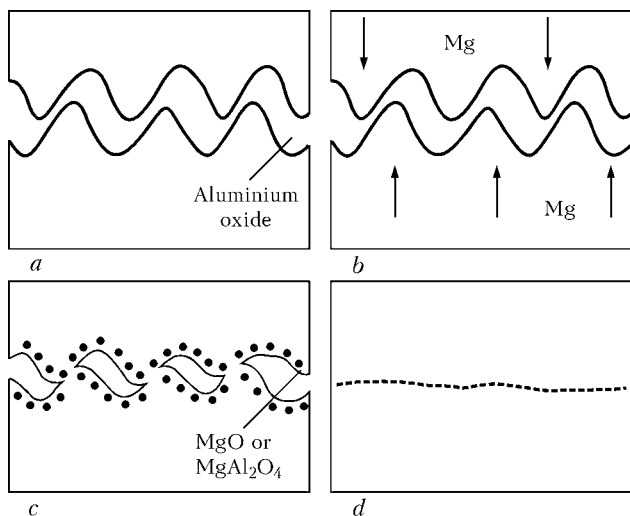


**Figure 1.** Schematics of the stage of welded joint formation [1]: a — physical contact; b — magnesium diffusion to the surfaces being joined; c — magnesium interaction with aluminium oxide; d — metal bond



Composition of the aluminium alloy (composite matrix) and interlayer, %

Alloy	Cu	Mg	Mn	Si	Fe	Ti	Zn	Al
AMg5	0.10	4.8–5.8	0.3–0.8	0.5	0.5	0.02–0.10	0.2	Rest
AD1	0.05	0.05	0.025	0.3	0.3	0.15	0.1	99.3

In [8] it is established that cyclic impact of pressure leads to increase of atom mobility in the metal by several orders of magnitude. Under such conditions, the loading temperature is not the dominating factor. It is shown that under the conditions of cyclic impact, mass transfer occurs by the interstitial mechanism of atom migration, while atom mobility decreases with increase of their dimensions.

It should be noted that the publications do not have any data on variation of the composition of the interlayer during deformation, or the ability to homogenize the composition of the initial interlayer from pure aluminium with that of the composite matrix during pressure welding. This was exactly the purpose of the research described below.

Investigations were conducted on CM based on AMg5 aluminium alloy with 23 % SiC strengthening phase, which was made by the casting technique --- mixing SiC ceramic particles into the matrix material melt with subsequent compacting. In the initial condition the composite structure is presented by  $\alpha$ -solid solution of aluminium, light-coloured inclusions of  $Al_3Mg_2$ ,  $Al_6(FeMn)$ ,  $MgSi$ , etc., inherent to the matrix aluminium alloy, and silicon carbide particles. Strengthening SiC particles of 6–20  $\mu m$  size are quite uniformly distributed in the matrix volume, they have an angular shape and 3–25  $\mu m$  interparticle distance. CM hardness in the initial condition is *HRB* 94–95, and the matrix alloy composition is given in the Table.

Comparative analysis of the composite weldability was conducted by vacuum diffusion welding (VDW) at cyclic application of pressure under the conditions of free deformation or with forced deformation of the contact zone when using the forming devices. CM

samples of 15 × 15 × 6 mm size were welded without the interlayer and with application of intermediate interlayer from commercial purity aluminium AD1 (see the Table) 0.15 mm thick (this thickness of the interlayer is determined as the optimum one in the authors' earlier research on CM weldability [3]).

VDW was conducted at the temperature  $T = 560\text{ }^\circ C$ , welding time  $t = 15\text{--}20\text{ min}$ , upset pressure  $P = 0.9\text{--}1.2\text{ MPa}$ , vacuum in the working chamber of  $1.33 \cdot 10^{-3}\text{ Pa}$ . Five loading cycles were applied at the average duration of one cycle of 3 min. Degree of plastic deformation of the samples was set on the level of  $\epsilon = 40\%$ . Total time of the welding process (heating up to welding temperature for up to 60 min, soaking under pressure for 15–20 min, item cooling) was equal to about 2.5–3 h.

Sample preparation for welding consisted in removing the work-hardened surface layer of about 0.2–0.3 mm thickness with a file, and its scraping. Samples for mechanical testing and sections for microstructural studies were cut out of the base material and welded joints, microstructural studies being performed in unetched condition, after chemical etching and electrolytical polishing in chloric acid electrolyte. Chemical etching of the samples was conducted in the solution of Keller reagent or 5 % solution of hydrofluoric acid. Microstructural studies were performed in MIM-8 and Neophot-8 microscopes and scanning electron microscope GSM-840. Sample microhardness was measured in PMT-3 microhardness meter at 0.2 N load. Elemental composition was determined in X-ray microanalyzer Camebax. Shear testing of samples of the initial CM and welded joints was performed.

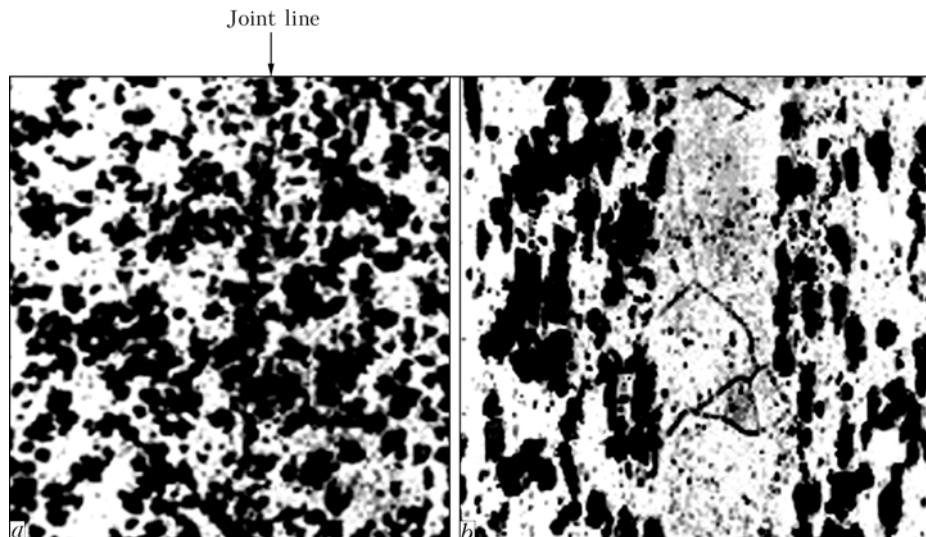
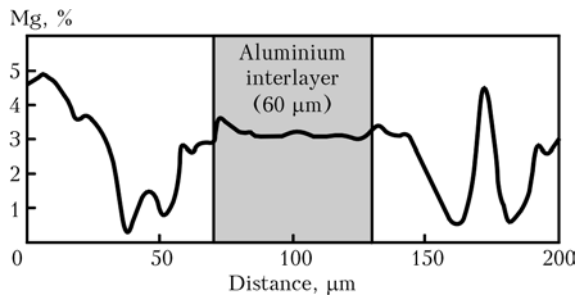


Figure 2. Microstructure of welded joints produced by VDW without (a) and with (b) the interlayer ( $\times 400$ )



**Figure 3.** Nature of magnesium distribution in the transition zone of CM welded joints at VDW in the forming devices

Magnesium content on CM surfaces to be welded and in the interlayer after their heating before welding (560 °C for 30 min at minimum pressure, sufficient only for adhesion on individual microprotrusions) was evaluated by the scanning microscopy method. After heating the produced joints were broken along the contact line. An increased magnesium concentration (up to 1.6 %) was found on the surface of the aluminium interlayer.

Thus, the obtained data are indicative of the fact that at the stage of preheating magnesium diffusion to the surfaces being welded, breaking up of the oxide film on the composite, magnesium sublimation and its deposition on the aluminium interlayer occur in the butt before application of welding pressure, i.e. conditions are in place for magnesium reduction of the oxide film on the composite and interlayer of commercial purity aluminium AD1.

Metallographic studies of welded joints showed that at direct welding of CM to CM the reinforcing particles, matrix intermetallics, oxides concentrate along the joint line. It is particularly clearly revealed in the areas of accumulation of the reinforcing particles (Figure 2, a), where pores and discontinuities are found. Shear strength of the joints is equal to  $\sigma_{sh} = 9$  MPa, which is attributable to a high rigidity of the composite and low ductility of near-contact layers of the material, so that an aluminium interlayer was used later on.

In CM welded joints produced by VDW under the conditions of free deformation no accumulation of reinforcing particles is found between the interlayer and matrix aluminium (Figure 2, b). Thickness of the aluminium interlayer during welding decreases from 150 to 100–120  $\mu\text{m}$ . Microhardness of the aluminium interlayer is equal to 650 MPa. Optical microscopy revealed that the nature of distribution of the reinforcing particles in the welding zone does not change. Shear strength of the joints is equal to 20–30 MPa. Welded joint fracture ran along the weld.

Weldability of CM with AD1 interlayer was studied at cyclic application of pressure and using a forming device for localizing plastic deformation directly on the interlayer and ensuring a directed flow of near-contact metal layers in the butt. No defects were revealed in the contact zone of the welded joint. Degree of interlayer deformation is equal to 46–60 %. Thickness of the aluminium layer varies between 80  $\mu\text{m}$  in the sample central part and 60  $\mu\text{m}$  along its edges,

i.e. along the edges of the welded joint the interlayer is thinner than in its central part. The found features are related to the fact that shear deformations are more intensive on the butt periphery. Microhardness of the aluminium interlayer in the joint zone is equal to 750 MPa, joint strength  $\sigma_{sh} = 124$ –132 MPa, fracture runs across the base metal. One of the main features of welded joints produced in the forming matrix, is the presence of flash, into which not only the soft interlayer, but also the adjacent CM layers are entrained, this promoting more intensive fracture of the oxide film on the surfaces being welded.

X-ray microprobe analysis revealed that saturation of AD1 interlayer by manganese up to approximately 0.1 % and magnesium up to 3 % occurs in welding in the forming devices. Comparison of the initial composition (see the Table) of the interlayer from commercial purity aluminium AD1 and its composition after welding in the forming devices (Figure 3) leads to the conclusion that after welding magnesium content in the interlayer rose up to 60, and that of manganese --- up to 4 times. Thus, in the butt the initial interlayer from AD1 is transformed during welding into Al–Mg alloy, which has higher strength values and lower ductility values compared to AD1. Such a change of the mechanical properties of the interlayer leads to an increase of the ductility properties in shear testing of welded joints. While in welding in the unrestrained condition the shear strength was 20–30 MPa, then in welding using the forming devices the joint strength corresponds to that of the composite --- 120–130 MPa, i.e. it rises 6 times.

In conclusion it should be noted that the developed technology of VDW for AMg5/23 % SiC composite allows increasing the shear strength of welded joints to the level of the composite strength due to the use of forming devices and cyclic application of welding pressure, as well as strengthening of the interlayer form commercial-purity aluminium AD1, as a result of diffusion of magnesium and manganese from the composite matrix.

1. Bushby, R.S., Scott, V.D. (1995) Joining of particulate silicon carbide reinforced 2124 aluminium alloy by diffusion bonding. *Mat. Sci. and Tech.*, 11(8), 753–758.
2. Ryabov, V.R., Kharchenko, G.K., Gurienko, V.P. et al. (1996) Welding of dispersion-strengthened material Al + 4 % C. *Avtomatich. Svarka*, 1, 59–61.
3. Ryabov, V.R., Muravejnik, A.N., Kharchenko, G.K. et al. (2003) Specifics of formation of structure of joints, made from dispersion-strengthened composite Al + 4 % C, in diffusion bonding. *The Paton Welding J.*, 12, 6–9.
4. Bolotov, G.P., Ganeev, T.R. (2004) Diffusion welding of dispersion-strengthened composite materials of Al–C group. *Visnyk Chernig. DTU. Series Eng. Sci.*, 21, 107–110.
5. Korsunskaya, I.G., Lyulichev, A.N., Maksimenko, G.I. (1970) Vacuum diffusion welding of magnesium with aluminium. *Svarochn. Proizvodstvo*, 7, 19–21.
6. Bakshi, O.A. (1981) *Mechanical heterogeneity of welded joints*. Part 1. Chelyabinsk: ChPI.
7. Abramov, V.V., Karakozov, E.S., Petrov, V.A. (1970) Kinetics of joint formation in solid-state welding by static and cyclic loading with preheating. *Fizika i Khimiya Obrab. Materialov*, 4, 107–113.
8. Mironov, V.M., Mazanko, V.F., Gertzriken, D.S. et al. (2001) *Mass transfer and phase formation in metals under pulse actions*. Samara: SGU.



# EFFECT OF LONGITUDINAL MAGNETIC FIELD ON THE EFFICIENCY OF WIRE MELTING IN SUBMERGED-ARC SURFACING

A.D. RAZMYSHLYAEV, A.A. DELI and M.V. MIRONOVA  
Priazovsky State Technical University, Mariupol, Ukraine

Causes of increase in the efficiency of the process of electrode melting in submerged-arc surfacing at a reverse-polarity current in the longitudinal magnetic field (LMF) were examined. It is shown that the effect of increase in the coefficient of melting of electrode wire depends upon its magnetic properties, and shows up not only in the case of permanent LMF, but also in the case of the alternating one with a frequency of 50 Hz.

*Keywords:* arc surfacing, longitudinal magnetic field, electrode metal droplet, electrode melting coefficient, magnetic properties, ferromagnetics

As shown in studies [1, 2], in submerged-arc welding under the effect of the permanent longitudinal magnetic field (LMF) the coefficient of melting of electrode wire,  $\alpha_m$ , at a reverse polarity of the process increases by 50 % and at straight polarity — by 30 %, whereas in welding at an alternating current it increases by 40 %. It is also established [2] that the alternating LMF with a frequency of 50 Hz does not affect the value of  $\alpha_m$  of the wire because of a high inertia of the molten droplet at the electrode tip. The above peculiarities were observed with ferromagnetic electrode wires Sv-08A 3–5 mm in diameter.

Studies [2, 3] attribute increase in  $\alpha_m$  of the wire during welding in the permanent LMF to the fact that a droplet in this case is rotated under the effect of electromagnetic forces, which causes decrease in its thickness in a direction along the electrode axis and reduces the time of its existence, thus improving conditions for heat transfer through the droplet.

The assumption of rotation (or the possibility of rotation) of a droplet under the effect of LMF is confirmed by the calculations of electromagnetic forces made in study [4], as well as by the data of kinetic diagrams of behaviour of the droplet in argon using non-magnetic wire EI-395 [5].

In studies [1–4], rotation of a droplet under the effect of LMF is attributed to the impact by volumetric electromagnetic forces, the vector of which in each elementary volume of a droplet has a tangential, i.e. azimuthal, direction. Presumably, the electromagnetic forces in the droplet are induced by interaction of an axial component of induction of LMF with a radial component of the current density in the droplet. As assumed in study [3], the radial component of the current density in the droplet constitutes half of the total current density in it, which is ungrounded, in our opinion, for the following reasons.

The data of study [6] on sizes of droplets at the electrode tip melted by the submerged arc were ob-

tained by X-ray filming of the submerged-arc welding process. So, only these data should be considered reliable. According to these data, for the reverse polarity of the welding process the mass of a droplet (within the welding current range of 500–750 A used to perform submerged-arc surfacing) is no more than 0.28 g. Hence, the volume of the droplet (in the form of a sphere at a liquid metal density of 7.0 g/cm<sup>3</sup>) is 0.04 cm<sup>3</sup>, and its diameter  $d_d$  is 4.3 mm, i.e. diameter of the droplet is smaller than that of the electrode  $d_d < d_e$  (in study [6] the electrode corresponded in cross section area to a diameter of 5.3 mm). With the above ratios of the droplet to electrode diameters, it might be expected that the droplet will be fully covered by the active spot of the arc. In our investigations, surfacing was performed with the 5 and 4 mm diameter wires. So, it can be assumed that the above ratio of  $d_d < d_e$  was also met.

As established in study [7] by modelling the process by the RR net method, the radial current density in a droplet is insignificant even on a condition that the droplet is fully covered by the arc spot.

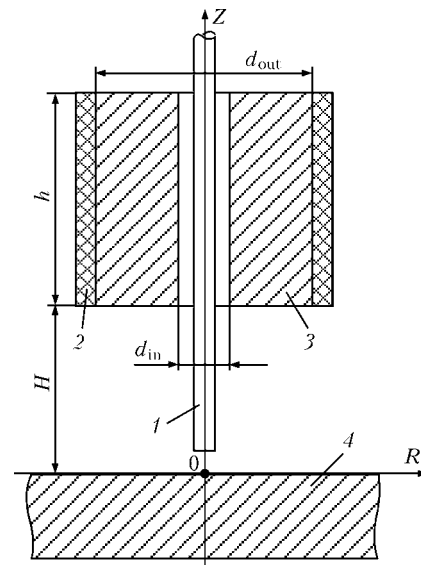


**Figure 1.** Schematic of system of bodies for calculation of distribution of induction of the magnetic field: 1 — electrode wire; 2 — solenoid winding; 3 — solenoid coil; 4 — workpiece (plate)



Affected by LMF, the rotating droplet cannot have a shape other than the ellipsoidal because of instability of other shapes of its surface [8, 9], which is also reported in study [3]. Of low probability is an assumption that under the effect of LMF the active spot of the arc is located in liquid droplet regions that are situated outside the electrode diameter (which would

have led to increase in the radial component of the current density in the droplet). The most probable case is that both in the conventional arc welding process and in the welding process affected by LMF the radial component of the current density in the droplet is much smaller than the axial component.

Calculations of induction of LMF in a non-magnetic gap ( $\Delta = 5$  mm) between the electrode wire tip and workpiece were made by the procedure described in studies [10, 11] (Figure 1). It is assumed that the droplet located in this gap (space) is non-magnetic

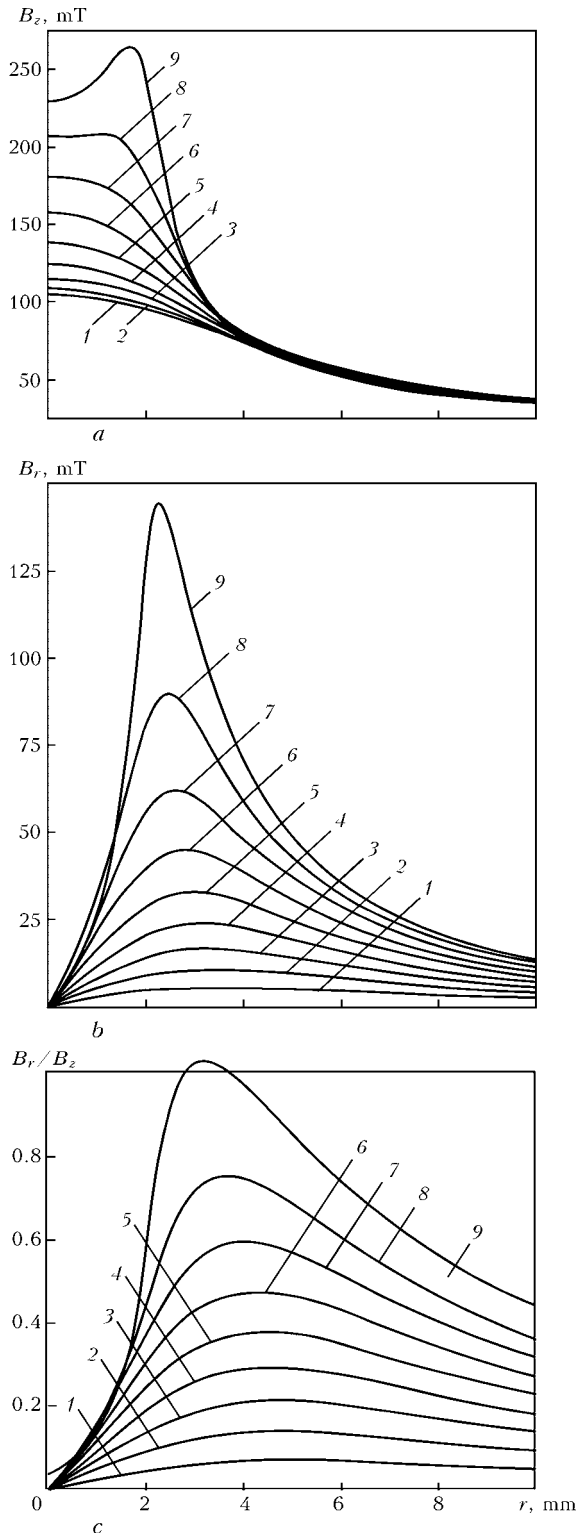


**Figure 2.** Distribution of induction components  $B_z$  (a),  $B_r$  (b) and  $B_r/B_z$  ratio (c) along axis  $r$  (layer-by-layer at different  $Z$ ) for a case where wire and workpiece are ferromagnetic ( $\mu = 500$ ): 1-9 —  $Z = 0.5, 1.0, 1.5, 2.0, 2.5, 3.0, 3.5, 4.0$  and  $4.5$  mm;  $I_w = 2000$  A

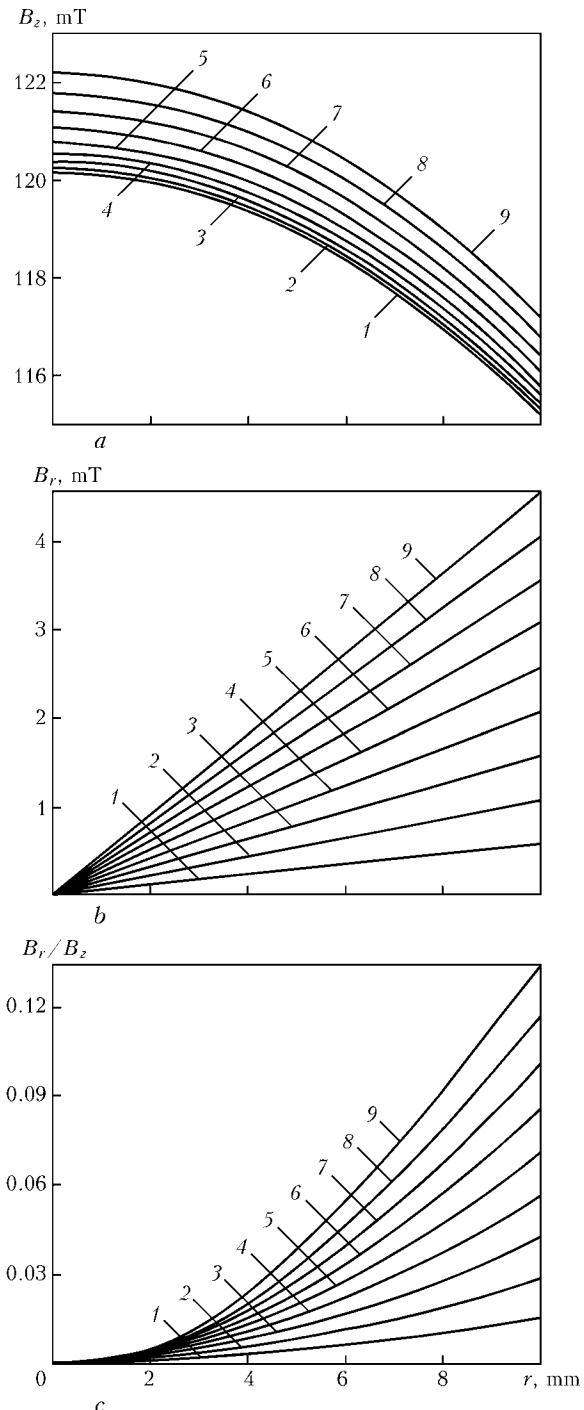


**Figure 3.** Distribution of induction components  $B_z$  (a),  $B_r$  (b) and  $B_r/B_z$  ratio (c) along axis  $r$  (layer-by-layer at different  $Z$ ) for a case where wire is non-magnetic ( $\mu = 1$ ) and workpiece is ferromagnetic ( $\mu = 500$ ); see designations of curves 1-9 in Figure 2



( $\mu = 1$ ) in the case of melting of wires of ferromagnetic materials, and that the temperature of heating of a wire at its extension (see Figure 1) is lower than the Curie point. The wire is ferromagnetic with a constant value of  $\mu$  (it is assumed that  $\mu = 500$ ), and length of the wire extension region adjoining the droplet and heated above the Curie point, as shown by the calculations, is no more than 1 mm. As also assumed in the calculations,  $\mu = 500$  both for ferromagnetic core 3 and workpiece 4, provided that it is ferromagnetic.

The calculations show that in surfacing on plates of magnetic and non-magnetic materials under the effect of LMF using electrode wires of magnetic materials (e.g. wire Sv-08A), the radial induction component  $B_r$  in the arc gap (in a zone at the electrode tip) is 0.3–0.5 of longitudinal  $B_z$  (Figure 2). In this connection, it can be suggested that the electromagnetic forces in a droplet, driving its rotation, are induced by interaction of the axial current density in the droplet (rather than the radial one) with the radial LMF induction component  $B_r$ . In surfacing using a non-magnetic wire ( $\mu = 1$ ) on a workpiece of ferromagnetic materials, the radial induction component  $B_r$  within the droplet zone is negligible (Figure 3). Therefore, the electromagnetic force is also insignificant, and an expected effect of increase in  $\alpha_m$  of electrode is insignificant as well.

The present study is dedicated to specifying the mechanism that causes rotation of a droplet at the electrode tip and increase in  $\alpha_m$  of the electrode under the effect of LMF in submerged-arc surfacing at a direct current of reverse polarity.

As increase in electrode melting coefficient  $\alpha_m$  under the effect of LMF is adequate to decrease in the surfacing current, in this study the level of increase in  $\alpha_m$  was estimated through a relative decrease in the surfacing current,  $\Delta I_s$ , i.e.  $\Delta I_s / I_s$  ( $I_s$  — surfacing current after switching on of LMF).

Experimental submerged-arc surfacing operations using flux AN-348A at a reverse-polarity current were performed with the automatic device ADS-1002 at an electrode feed speed, which was independent of the arc voltage of rectifier VDU-1201 with a drooping external characteristic. Surfacing parameters  $I_s$  and

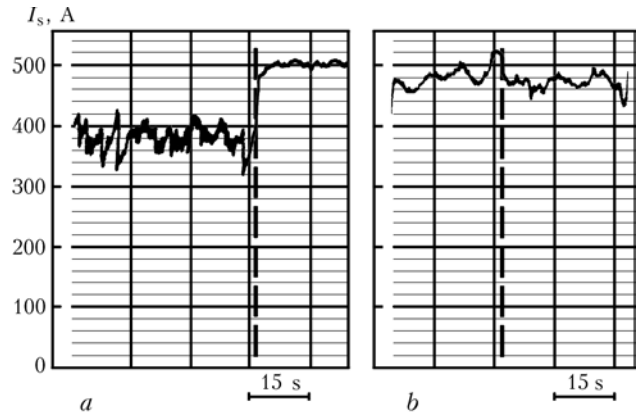


**Figure 4.** Diagrams of current in submerged-arc surfacing using ferromagnetic wire Sv-08A (a) and non-magnetic wire Sv-12Kh18N10T (b): regions on the right — surfacing without LMF; regions on the left — with LMF

$U_a$  were fixed with recorders of the N390 type during the surfacing process. In all the experiments the surfacing parameters without the application of LMF, established preliminarily using pointer indicators, were as follows: for  $d_e = 4$  mm  $I_s = 500$ –520 A,  $U_a = 28$ –30 V, and for  $d_e = 5$  mm  $I_s = 700$ –750 A,  $U_a = 30$ –32 V, the surfacing speed was  $v_s = 30$  m/h. And in all the experiments the measured longitudinal induction component  $B_z$  was 70–85 mT. The distance from the electrode tip to the plate surface was  $\Delta = 5$  mm. For  $d_e = 5$  mm the electrode extension was  $H = 40$  mm, and for  $d_e = 4$  mm the electrode extension was  $H = 35$  mm. The lower end of the solenoid generating LMF was also at the said distance from the plate treated (40 and 35 mm, respectively). After 20–30 s of the surfacing process, the constant or alternating LMF with a frequency of 50 Hz was switched on, and the surfacing process was continued by recording the surfacing parameters ( $I_s$ ,  $U_a$ ) for 20–30 s. 5–10 depositions were made at each process conditions. The averaged experimental data are given in the Table.

In series 1 of the experiments, surfacing was performed with wire Sv-08A (ferromagnetic material) 4 mm in diameter on a 20 mm thick plate of steel 09G2S (also ferromagnetic). Surfacing current  $I_s$  (Figure 4, a) decreased and arc voltage  $U_a$  increased after switching on of permanent LMF. As shown by the data, decrease in  $\Delta I_s / I_s$  (hence, increase in  $\alpha_m$ )

Conditions for making experimental depositions with different electrode melting coefficient

No. of experiment series	Base metal	Welding wire	Wire diameter, mm	LMF frequency, Hz	Increase in $\alpha_m$ , %
1	09G2S	Sv-08A	4	Permanent LMF	30.3
2	09G2S	Sv-12Kh18N10T	4	Same	0
3	12Kh18N10T	Sv-08A	4	»	34.5
4	09G2S	Sv-08A	4	50	22.0
5	09G2S	Sv-12Kh18N10T	4	50	0
6	09G2S	Sv-08A	5	Permanent LMF	32.0
7	09G2S	Sv-08A	5	50	18.1
8	09G2S	Sv-12Kh18N10T	5	Permanent LMF	0

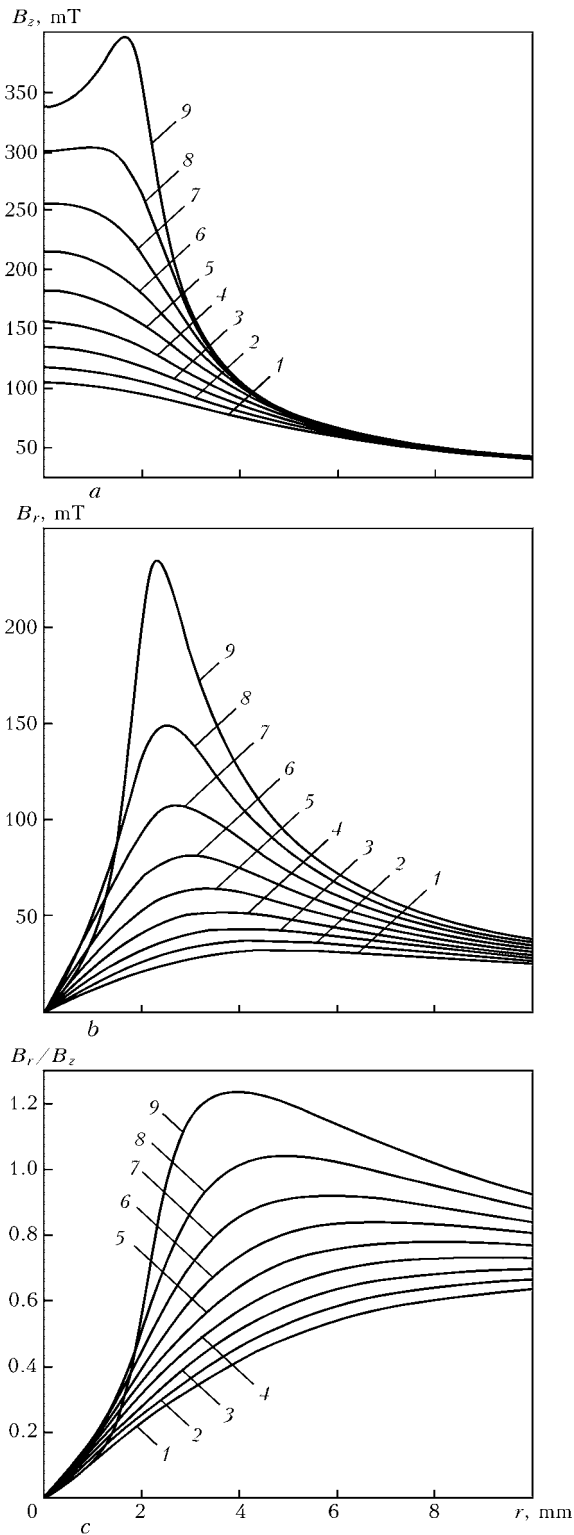


**Figure 5.** Distribution of induction components  $B_z$  (a),  $B_r$  (b) and  $B_r/B_z$  ratio (c) along axis  $r$  (layer-by-layer at different  $Z$ ) for a case where wire is ferromagnetic ( $\mu = 500$ ) and workpiece is non-magnetic ( $\mu = 1$ ):  $I_w = 2700$  A; see designations of curves 1–9 in Figure 2

in this case is 30.3 %, which corresponds to the data of studies [1, 2].

In surfacing using non-magnetic 4 mm wire Sv-12Kh18N10T (series 2, Table), switching on of the permanent LMF did not lead to decrease in the sur-

facing current, i.e.  $\Delta I_s = 0$  (Figure 4, b), and  $\alpha_m$  of the electrode did not increase.

In surfacing using 4 mm wire Sv-08A on a plate of non-magnetic steel 12Kh18N10T (series 3, Table), switching on of the permanent LMF caused a 34.5 % decrease in  $\Delta I_s/I_s$  (hence, increase in  $\alpha_m$ ). The effect of increase in  $\alpha_m$  of the electrode under the effect of LMF in this case is not lower than in the case of series 2 of the experiments, as the ratio of induction components  $B_r/B_z$  (Figure 5) is not lower than for a case where a workpiece is made from ferromagnetic steel (see Figure 2).

The experiments show that if the welding wire is made from a non-magnetic material and LMF induction component  $B_r$  within the electrode droplet zone is equal to zero, no increase in  $\alpha_m$  of the electrode occurs under the effect of LMF. In melting of the electrode of a ferromagnetic material, where LMF induction component  $B_r$  is substantial,  $\alpha_m$  of the electrode grows. This confirms the above assumption that rotation of a droplet at the consumable electrode tip under the effect of LMF (hence, improvement of conditions for transfer of the arc heat through a droplet and increase in  $\alpha_m$ ) is caused by electromagnetic forces in the droplet due to interaction of the radial LMF induction component (in the droplet) with the axial (along the electrode axis) component of density of the current spreading in the droplet.

Depositions were made using the 4 mm wire Sv-08A on a plate of steel 09G2S under the effect of LMF with a frequency of 50 Hz ( $B_r = 85$ – $89$  mT). In this case the surfacing current decreased as well (22 %, series 4, Table), whereas in surfacing using the 4 mm wire Sv-12Kh18N10T on steel 09G2S under the effect of LMF with a frequency of 50 Hz no changes occurred in  $I_s$  ( $\alpha_m$ ) (series 5, Table). Similar effects were observed also in surfacing using a 5 mm diameter wire (series 6–8, Table).

Therefore, the process of submerged-arc surfacing at a direct current under the effect of LMF is accompanied by decrease in thickness of a droplet in a direction along the electrode axis, and improvement of conditions for heat transfer through the droplet caused by rotation of the droplet under the effect of electromagnetic forces due to interaction of the radial component of induction of LMF with the axial component of the current density in the droplet. This is the difference between the results of this study and data of studies [2, 3], where it was assumed that the electromagnetic forces in surfacing under the permanent LMF conditions are induced by interaction of the longitudinal component of induction of LMF with the radial current density in the droplet. It is established that, unlike the data of study [2], the alternating LMF with a frequency of 50 Hz also causes increase in  $\alpha_m$  of the electrode with a diameter of 4 and 5 mm, although to a lesser degree than the permanent LMF. Moreover, the effect of increase in  $\alpha_m$  of the electrode depends upon the magnetic permeability of the electrode material. So, as might be expected, under the



effect of LMF it will be proportional to increase in a value of  $\mu$  of the electrode.

In addition, it is necessary to investigate the effect of growth of  $\alpha_m$  in the alternating LMF with a frequency of 50 Hz. Similar investigations should be conducted also for the straight polarity of the submerged-arc surfacing process under the LMF conditions.

## CONCLUSIONS

1. Application of electrode wire of ferromagnetic material leads to formation of a substantial radial induction component in a droplet, which causes distortion of structure of the magnetic field in a region under the electrode tip. When using electrodes of non-magnetic materials, the radial LMF induction component  $B_r$  is insignificant.

2. Rotation of droplets of an electrode metal at the electrode tip in arc welding and surfacing affected by LMF, and an associated increase in  $\alpha_m$  of the electrode are caused by electromagnetic forces in liquid metal of the droplet due to interaction of the radial (rather than longitudinal) LMF induction component with the axial (rather than radial) component of density of the welding current in the droplet.

3. Increase in the electrode melting coefficient occurs under the effect of the permanent LMF, as well as LMF with a frequency of 50 Hz, in surfacing on workpieces of ferromagnetic and non-magnetic materials using ferromagnetic wire. No increase in the elec-

trode melting coefficient is observed in surfacing using non-magnetic materials under the LMF conditions.

1. Boldyrev, A.M., Birzhev, V.A., Chernykh, A.V. (1989) Increase in the efficiency of electrode wire melting in longitudinal magnetic field welding. *Svarochn. Proizvodstvo*, **4**, 18–19.
2. Birzhev, V.A. (1997) *Theoretical and technological principles of increase in productivity of arc welding and surfacing in external axial magnetic field*: Syn. of Thesis for Dr. of Techn. Sci. Degree. Lipetsk.
3. Boldyrev, A.M., Birzhev, V.A., Chernykh, A.V. (1991) Specifics of electrode metal melting in longitudinal magnetic field welding. *Svarochn. Proizvodstvo*, **5**, 28–30.
4. Patskevich, I.R., Zernov, A.V., Serafimov, V.S. (1973) Influence of longitudinal magnetic field on melting and transfer of electrode metal. *Ibid.*, **7**, 8–10.
5. Kuznetsov, V.D., Malinkin, I.V., Syrovatka, V.V. et al. (1972) Behaviour of arc and transfer of electrode metal in longitudinal magnetic field welding. *Ibid.*, **4**, 3–4.
6. Pokhodnya, I.K., Kostenko, B.A. (1965) Melting of electrode metal and its interaction with slag in submerged-arc welding. *Avtomatich. Svarka*, **10**, 16–22.
7. Voropaj, N.M., Kolesnichenko, A.F., Lunkova, O.N. (1982) Electromagnetic forces in droplets during melting of cylindrical electrode by electric arc. *Tekhn. Elektrodinamika*, **6**, 11–15.
8. Kolesnichenko, A.F., Voropaj, N.M., Lunkova, O.N. et al. (1977) Numerical method of determination of the free surface of droplets of electrode metal in its transfer in the magnetic field of electric arcs. *Magn. Gidrodinamika*, **3**, 121–126.
9. Berezovsky, B.M., Sudnik, V.A. (2000) Mathematical modelling of formation of a droplet at consumable electrode tip in arc welding. In: *Welding — Testing. Results of the 20th Century*: Proc. of 19th Sci.-Techn. Conf. of Ural Welders. Chelyabinsk: ZAO MT, 24–27.
10. Lazarenko, M.A., Razmyshlyayev, A.D., Chichkarev, E.A. (1999) Computation of controlling magnetic fields for welding and surfacing processes. *Vestnik Priazov. GTU*, Issue 8, 147–150.
11. Razmyshlyayev, A.D., Deli, A.A., Mironova, M.V. (2006) Calculation of induction of the controlling longitudinal magnetic field allowing for magnetic properties of the core, wire and workpiece as applied to arc surfacing. *The Paton Welding J.*, **8**, 10–13.

## DIFFUSION WELDING OF METALS AND ALLOYS

Technological processes of diffusion vacuum welding of different combinations of metals and alloys (copper–tungsten, copper–stainless steel, aluminium–titanium, bronze–steel, heat-resistant alloys of different systems of alloying and others) with and without use of interlayers have been developed.

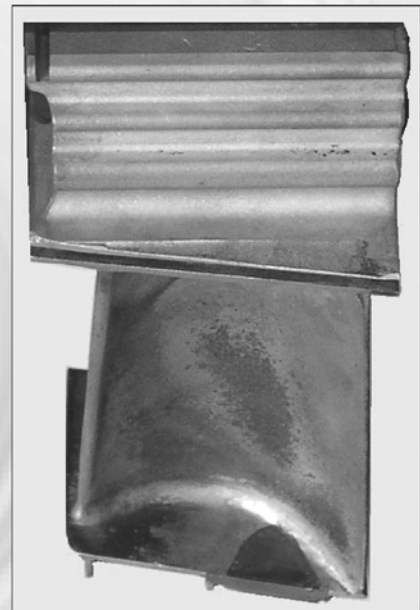
Technological processes and designed equipment guarantee the required properties and high quality of the joints.

**Purpose and application.** Technological processes are designed for welding special products, including those from dissimilar metals and alloys. They are used in different branches of machine building, for example, in manufacture of powerful cathodes of metallurgical plasmotrons, plate heat exchangers of high pressure, parts of precision pairs of friction of hydraulic units, parts of a hot path of gas turbines and so on.

**Status and level of development.** Technology and equipment for manufacture of plate heat exchangers are implemented in OJSC «Kriogenmash», bronze–steel parts of hydraulic units at Kharkov machine-building plant «FED».

**Proposals for co-operation.** Signing of contract is possible.

**Main developers and performers:** Prof. Yushchenko K.A., Dr. Nesmikh V.S., Lead. Eng. Kushnaryova T.N.



Contacts: Prof. Yushchenko K.A.  
Tel./Fax: (380044) 289 9087, 287 1088

# EVALUATION OF TECHNICAL STATE OF WELDED JOINTS ON HPS STEAM LINES ALLOWING FOR HYDROGEN-INDUCED DEGRADATION OF METAL IN OPERATION\*

G.N. NIKIFORCHIN<sup>1</sup>, O.Z. STUDENT<sup>1</sup>, S.M. STEPANYUK<sup>2</sup> and A.D. MARKOV<sup>2</sup>

<sup>1</sup>G.V. Karpenko Physico-Mechanical Institute, NASU, Lvov, Ukraine

<sup>2</sup>E.O. Paton Electric Welding Institute, NASU, Kiev, Ukraine

Loss of performance of degraded metal from different zones of real (~2·10<sup>5</sup> h) and model (repair) welded joints on live steam lines of heat power stations (HPS) was evaluated. It is established that current state of the base metal in operation can be evaluated only from local (short-time crack resistance) mechanical properties, whereas that of the weld metal can be evaluated also from integrated (strength, ductility, hardness) properties. It is shown that mechanical properties of the weld metal in operation are deteriorated more intensively, compared with the base metal. It is recommended to allow for the revealed peculiarities of degradation of metal of welded joints in evaluation of the current state of the weld metal and estimation of the remaining life of welded structures.

*Keywords:* arc welding, HPS steam line, degradation of metal, hydrogen-induced embrittlement, welded joint, weld metal, short-time crack resistance, integrated mechanical properties

Evaluation of performance of heat power equipment is of particular importance now for Ukraine. Firstly, as of the end of 2005, the quantity of HPS units with service life of more than 30 years was about 80 % [1]. Therefore, to substantiate periodicity of their examinations and possibility of leaving them in operation, it is necessary to reliably evaluate the current state of metal degraded under service conditions. Secondly, welded joints (WJ) are indispensable in assembly of any large-size object, while statistics of service damages shows that they are the most vulnerable link of structures.

Methodology of evaluation of the current state of metal in operation should allow for the maximal number of factors affecting its performance. First of all, this is the effect of stops and starts of equipment in operation of HPS units, which is accompanied by heating and cooling of structural elements, as well as by formation of resulting thermal stresses. Along with working stresses, they may amount to a super critical level [2–4]. In addition, it is not always possible to avoid microdefects in welded joints on large-size structures. Under the simultaneous effect by high stresses and process environment (high temperature and pressure steam or water), they may transform into macrocracks [5]. Results of investigations of properties of metal in operation (for more than 2·10<sup>5</sup> h) indicate that fracture of steam lines often occurs even in spite of a satisfactory level of strength and impact

toughness characteristics [3, 4]. As the cause is a substantial decrease in crack resistance [6–9], it is this factor that should be taken into account in the first place in evaluation of performance of steam lines. Their operation at a temperature of 540 °C and steam pressure of up to 22 MPa, as well as location outside the boundaries of a boiler, make through damages of steam lines especially dangerous for personnel. Periodic ultrasonic inspection of welded joints allows the damaged regions to be detected and repaired. Because of macro heterogeneity of structure and chemical composition, metal of the welded joints is particularly sensitive to a combined long-time effect by high-temperature environment and loads [3]. Microvoids in the weld metal (WM) [2] and structural defects are energetically convenient traps for localisation of hydrogen, which gets into metal during welding operations [6] and from the process environment [4]. It is reported [4] that the local concentration of hydrogen near the fracture surfaces from elements of steam lines damaged during operation is by an order of magnitude higher than the average concentration of hydrogen in degraded metal, which indicates to the need to allow for the hydrogen factor in development of a metal damage.

The purpose of this study was to evaluate mechanical properties of metal from different zones of a welded joint after operation at a HPS steam line, as well as to compare the metal in operation and that which is not operating in terms of their sensitivity to hydrogen-induced embrittlement.

**Investigation object and procedures.** Investigations were conducted on metal taken from different

---

\*The article is based on the results of the integrated target program of the NAS of Ukraine «Problems of life and safety of operation of structures, constructions and machines» (2004–2006).



Chemical composition of metal from different zones of repair and operating welded joint, %

WJ metal	C	Cr	Mo	V	Ni	Mn	Si	Cu	S	P	Ti	Al	Co
Operating:													
WM	0.050	1.06	0.68	0.20	0.18	1.09	0.344	0.21	0.016	0.031	0.002	0.0122	0.016
BM	0.154	1.33	1.02	0.26	0.17	0.59	0.423	0.20	0.011	0.021	0.002	0.0167	0.015
Repair:													
non-operating BM	0.157	1.39	0.97	0.29	0.20	0.91	0.296	0.22	0.017	0.021	0.001	0.0114	0.017
operating BM	0.136	1.33	1.02	0.25	0.12	0.75	0.285	0.02	0.012	0.027	0.003	0.0440	0.009
non-operating WM	0.090	1.13	0.57	0.19	0.07	0.69	0.184	0.10	0.009	0.021	0.030	0.0113	0.010

zones of welded joints on 15Kh1M1F steel pipes with outside diameter and wall thickness of 325 and 60 mm, respectively. One welded joint was cut from the HPS steam line after operation for  $19 \cdot 10^4$  h, and the other --- from a non-operating (repair) welded joint. Both welded joints were made by multi-pass electric arc welding by keeping to an operating practice used to perform corresponding operations. The repair welded joint simulated replacement of the damaged region of a pipe by a non-operating pipe. This welded joint comprised an operating base metal (BM) on the one side, and non-operating BM on the other side. WM of such a welded joint was not in operation. Therefore, it was considered to be WM in the initial state, and its properties were compared with those of WM after operation. Chemical compositions of BM and WM, both operating and non-operating, are given in the Table.

The state of metal was evaluated from the values provided for by the regulatory documents in force (hardness *HRB*, characteristics of strength and ductility), as well as from static crack resistance. Smooth cylindrical specimens with a gauge part diameter of 3 mm, oriented across the pipe wall, were stretched with the UME-10TM machine at a speed of movement of the active clamp equal to  $3 \cdot 10^{-3} \text{ s}^{-1}$ . The specimens were preliminarily electrolytically hydrogenated in electrolyte (5 % solution of  $\text{H}_2\text{SO}_4$  in water with an addition of 0.05 % of sodium thiosulfate) for 15 min at a current density of 0.05 A/cm<sup>2</sup>. One part of the specimens was loaded to fracture with hydrogenation, and other part --- without hydrogenation in air. Static crack resistance under an active load (critical value of *J*-integral  $J_{Ic}$ ) was evaluated, according to requirements [7], on one specimen by repeatedly partially unloading it. Fractography of fractures of the specimens after the tests was conducted using a scanning microscope.

**Results and discussions.** In the initial state, hardness of WM of a repair welded joint is higher than that of BM (Figure 1), which satisfies requirements of regulatory documents in force. As hardness of the welded joint under investigation, taken from an operating steam line, is unknown before operation, it was assumed that it was of the same order as hardness of the repair welded joint and higher than hardness of BM.

Hardness of BM on both sides of the welded joint remained almost unchanged after long-time operation, which is indicative of a low sensitivity of integrated mechanical characteristics of strength and hardness to degradation of low-alloy heat-resistant steels [8]. At the same time, hardness of WM was substantially decreased (approximately from *HRB* 100 in the initial state against *HRB* 75 after operation). This suggests that such an integrated property as hardness is sufficiently sensitive to high-temperature degradation only in the case where it occurs at a high intensity in time and reaches the level of hardness of operating WM, i.e. becomes inadmissibly lower than hardness of BM. The results obtained also indicate to the fact that it is WM (compared to BM) that is particularly sensitive to high-temperature degradation.

As established (Figure 2) in the course of investigations into short-time crack resistance of different zones of a welded joint [9], including HAZ, WM and HAZ in a repair welded joint on the side of the non-operating BM have the highest values of  $J_{Ic}$ , compared with BM and HAZ on the side of the operating metal. Therefore, WM prior to operation has the best properties not only in terms of hardness, but also in terms of crack resistance, which is lower in all zones of the operating welded joints, compared with the repair welded joint. However, its maximal decrease was fixed particularly for WM, which is in agreement with the hardness measurement results and confirms that

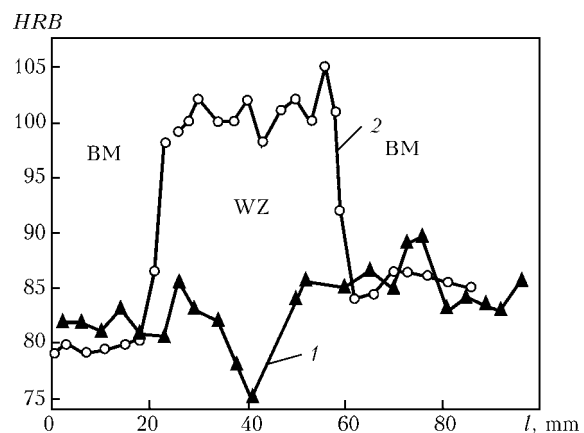
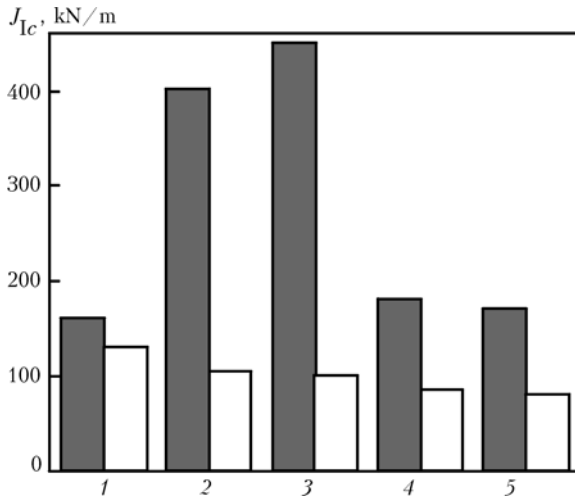


Figure 1. Hardness *HRB* across operating (1) and non-operating (2) welded joint



**Figure 2.** Crack resistance  $J_{Ic}$  of operating (light columns) and non-operating (dark columns) metal taken from different zones of welded joint: 1, 5 — BM on different sides of repair (1 — operating, 5 — non-operating) and operating welded joint; 2, 4 — HAZ; 3 — WM

it is the weld metal that is characterised by the highest sensitivity to degradation during long-time operation.

Therefore, hardness and short-time crack resistance decrease under service conditions because of degradation of WM. If we assume that strength (hardness usually correlates with strength) characterises resistance to tough fracture and crack resistance characterises resistance to brittle fracture, the fixed decrease in hardness of the operating WM is indicative of its low resistance to tough fracture, and decrease in crack resistance is indicative of its low resistance to brittle fracture. Therefore, a more intensive degradation of WM in operation may facilitate fracture of welded structural members both by the tough and brittle mechanisms.

The more intensive degradation of WM is confirmed by fractography of fractures of the specimens

tested to crack resistance [9]. Initiation (start) of a crack in WM of the repair and operating welded joints occurs by the tough mechanism through formation, growth and coalescence of microvoids. And on the contrary, relief of fracture details in operating WM is much smaller, and quantity of cleavage and secondary cracking elements grows with propagation of the crack (Figure 3, *b, c*). All these features are indicators of decrease in the consumption of energy for fracture, which is in agreement with the crack resistance test results.

For both welded joints (in the repair welded joint on the side of operating BM), initiation of crack in HAZ occurs also by the tough mechanism to form a characteristic elongation zone. Nevertheless, after an insignificant growth of the crack, fracture occurs by the intergranular mechanism to form deep secondary microcracks (Figure 3, *d, e*). Large grain conglomerates form a coarse relief, and traces of local plastic deformation in the form of tear ridges are identified on intergranular facets.

The classical tough fracture in non-operating BM changes into the classical chamfer mechanism to form fan-shaped relieves on cleavage facets in operating BM (Figure 3, *f*). The latter, together with fractographic features of fracture in HAZ, is indicative of the lowest consumption of energy for fracture, which seems to be related not only to the degradation of metal, but also to the effect of hydrogen accumulated in it during operation.

As established by the results of the air tests of smooth specimens cut from different zones of the repair and operating welded joints, the characteristics of strength  $\sigma_{0.2}$  and  $\sigma_t$ , as well as ductility  $\psi$  of BM remain almost unchanged after operation (Figure 4, *a-c*), which is in agreement with the results [8] on low sensitivity of integrated indicators of performance

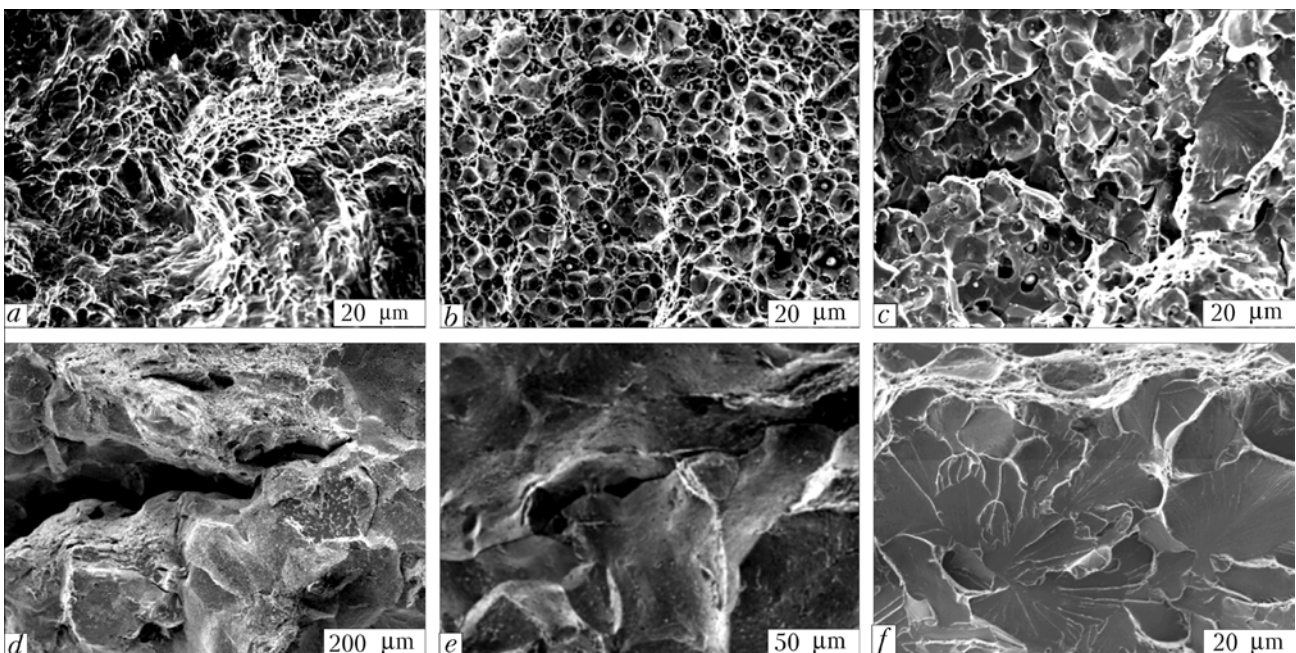


**Figure 3.** Fractographic features of fractures after crack resistance tests of WM (*a-c*), HAZ (*d, e*) and BM (*f*): *a, d* — repair welded joint; *b-f* — operating welded joint

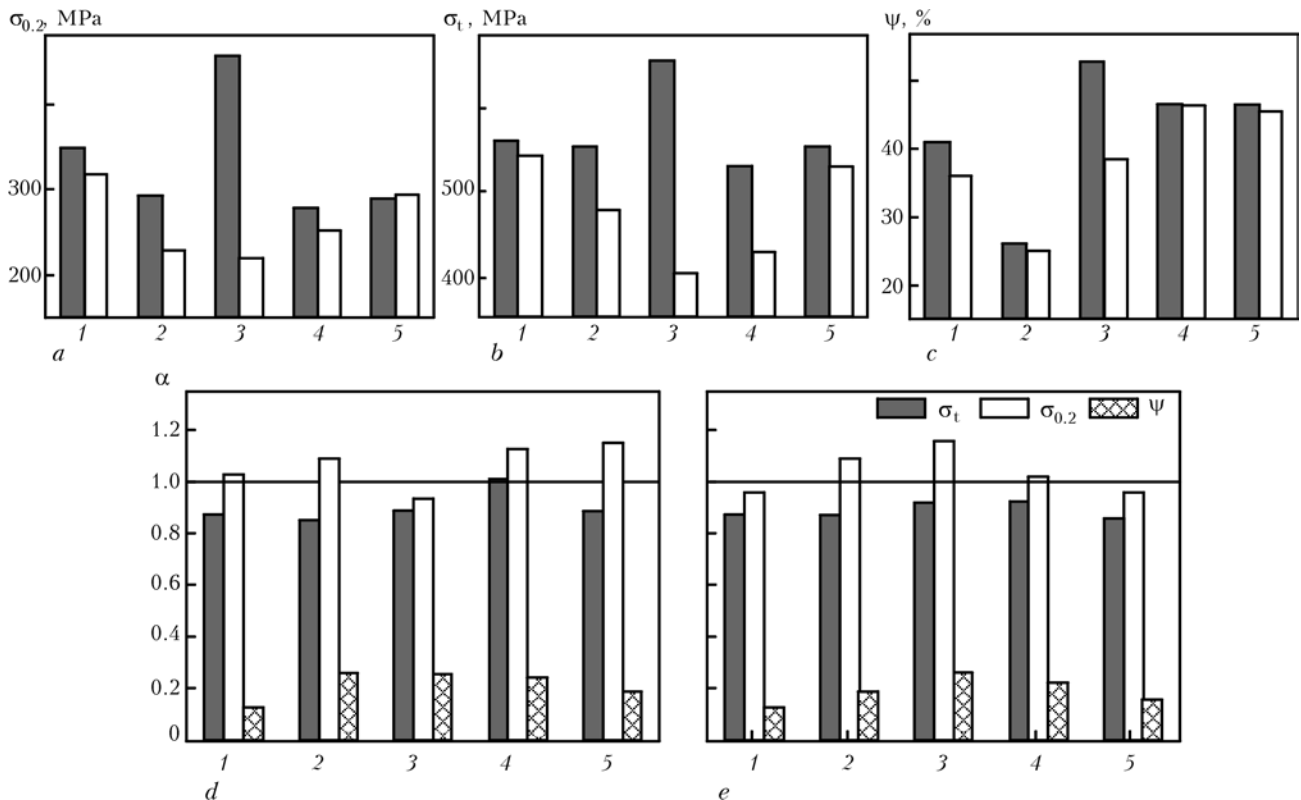


**Figure 4.** Mechanical properties of metal from different zones of repair (dark columns) and operating (light columns) welded joints in tests conducted in air (a–c), and comparison of mechanical properties of different zones of repair (d) and operating (e) welded joints by hydrogenation effect coefficient  $\alpha$  as a ratio of corresponding indicators for hydrogenated to non-hydrogenated metal (see designations of welded joint zones 1–5 in Figure 2)

to variations in the state of metal because of its degradation under service conditions. After operation, the strength characteristics of the HAZ metal decrease to some extent. However, the strength and ductility characteristics decrease to the highest extent particularly for WM ( $\sigma_{0.2}$  — by 53 %,  $\sigma_t$  — by 37 %, and  $\psi$  — by 28 %). Besides, if strength of WM in the initial state is higher than that of BM and meets requirements of the welding technology, after operation the strength characteristics of WM are lower than those of BM, which makes further operation of WM inadmissible. These results are in agreement with the data of measuring hardness of the welded joints. Therefore, it can be concluded that, unlike BM, the strength characteristics of WM are more sensitive to high-temperature hydrogen-induced degradation. In addition, they also prove a more intensive degradation of WM compared with other zones of a welded joint.

The effect of hydrogenation on properties of metal from different zones of the repair (Figure 4, d) and operating (Figure 4, e) welded joints was evaluated from coefficient  $\alpha$ , which characterises a relative variation in corresponding indicators of strength and ductility in electrolytic hydrogenation and in air. Hydrogenation causes some decrease in the strength limit of metal of almost all the zones of both repair and operating welded joints. And vice versa, yield limit  $\sigma_{0.2}$  of metal in the majority of the zones of a welded joint increases to some extent after hydrogenation. No effect of hydrogenation was observed only on the level of  $\sigma_{0.2}$  of WM of the repair welded joint (Figure 4, d)

and BM of the operating welded joint (Figure 4, e). And only reduction in area  $\psi$  under the effect of external hydrogenation is unambiguous and substantially decreases for all the zones, without any exception, of both repair and operating welded joints. Note that a relative variation in the integrated indicators of strength and ductility, caused by hydrogenation, is practically a value of the same order for the corresponding zones of the operating and repair welded joint. Therefore, a change in the state of the degraded metal can not be estimated from a change in coefficient  $\alpha$ , which is caused by electrolytic hydrogenation of specimens both before and during testing. This provided the effect of hydrogen both on the zone of volumetric tension in the central part of section of a specimen (internal hydrogen), and on the side of the generating line of the specimen surface (external hydrogen).

There may be almost no difference in energy consumption for initiation of local damages from the generating line of surfaces of specimens of operating and non-operating metal under the hydrogenation conditions used, as damage is stimulated from the surface of specimens by almost identical flows of hydrogen along the slip line. Fractographic analysis (Figure 5) of fractures of the specimens in electrolytic hydrogenation proves that practically in all the cases (independently of the zone from which the metal was taken) there were many local nuclei of damages from the side surface of the specimens, which coalesced during tension by the mechanism of tough fracture of

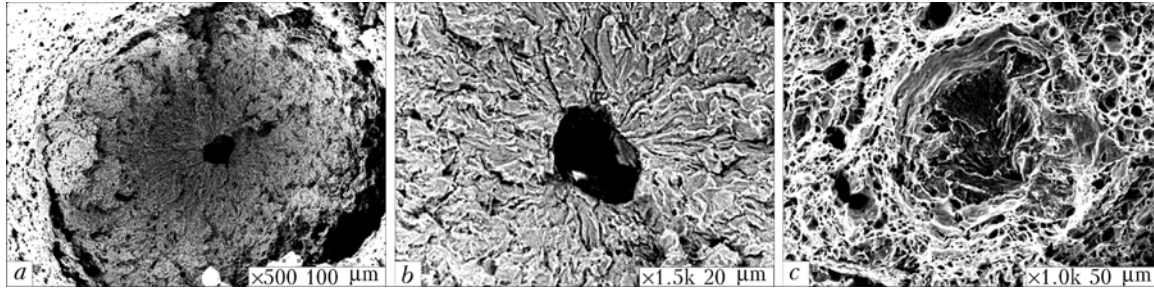


**Figure 5.** Fractographic peculiarities of fractures of preliminarily hydrogenated smooth specimens cut from the welding zone (a, b) and BM (c) after tension in air

partitions between them. Despite the presence of tough elements of a pit-like relief, some brittle regions in the form of a circle with a big pit at the centre and characteristic radial orientation of tear ridges can be seen at the centre of fracture. These ridges separate regions of local cleavages in parallel, but distant planes (Figure 5, a). The above-mentioned elements may be manifestations of internal hydrogen, which is molised at defects, while migrating into a region of the volume-stressed state, and creates high pressure, which leads to such local fractures.

To verify this hypothesis, investigations were conducted to study fracture surfaces of the specimens taken from different zones of a welded joint, which were tested in air after preliminary electrolytic hydrogenation. In this case, any ingress of hydrogen into metal along the slip lines was eliminated, thus leaving only the effect of internal hydrogen. The investigation results confirmed that despite a macro-tough character of fracture of the cup-cone type, at its central part, against the background of a typical pit-like relief, there were almost round regions of a cleavage character and different size, having holes at their centres (Figure 5, b, c). As nothing of this kind was observed in metal which was not saturated with hydrogen, it can be logically assumed that these fracture elements are manifestations of internal hydrogen. Moreover, they were larger in quantity, but smaller in size, compared with the combined effect by external and internal hydrogen. Besides, these peculiarities of the relief in non-operating metal should be regarded as exceptions, whereas in the operating metal they are dominant; hence, their area could serve as a quantitative fractographic indicator of the state of the degraded metal.

Therefore, long-time high-temperature service of welded joints under the effect of a hydrogenated environment leads to degradation of metal in all the

zones of a welded joint. This causes a substantial decrease in the integrated characteristics of strength, ductility and hardness of WM, which remain almost unchanged for the other zones of a welded joint. Short-time crack resistance allows evaluation of the level of degradation of all the zones of the welded joint. However, its maximal decrease was observed only for WM. The highest sensitivity to hydrogen-induced embrittlement of metal was fixed by the value of reduction in area of specimens. Fractographically, degradation of metal of all the zones of the welded joint is a low-energy consuming intergranular or cleavage fracture, which is in agreement with decrease in static crack resistance, i.e. the local indicator of the state of metal that degraded under service conditions. Fractography shows promise for evaluation of the state of the degraded metal by the area of local cleavages in the zone affected by volume stresses induced by internal hydrogen.

1. Zabara, Yu. (2002) There is always a solution. *Obrij PIB*, 82(24).
2. Karzov, G.P., Leonov, V.P., Timofeev, B.T. (1982) *Welded high pressure vessels*. Leningrad: Mashinostroenie.
3. Bugaj, N.V., Mukhopad, G.V., Krasovsky, A.Ya. (1986) *Improvement of reliability of electric power station boilers*. Kiev: Tekhnika.
4. Vajnman, A.B., Melekhov, R.K., Smiyan, O.D. (1990) *Hydrogen-induced embrittlement of elements of high pressure boilers*. Kiev: Naukova Dumka.
5. Kolachev, B.A. (1985) *Hydrogen brittleness of metals*. Moscow: Metallurgiya.
6. Pokhodnya, I.K. (1998) Problems of welding of high-strength low-alloy steels. In: *Current materials science of the 21st century*. Kiev: Naukova Dumka.
7. Romaniv, O.N., Tkach, A.N., Dzioba, I.R. et al. (1989) Influence of long-term thermomechanical impact on crack resistance of 12Kh1MF steel. *Fiz.-Khim. Mekhanika Materialov*, 2, 87–92.
8. Student, O.Z., Lonyuk, B.P. (1997) Growth of fatigue cracks in steel 15Kh2MFA held in high-temperature hydrogen. *Ibid.*, 33(4), 121–126.
9. Nikiforchin, G.M., Student, O.Z., Dzioba, I.R. et al. (2004) Degradation of welded joints of electric power station steam pipelines in hydrogenated medium. *Ibid.*, 40(6), 105–110.

# SECONDARY STRESSES IN WELDED GANTRY CRANES

O.A. EMELIANOV<sup>1</sup>, R.L. SLAVINSKY<sup>2</sup> and D.V. YAREMENKO<sup>3</sup>

<sup>1</sup>Donbass State Machine-Building Academy, Kramatorsk, Ukraine

<sup>2</sup>Company NKMZ (Novo-Kramatorsk Machine-Building Works), Novo-Kramatorsk, Ukraine

<sup>3</sup>Kharkov Polytechnic University, Kharkov, Ukraine

Formation of secondary stresses and their effect on fatigue of welded gantry cranes are considered.

*Keywords:* welded gantry cranes, secondary stresses, generation sites, fatigue strength, cycle fatigue life

Fatigue failures of gantry metal structures, occurring only under the influence of alternating loading, are the main reason of crane unfitness for future operation. Crane loading are all the external forces applied to the crane, the main of them are the dead weight and support reactions. The load change happens in the case if weight loads or their application sites change, as well as due to the action of some force and deformation factors.

The Laboratory of Technical Diagnostics of Donbass State Machine-Building Academy has conducted studies on improvement of welded structures of load-carrying machines since 1978. Diagnostic of 1800 gantry cranes has been performed during this time. It was established that up to 60 % of the examined machines have fatigue damage.

The aim of this study is to clarify the reasons of mass fatigue damage of «weakly loaded» areas of structures of welded gantry cranes.

The work that the crane performs can be divided into three periods: cargo lifting and lowering, its displacement by the carriage, and cargo displacement by the crane gantry along the span.

During the first period the cargo is suspended from the hook. When the hoisting mechanism operates, the cargo weight is transferred step by step to the crane girders by the following chain: drum–drum supports–reducer and hoisting mechanism motor supports–cargo carriage frame–carriage wheels–main crane beams–end beams–gantry wheels. Each of the above-mentioned components transfers almost equal load, which value is equal to the mass of lifted load, from the hook to crane girders, allowing for the losses for friction, etc. The point of load transfer to each component and its value can be determined rather precisely.

During the second period the load hanging from the hook is moved on the carriage along the main beams of the gantry. The points of load transfer to the main and end beams and the forces in each cross-section can be exactly determined by influence lines. Therefore, in the first period the load variability is obtained as a result of variation of the tightening force in the suspension ropes, in the second — when the carriage changes its position on the main beams.

Fatigue strength (cyclic life) for welded components of the gantry crane and its elements can be determined with sufficient accuracy for practice by the procedure (third period) set force in SNiP 11-23--81 [1] in the case of their operation in the first and in the second periods.

Further on (third period), the cargo suspended from the hook is displaced when the crane travels along the span; the load value and the point of its application to the construction do not change. Formally, no fatigue damage should occur, however, it is observed in reality.

The discovered features can be explained in the following way. In the third period the electric motor of the crane (or cargo carriage) travel mechanism drive performs the work, required for crane travel along the span and for different unproductive losses, namely deformation and wear of parts making up the crane structures, formation of secondary stresses and fatigue cracks and so on. Variation of forces in gantry elements may appear in this situation, if the work of unproductive losses influences the values of its supporting reactions, i.e. vertical and horizontal forces in the running wheel–rail contact. These forces, continuously changing at wheels rolling, cause a change of forces in the gantry metal structure parts and in the crane travel drive [2, 3], thus promoting the development of fatigue damage in them.

Therefore, in the third period the fatigue resistance of crane metal structures depends on unproductive power losses of crane travel drive during its travel along the span.

The losses are determined by the rationality of the gantry circuit design solution and design of its welded components; precision of component manufacturing, quality of component assembly; condition of elements of crane track and crane travel drive, as well as violation of safe operation rules.

Mechanisms of the drives of hoisting, carriage and gantry travel are usually mounted on the gantry crane. Efficiency factor of each drive depends on the conditions of performed work and design features. The smaller the number of parts, elements and kinematic pairs of the mechanism, crane and scaffold gantry involved in its manufacturing, the smaller are the unproductive losses of energy produced by motor drive and the higher its efficiency factor. The lifting mecha-



nism has the highest efficiency factor, and the crane travel drive has the lowest efficiency factor.

Vibratory processes of secondary stresses can be generated and maintained, depending on the drive efficiency factor, during crane operation both in the first and in the second period, as a result of the losses of energy produced by the motor, promoting the development of fatigue damage in the gantry structure.

Operation practice of welded gantry cranes shows that fatigue damage develops in them after 1–3 years of operation, i.e. much earlier than it is specified by different standards. Premature cracks appear in those elements, in which they were not expected, and which, therefore, were not analyzed for fatigue.

Fatigue cracks were observed in all the types of steel welded span structures, especially those which have stiffeners, plates and transverse beams welded to the beams, as well as different cuts to accommodate the welds.

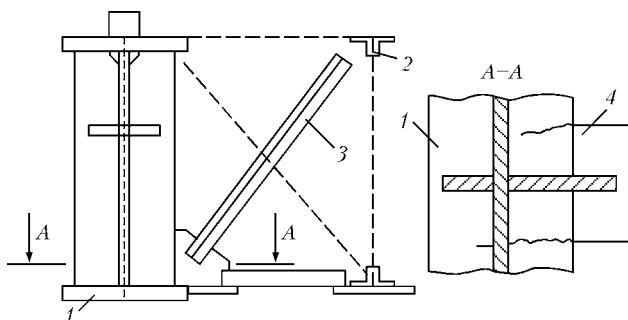
The majority of gantry cranes where cracks are found, are subjected to cyclic loads, however, the number of loads up to the moment of cracks formation was small. J. Fisher and D. Mertz [4] believe that such cracks formation is caused by secondary stresses, induced by deformation of the gantry span structure and its separate elements.

Operating practice of hoisting-transportation mechanisms shows that the problem of secondary stress formation and their influence on cyclic life of gantry cranes is urgent and requires a solution.

It is rational to classify the alternating loadings acting on the crane, and forces and stresses caused by them in the gantry structure into two groups, depending on the reasons of their formation: the principal and secondary.

The principal ones are the stresses caused by the increase or decrease of forces in the elements of gantry crane structure, at the change of the point of carriage mounting on the main beams of the gantry or the force of tensioning in suspension from the load  $G_1$  lifted or lowered by the crane.

The value of the main forces in gantry elements and in support reactions, balancing the weight loads, can change at the change of the force in the suspension of the lifting mechanism during its tension until the load is lifted from the base (or weakening when it is



Schematic of crack formation in the main beam lower girth on the edges of butt-welded horizontal gusset (for designations see the text)

placed on the base) or the point of carriage mounting on the main gantry beams.

Beams are loaded by transverse bending, torsion and local pressure, the main forces  $M$ ,  $Q$ ,  $M_t$ ,  $F$  and the main stresses  $\sigma_x$ ,  $\tau_{xy}$ ,  $\sigma_{fy}$ ,  $\sigma_{loc}$ ,  $y$  formed in them [1, items 13 and 14]. In some cases, in addition to the principal ones, alternating secondary stresses can form, which are caused by displacement of auxiliary elements and structures of the gantry (bar girders, brake areas, service platforms, stairs, cabins and so on) at their forced deformations together with the main load-carrying structures, to which they are joined by electric welding.

Fatigue cracks appear in the main load-carrying structure already loaded by the principal stresses under the influence of secondary stresses in the points of fastening of different auxiliary structural elements to it.

Auxiliary part fastened by welding is an additional stress raiser, in the zone of which the residual stresses from welding and secondary stresses from the load acting on the auxiliary part, are added. Therefore, additional site of possible fatigue crack formation appears, but with allowance for the side effect of secondary stresses. The greater the number of such areas, the greater the number of damages that depending on the circumstances can appear in weakly loaded areas already at the early stage of gantry operation.

An example of fatigue crack initiation in the main load-carrying structure is shown in the Figure — the lower girth of the main beam 1 of gantry crane, connected by electric welding with the upper belt of auxiliary truss 2 by diagonal brace 3. The main beam deflection causes stretching of brace 3 and simultaneous deflection of auxiliary truss 2, at the carriage with load driving over it. Tensile force of brace 3 bends gusset 4 and causes fatigue crack formation in the points of the gusset fastening to the main beam girth.

Secondary stresses can also form in other areas on the main and end beams of the crane gantry. This can be explained by that depending on the perfection of the design of crane travel drive mechanism and its actual state, part of energy produced by the motor, is spent on different unproductive losses (deformation and wear of parts that make up the structure, formation of secondary stresses and fatigue cracks and so on).

Magnitude of supporting reactions at motion of gantry crane mainly depends on ensuring the straightness and uniformity of crane travel (cargo carriage) along the rail way as well as on:

- value and direction of angle of assembly wheel skewing relative to the direction of crane travel speed;
- deflection of rail head level from its nominal value by the height near the butts and between the columns in the row;
- value of friction coefficient in the wheel-rail contact;
- plastic dragging of metal on the contact surface of wheel and rail.



As it is seen from above-mentioned, this information is useless for direct evaluation of fatigue resistance, it is necessary to create a procedure allowing determination of the generation point, cause for formation and influence of secondary stresses of the crane operating life in the third period.

Two principles are valid in the engineering practice: local strength (straps, reinforcing ribs, bosses, local thickening or structural element widening, etc.) and local weakness (openings, hatches, cutouts, angles of incidence, local thinning and narrowing, etc.), which lead to total lack of strength, as local changes of the structure rigidity cause stress concentration (SC) and are hazardous. SC, as a rule, promotes fatigue damage development at alternating load. In these cases it is necessary to remove SC in its gantry elements or lower the range of supporting reactions in its travel along the span.

Secondary stresses develop in the main load-carrying elements of the gantry, in the points of location of different structural stress raisers that can form in the points of auxiliary element welding to the main part.

High stresses in the points of auxiliary element fastening to the main ones, develop as a result of summation of the force flow transferred by them, with residual stresses from welding, as well as with concentration of principal stresses, formed in the points of auxiliary elements abutting to the main ones. This accounts for fatigue crack formation in the structure areas «weakly loaded» by the principal stresses.

Methods of improving the fatigue strength of welded joints and crane structures can be divided into three principally different groups: increase of fatigue resistance by local treatment of welds, rational design of welded components and rational circuit-design solution of gantry cranes in general.

The first group of methods was studied in detail in [2] and is widely applied currently for increasing the fatigue resistance of welded joints.

The issues of rational design of welded components included into the gantry crane design are described in study [3]. This method allows providing a uniform transmission of force flow in the elements of gantry structure forming the component, i.e. eliminating SC by design means within the welded component and the adjacent elements, decreasing the influence of residual stresses on fatigue resistance of welded joints and the component in general, eliminating strain ageing of steel in the welded joints.

The third group was designed in the Donbass State Machine-Building Academy. It includes the methods of eliminating the factors [3] causing fatigue damage of the welded gantry during its travel along the span. These methods are based on improvement of the diagram-component solution of the gantry and the crane as a whole, with the aim of eliminating or essentially

reducing the range of reaction forces in wheel-rail contacts, i.e. eliminating the change of forces and stresses in gantry structure at crane travel along the tracks deviating from the design dimensions, as well as eliminating the possibility of vibration occurrence.

Therefore the gantry load can be decreased by adjustment of vertical and decrease of horizontal support reactions. It is rational to call all the methods that allow solving this problem --- «improvement of crane travel properties».

The first two methods are passive as they do not influence the general loading of the crane or crane trestle gantry, or the unproductive power losses consumed in crane travel. The third (design) method lowers the gantry and crane trestle loading at crane travel, as well as unproductive power losses, decreases or eliminates the range of amplitude of forces and stresses in structure. The method is based on crane travel property improvement.

Over 20 years of gantry crane operation, fatigue cracks can form mainly under the impact of secondary stresses, manifested in punching of the upper girth sheet by the rail, detachment of «risers» that fix the rail to the beam, detachment of carriage dead ends, crack formation in the points of welding the bracket frames to beam webs for mounting the drives and cabinets with electric equipment in the points of fastening the main beams to the end beams, etc.

It is obvious that in such cases fatigue damage of the main beams by the loads at load handling by the hoist, lifting and displacement by the carriage can be prevented by elimination of factors causing secondary stresses.

## CONCLUSIONS

1. Cycle fatigue life of welded gantry cranes manufactured to the standards for T and VT modes, which is achieved under production conditions, in the majority cases is much lower than the calculated value, as the influence of secondary stresses is not taken into the account.
2. Further increase of fatigue strength of gantry welded structures, requires investigation of the reasons of formation and the points of alternative secondary stress generation.
3. It is necessary to continue work on improvement of the already existing and creation of new modifications of statically determinate cranes that allow an essential lowering of secondary stresses during their travel.

1. SNiP 11-23-81.
2. Trufyakov, V.I. (1998) Increase of fatigue resistance of welded joints and structures. *Avtomatich. Svarka*, **11**, 11-19.
3. Emelianov, O.A., Shepotko, V.P., Pikhota, Yu.V. et al. (2004) Fatigue damages of welded crane bridges. *The Paton Welding J.*, **5**, 29-35.
4. Fisher, J., Mertz, D. (1985) Crack formation in steel bridges. *Grazhdanskoe Stroitelstvo*, **2**, 9-13.



# EFFECT OF THE STATE OF SURFACE OF ELECTRODES ON STABILITY OF GLOW DISCHARGE UNDER WELDING CONDITIONS

G.P. BOLOTOV

Chernigov State Technological University, Chernigov, Ukraine

The effect of cathode processes on stability of the glow discharge is determined. It is shown that under conditions of heating by the high-current glow discharge the presence of non-uniform dielectric films on the anode surface caused by its contamination during operation leads to formation on the anode of local regions with a higher current density, which promote transformation of the glow discharge into the arc one.

*Keywords:* electrodes, low-temperature plasma, glow discharge, stability, surface state

Low-temperature plasma of the glow discharge of a medium (1–15 kPa) pressure in inert or active gases is applied to advantage as an energy source for technological processes accompanied by a substantial long-time heating of parts, such as thermochemical treatment, diffusion bonding and brazing. The parts treated or joined by these processes act as one of the discharge electrodes, i.e. cathode. Heating is provided through the cathode spot on their surfaces.

At the same time, the glow discharge does not feature a sufficient stability, and under certain conditions it transforms into the electric arc. The concentration of energy grows in local heat spots formed in this case, thus leading to burns-through and melting of individual regions of the parts joined to form irreparable defects. The processes occurring at the cathode and in the near-cathode region are of special importance for the electric discharges in gases.

Numerous studies conducted at present [1–3], which relate to the problem of stability of the glow discharge, consider mostly the effect of the cathode processes on the shape of the discharge. It has been established that the probability of transformation of the glow discharge into the electric arc is determined by characteristics of the surface layer of the cathode material (chemistry, microrelief, presence of oxide films and contaminants that provide existence of spots of an increased electron emission), as well as formation of slots and gaps of a certain size on the cathode, where the effect of a hollow cathode may take place, thus leading to a local growth of the current density. Treatment of parts for surface finish class 3–5, their washing in solvents, and removal of slots and gaps 0.01–1.00 mm in size from the heating zone are the sufficient measures to avoid transformation of the glow discharge into the arc one.

As reported in [4], with a geometry of electrodes used for glow-discharge welding (steel wire profile-anode, and relatively massive workpieces-cathode), the current density in the near-anode region is 5 to 8

times as high as at the cathode, which makes this region very sensitive to local fluctuations of the current density and may affect stability of the discharge even at the absence of unfavourable factors on the cathode.

As noticed, during operation an initially weak uniform anode glow gradually changes its state. Occasional glowing spots, located arbitrarily, emerge at the anode (Figure 1, a, top). With time they transform into channels of increased conductivity (Figure 1, b, top). Increase in the discharge current leads to development of the electric arc in these channels (Figure 1, c, top). The cause is that the state of the anode surface substantially changes during operation because of deposition of oil vapours on it, which are polymerised in the discharge and get into the chamber from vacuum pumps and pipelines, oxidation of the anode surface due to the presence of oxygen impurities in gases, and deposition on the anode of the cathode material particles sputtered by ion bombardment. All this leads to formation on the anode surface of uncontrollable films having increased resistance, compared with the anode material, and favour shorting of the glow discharge current at the anode.

Investigations of the character of current conduction on the anode surface (Figure 2, a) were performed using the rotating probe method by recording results with the light-beam oscillograph. The anode was made from a piece of St3 rod 0.005 m in diameter and 0.05 m long. To simulate the state of the anode surface formed during operation, the anode was subjected to oxidation in air at a temperature of 873–973 K for 10 min up to formation of a marked layer of oxides. After that the anode surface was cleaned in two regions up to formation of metallic lustre. The path of the probe tip was at a distance of 1.0–1.5 mm from the anode surface. It can be seen from the previous oscillograms (Figure 2, b) that the major part of the discharge current gets to the anode particularly through the regions free from surface contaminants. This leads to increase in the local current density at the anode and, accordingly, in the adjoining regions of the positive discharge column.

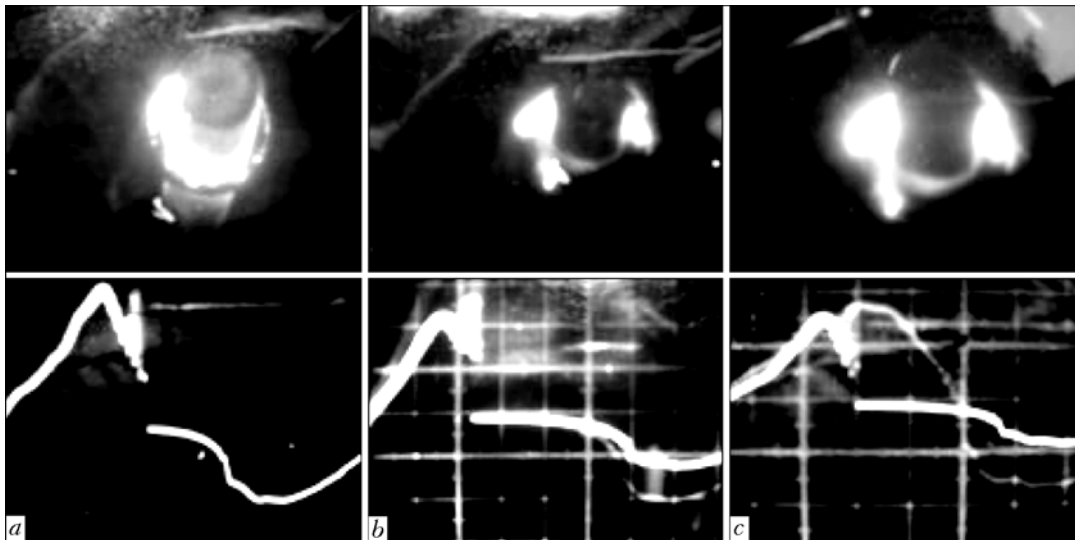


**Figure 1.** Character of variations in appearance of the anode glow during operation of the glow discharge anode (top), and oscillograms of the discharge current (bottom): a–c — see in the text

As the discharge power is increased, the high-frequency oscillations appear on the discharge current oscillograms. These oscillations are formed at a moment that follows passing the amplitude value by the current curve (see Figure 1, a, bottom). Measurement of the frequency of these pulses using the frequency spectrum analyser of the S4-25 type made it possible to find its characteristic values, which are equal to  $1 \cdot 10^5$ – $1 \cdot 10^6$  Hz. Some time after formation of the high-frequency current pulses the low-frequency oscillations are formed. The latter have frequency of the mains that powers the discharge, the amplitude of which may grow up to transformation of the glow discharge into the arc one (see Figure 1, c, bottom). This process may be caused by the fact that increase in the electric current leads to growth of its density in regions of an increased conductivity on the anode surface and their probable heating up to the metal melting and evaporation points. Metal vapours formed in the inter-electrode gap decrease the efficient potential of ionisation of the gas medium, which may promote increase in conductivity of this gap with increase in the electric current in it. Explanation to this phenomenon is given in study [5], which reports that intensive evaporation of metal from the cathode surface can lead to formation of the electric arc channel in the glow discharge inter-electrode gap.

Investigation of the process of electron beam treatment (EBT) of metals [6] shows that evaporation of metal from the surfaces of workpieces under the effect of a flow of accelerated electrons occurs periodically, rather than permanently, i.e. the process consists of a sequence of elementary heating–boiling–dissipation (evaporation) cycles, the frequency of which under the EBT conditions is  $1 \cdot 10^3$ – $1 \cdot 10^6$  Hz.

To establish whether the high-frequency oscillations of the electric current in the glow discharge are caused by evaporation of the anode material, it is necessary to determine the probable temperature of heating and characteristic time of energy accumulation, leading to overheating and evaporation of metal

from the anode surface in regions of the increased current density.

Assuming simplistically that the electric arc formed on the anode surface is a spot heat source acting on the surface of a semi-infinite solid, the ultimate temperature within the heating zone can be determined, according to [7], as

$$T = T_0 + \frac{q}{2\pi\lambda r}, \quad (1)$$

where  $T_0$  is the initial anode temperature (amounting to 873–1073 K under the glow discharge conditions);  $q$  is the power of the heat source (arc);  $\lambda$  is the coefficient of conductivity of the anode material; and  $r$  is the radius of the heat spot determined approximately from the erosion (melting) traces on the anode surface.

Measurement of transverse traces of the arc showed that they are no more than 0.001–0.002 m in size. Allowing for this fact, for a discharge current of 10 A

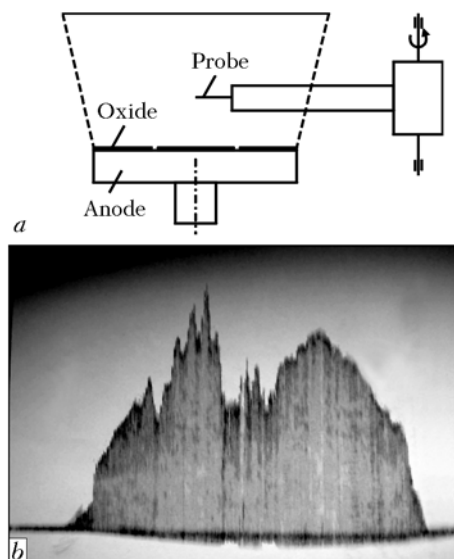


**Figure 2.** Scheme of measurement of the current density (a), and oscillograms of its distribution (b) on the glow discharge anode surface



and anode potential drop of 15 V (its value is 14–16 V for nitrogen, argon and hydrogen), according to (1), the temperature at the heat spot may amount to 3500–4000 K, which is higher than the temperature of the beginning of marked evaporation of a steel anode (about 3000 K).

The time of energy accumulation depends upon the density of a heat flow and physical properties of metal. As the anode under the glow discharge conditions is bombarded, like in EBT, by electrons accelerated in a range of the anode potential drop, the time of the metal heating–evaporation cycle can be estimated using relationships that are employed in the EBT theory [6, 8]. In this case, the time of energy accumulation is

$$\tau = \frac{M^{2/3}(4\rho)^{-2/3}}{4a} \text{ [s]}, \quad (2)$$

where  $M$  is the mass of a metal covered by boiling, g;  $\rho$  is the metal density, g/cm<sup>3</sup>; and  $a$  is the thermal diffusivity of metal, cm<sup>2</sup>/s.

The mass of a material covered by energy release is related to parameters of the electron flow (using the Shenland formula [9]) as follows [8]:

$$M = 1.65 \cdot 10^{-12} d^2 U^2 \text{ [g]}, \quad (3)$$

where  $d$  is the characteristic size of the evaporation zone (arc affected zone), cm; and  $U$  is the potential of acceleration of electrons, V.

For the values of  $d$  and  $U$  indicated earlier, as well as for corresponding thermal-physical characteristics of the anode, according to relationships (2) and (3), the characteristic time of energy accumulation is  $\tau = 2 \cdot 10^{-8}$ – $10^{-7}$  s. Hence, the probable frequency of vapour formation is  $f = 1 \cdot 10^7$ – $0.5 \cdot 10^8$  Hz, which is very

close to the frequency of the electric current oscillations observed in experiments, and, therefore, may serve as a confirmation of the suggested hypothesis.

## CONCLUSIONS

1. To avoid formation of centres of a marked evaporation of the anode, it is recommended to make it from refractory metals (molybdenum, tungsten).

2. As the formed discharge current oscillations get into the radio-frequency range, they can be readily detected using any radio-broadcasting receiver with a medium-wave range, and serve as a signal to timely adjust the process mode.

3. Instability of the discharge current is related not to the presence of dielectric films on the anode surface, but to the heterogeneity of their thickness and composition, which requires periodic replacement or cleaning of the anode.

1. Leeb, L. (1950) *Main processes of electric discharges in gases*. Moscow-Leningrad: AN SSSR.
2. Gajsin, F.M., Sattarov, R.K., Khalikov, R.A. (1975) *Study of transition of glow discharge into electric arc at high temperatures*. Kazan: KAI.
3. Golubev, V.S. (1990) *Increased-pressure glow discharge*. Moscow: Nauka.
4. Bolotov, G.P., Satyukov, A.I. (1998) Theoretical estimate of stability threshold of glow discharge in diffusion bonding. *Avtomatich. Svarka*, **4**, 13–15.
5. Plesse, H. (1935) The effect of temperature on the electrode glow discharge at low pressure. *Ann. d. Phys.*, **22**, 423.
6. Rykalin, N.N., Zuev, I.V., Uglov, A.A. (1978) *Principles of electron beam treatment of materials*. Moscow: Mashinostroenie.
7. Rykalin, N.N. (1951) *Calculation of thermal processes in welding*. Moscow: Mashgiz.
8. Nikolaev, G.A., Olshansky, N.A. (1966) *New methods for welding of metals and plastics*. Moscow: Mashinostroenie.
9. Nazarenko, O.K. (1981) *Electron beam welding*. Moscow: Mashinostroenie.

## TECHNOLOGY AND EQUIPMENT FOR REFINING OF CRUDE RARE-EARTH METALS

Metal-thermic reduction is the most common method used to commercially produce the majority of REM. Calcium, aluminium or carbon are most often employed as reducing agents. Crude rare-earth metals produced by this technology contain from 0.7 to 2.0 % calcium. Therefore, they should be additionally refined in arc skull furnaces. This process is characterised by increased power and labour consumption.

The E.O. Paton Electric Welding Institute developed the technology and built the pilot unit for refining of crude REM, based on induction remelting with formation of ingots in sectional water-cooled mould. Intensive stirring of the metal melt in the high-frequency electromagnetic field provides a several times increase in the rate of evaporation of calcium from the metal melt, compared with traditional arc melting. The refining process is performed in the inert gas atmosphere, and pressure in the melting chamber can be varied over a wide range. The pilot unit allows melting of high-purity REM ingots with a diameter of 100 to 200 mm and weight of up to 80 kg. The annual output of the unit is up to 30 t.

**Purpose and application.** The technology is intended for refining of crude rare-earth metals having a melting point of not lower than 1200 °C. The technology and equipment have been applied at the Kirgiz Mining Works to produce pure yttrium of the Itm1 grade with a calcium content of up to 0.01 %.

**State and level of development.** Experimental-industrial verification at the Kirgiz Mining Works.

**Principal performers and developers:** Shapovalov V.A., Dr. of Techn. Sci.; Shejko I.V., Dr. of Techn. Sci.

Contacts: Prof. Shapovalov V.A.  
E-mail: shapovalov@paton.kiev.ua

# AUTOMATION OF TRAINING PROCEDURES OF PUMA FAMILY ROBOTS

G.A. TSYBULKIN

E.O. Paton Electric Welding Institute, NASU, Kiev, Ukraine

An algorithm is proposed, which allows automating certain robot training procedures. The algorithm is based on approximation of the trajectory elements in virtual systems of coordinates. Results of the experiment are presented.

*Keywords:* trajectory of movement, algorithms, training, programming, automation of training, manipulation robots

Programming of the movement trajectory of welding robots is most frequently performed by means of demonstration or so called training [1, 2], when an operator, using manual control panel, moves a welding torch from one point of the programmed trajectory to the other. Having established the torch into the next in turn point of the trajectory and oriented it in a respective way, the operator registers by means of the storage device coordinates of the torch position, after which the torch is moved into a new point, and the training procedure is repeated.

The time necessary for training directly depends upon complexity of the billet and constitutes from several minutes up to 10–20 h [1]. It is especially long if the robot control system does not ensure circular interpolation because of a rather limited volume of memory, like in the PUMA-560 (PM 01) robot. As far as significant share of the robots, which were used till now, relate exactly to this type, solution of the task, directed at expansion of functional possibilities of these robots for the purpose of increasing efficiency of their training, is rather actual.

In this work one of the algorithms is proposed, which expands possibilities of training of the PUMA family manipulation robots in programming of the welding torch movement trajectory, including circumference arcs. Idea of the algorithm construction is based on approximation of these elements in certain virtual systems of coordinates, whereby included into the VAL language procedures of orthogonal transformation, by means of which connection is established between the virtual and the base systems of the robot coordinates, are actively used.

**Training algorithm synthesis.** For simplicity of the presentation, let us consider the case when it is necessary to program a fragment of the arc of  $L$  length and  $R$  radius located on a certain plane within working space of the robot. Let us select on this plane Cartesian system of coordinates  $Oxy$  in such way that center of the circumference coincided with origin of the coordinates  $O$ , and axis  $x$  passed through the initial point of arc  $A$  (Figure). Then coordinates  $x_B, y_B$  of point

$B$  and increments of the coordinates  $\Delta x = x_B - x_A$  and  $\Delta y = y_B - y_A$  are connected by the relations

$$x_B = R \cos \alpha, \quad y_B = R \sin \alpha. \quad (1)$$

Increments  $\Delta x$  and  $\Delta y$  can be determined by the formulas

$$\Delta x = R(1 - \cos \alpha), \quad \Delta y = R \sin \alpha. \quad (2)$$

Let us select angle  $\alpha$ , proceeding from requirements to accuracy of approximation of the arc:

$$\alpha \leq 2 \arccos(1 - \delta R)^{-1}, \quad (3)$$

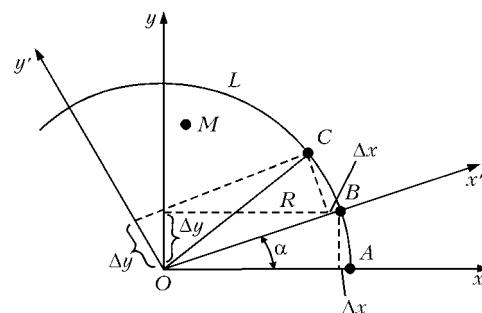
where  $\delta$  is the allowable error of approximation.

Let us set now a new system of Cartesian coordinates  $Ox'y'$ , in which axis  $x'$  passes through point  $B$ . Having used relations (1) and preliminary calculated according to formula (2) values of increments  $\Delta x$  and  $\Delta y$ , we will find the next points  $C$ , but this time in the system of coordinates  $Ox'y'$ :

$$x_C = R \cos \alpha, \quad y_C = \Delta y.$$

Continuing in this way setting of new virtual systems of coordinates and calculating coordinates of subsequent points using formulas (1), we get, as a result, coordinates of all equidistant from each other points  $n$  on the programmed arc, number of which is  $n \leq L / \alpha R$ .

It is necessary to pay attention to one very important issue, namely, when determining coordinates of the arc points, we do not need to calculate each time values of increments  $\Delta x$  and  $\Delta y$ , because according to (2) they are constant at  $\alpha = \text{const}$ . Exactly this peculiarity of the proposed algorithm allows significant reducing of the number of operations, needed for determining coordinates of the nodal points, under con-



Virtual systems of coordinates



ditions of rather limited calculation resources of the robot.

So, the algorithm of training works as follows. At the beginning, in the manual control mode the welding torch is set into initial position (for example, into point A) and oriented in necessary direction. The coordinates of points O, A, and some other point on the plane are entered. Calculated values  $\Delta x$  and  $\Delta y$  are entered into the control program and the automatic training program is started, which performs three main groups of operations: setting on the basis of two points on the plane of a virtual system of orthogonal coordinates; movement of the torch in this system of coordinates from the previous point into the next one located at the distance  $d = (\Delta x^2 + \Delta y^2)^{1/2}$ ; registration of the subsequent point coordinates and transformation thereof into the coordinates of the robot base system of coordinates. Using the program cycles, the robot «passes» all nodal points of the trajectory being programmed and stores all their coordinates, i.e. is automatically trained (self-trained) to move over the needed trajectory for its subsequent reproduction.

**Experimental check of the training program.** The experiment was carried out for the purpose of checking working efficiency of the program developed on the basis of the synthesized training algorithm. For this purpose, instead of the welding torch located on the last link of the PM 01 robot, a writing mechanism was fixed, which was installed by means of the manual control panel in center of the flat surface located within working space of the robot, having oriented it in such way that its longitudinal axis be perpendicular to this surface. At the same time in the robot storage device coordinates of three points, not lying on the same straight line --- O, A, and M, were fixed (see the Figure).

Circumference of  $R = 50$  mm radius was taken as the trajectory for programming, whereby allowable error of approximation of circumference  $\delta$  was accepted equal to 0.3 mm. Then, according to (3), angle  $\alpha$  was accepted equal to  $12^\circ$ . Values of increments  $\Delta x = -1.09$  mm and  $\Delta y = 10.4$  mm, which were entered into the control program, were calculated according to formulas (2).

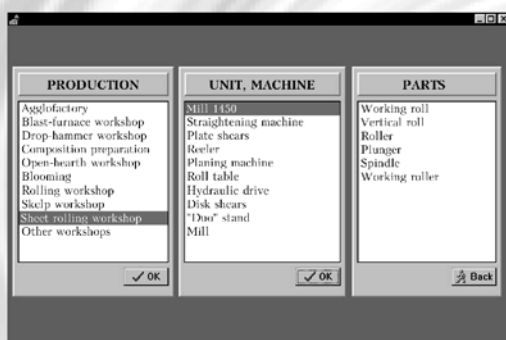
After these preparatory measures the training program was started. As a result of its optimization coordinates of thirty points, equidistant from each other on the circumference being programmed, are entered into the storage device.

In order to estimate efficiency of the robot training, operations of calculation of distance  $s$  between initial and final points of the trajectory and training time  $\tau$  are envisaged in the program. In this experiment  $s = 0.8$  mm, and  $\tau = 65$  s. Judging from the fact that values  $s$  and  $\delta$  in this experiment are of the same order, accuracy of setting of the nodal points is sufficiently high. It is rather difficult to achieve such accuracy in manual mode of training. As far as the time spent for automatic training of the robot is concerned, it should be noted that it is several dozen times shorter than that spent for training of the robot in manual mode.

So, the experimental check demonstrated sufficiently high efficiency of the proposed algorithm of the robot automatic training. Due to exclusion of the operator directly from the training conditions, it became possible to significantly reduce the robot training time, simplify this procedure, and noticeably increase accuracy of setting of the trajectory reference points.

1. Gettert, W., Gerden, H., Guttner, H. et al. (1988) *Welding robots*. Moscow: Mashinostroenie.
2. Kozlov, Yu.M. (1996) *Adaptation and training in robotics*. Moscow: Nauka.

## COMPUTER SYSTEM TO DESIGN TECHNOLOGIES FOR REPAIR AND HARDENING OF METALLURGICAL EQUIPMENT PARTS



Selection of a part to be surfaced

**Purpose.** The system is intended to design technologies for repair and hardening of metallurgical equipment parts by the electric arc surfacing methods. The computer system is based on the experience accumulated by 16 metallurgical plants in the field of surfacing. It allows design of a surfacing technology for 350 different parts (selection of surfacing consumables, methods, conditions, equipment, etc.) at a level of a highly skilled specialist. The system operation result has the form of a process sheet.

**Application.** The system can be used at metallurgical enterprises. It is intended for welding technologists working at a plant engineering department.

Contacts: Prof. Makhnenko V.I.  
E-mail: d34@paton.kiev.ua

# STEREOSCOPIC MEASUREMENT OF SPATIAL COORDINATES OF JOINTS IN WELDING PRODUCTION

V.A. KOLYADA and E.V. SHAPOVALOV

E.O. Paton Electric Welding Institute, NASU, Kiev, Ukraine

Stereoscopic technical vision system was developed to measure spatial coordinates of butt-welded joints. The system can be used for automatic directing of the welding tool to a joint in welding using robotic systems.

*Keywords:* welding production, automation, welding object, stereoscopic measurement, spatial coordinates, robotic complex, epipolar lines, conjugated points

At present, optical sensors based on the method of light section, which allows determining within one measurement cycle 2D coordinates of the object profile in the light section plane, are used most frequently in automation of the welding production. However, when it is necessary to estimate spatial orientation of the object before performance of a welding operation, application of optical sensors with light section causes significant difficulties.

For example, in welding with application of robotic complexes, the task frequently occurs connected with directing of a welding tool to the joint at the right angle to the welding object plane, which requires for determining spatial orientation of the structures being welded. Solution of this task in case of application of a sensor with the light section requires for fulfillment first of multiple scanning of different areas of the object surface and then calculation on the basis of the scanning results of the surface relief spatial coordinates.

The procedure of spatial orientation determination of the welding objects can be significantly simplified by means of the stereoscopic measurement method, in which determination of the 3D coordinates of the object surface is fulfilled within one measurement step, whereby additional scanning movements of the sensor unit are not needed. Separate cases of using stereoscopic technical vision means in welding production are known. For example, American company «Automatics Robotic Systems» used a binocular system for planning movement trajectory of the welding torch in welding of inserts to heavy frames of the bunker car carriages during their repair [1]. The main shortcoming of this system and all other similar solutions consists in the fact that each such system is oriented for solution of a limited range of tasks and can not be used for automation of existing welding installations.

In the E.O. Paton EWI a stereoscopic system of technical vision for measurement of spatial coordinates of the butt joints, which are most frequently used in the welding production, was developed. Scheme of the system sensor unit is shown in Figure 1. Two CCD

video cameras function as video sensors. For lighting of the measurement object surface, sources of scattered light, which represent a matrix from the laser light diodes, are used. Before lenses of each video camera light filters are installed, transmission band of which matches radiation wavelength of the laser light diodes. Video signals from the video cameras are processed in the system controller, using special software.

Software of the developed stereoscopic system is designated for preliminary processing of the digital images, search of the conjugated points, and determination of spatial coordinates of the points by images thereof.

At the stage of preliminary processing of the images singling out of certain characteristic areas on two images for their subsequent identification is performed. Normalization and shadow-mask filtration of the images are performed for solution of this task. Normalization of the images, i.e. enhancement of the level of their similarity, is performed by means of the video capture device by change of brightness and contrast of the input video signals. Shadow-mask filtration in this case is performed according to the program and allows significant reducing white noise level and emphasizing characteristic elements on the object images.

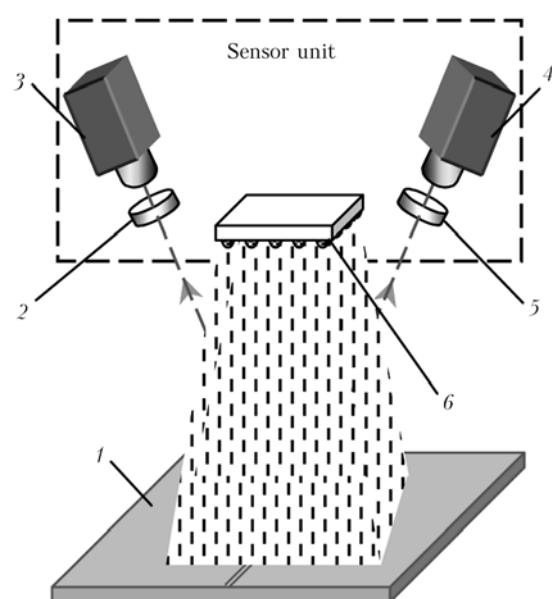


**Figure 1.** Scheme of sensor unit: 1 — object of measurement; 2, 5 — light filter 1 and 2; 3, 4 — video camera 1 and 2; 6 — dissipated light source

Search of the conjugated points is central problem of stereovision. The task of automated search of the conjugated points consists in the following: on one of the images point  $m'$  is selected, which is a projection of a certain point  $M$  of the 3D space. On second image it is necessary to find point  $m''$  --- projection of the same point. Correlation methods of search of the conjugated points, which are most frequently used in practice, have low efficiency concerning processing of the joint images because in general case an image of the joint has a homogeneous structure and a selected area of the joint on one image can correlate with several areas of the second image. That's why in this case of the point identification, the method connected with finding of the epipolar lines is used, physical idea of which can be formulated as follows. If one video camera «sees» the point, it is possible to consider that it «looks» at the «end» of a straight line in space. Then the second video camera located at a certain angle to the first one will «see» a straight line, which contains the conjugated point. Knowing the positions and angles of observation of the video cameras, for each point on the first image it is possible to calculate epipolar line on the second image, which significantly reduces zone of search of the conjugated points.

Identification of own and adjustment parameters of the sensor unit video cameras is performed independently for each video channel, using the methodology presented in [2]. The result of identification are two matrixes  $A_1$  and  $A_2$  of  $4 \times 4$  size, which describe spatial position and orientation of the video cameras relative reference system of the coordinates. If position of a point in the reference system of coordinates is assigned by vector  $\mathbf{r}_0$ , and positions of the same point in systems of coordinates of the video cameras --- by vectors  $\mathbf{r}_1$  and  $\mathbf{r}_2$ , then the following expression will be fair:

$$\mathbf{r}_0^P = A_1 \mathbf{r}_1^P, \quad \mathbf{r}_0^P = A_2 \mathbf{r}_2^P. \quad (1)$$

Transformation of the perspective serves for transition from systems of coordinates of the video cameras to the systems of coordinates of respective images:

$$x_k^i = \frac{x_k}{z_k/d_k} + \frac{W}{2}, \quad y_k^i = \frac{y_k}{z_k/d_k} + \frac{H}{2}, \quad k = 1, 2, \quad (2)$$

where  $x_k^i, y_k^i$  are the coordinates of conjugated points on the images;  $x_k, y_k, z_k$  are the coordinates of conjugated points in systems of coordinates of the video cameras;  $d_k$  is the distance from the points of front focus of the video cameras to the origin of the reference system coordinates;  $W, H$  are the width and the height of the images in pixels;  $k$  is the camera number.

Expressions (2) may be rewritten in the form of

$$x_k = c_k^x z_k, \quad y_k = c_k^y z_k, \quad k = 1, 2, \quad (3)$$

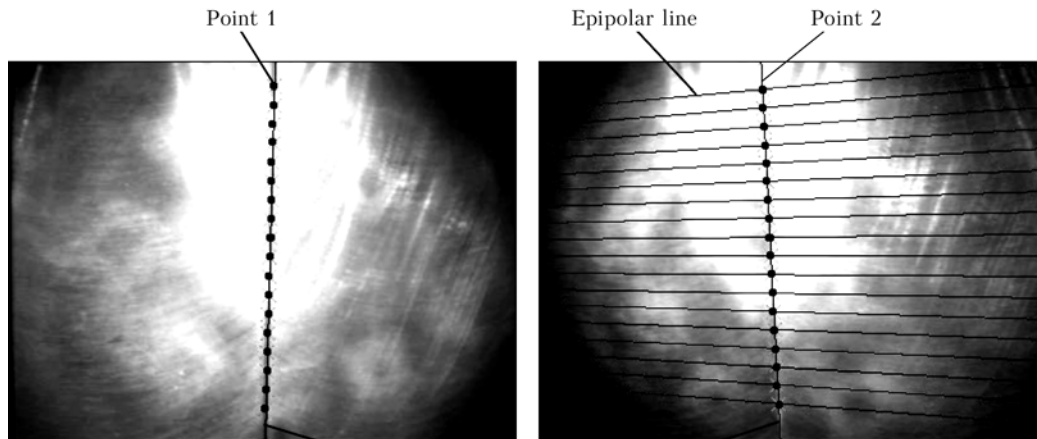
where  $c_k^x = \frac{x_k^i - (W/2)}{d_k}$ ;  $c_k^y = \frac{y_k^i - (H/2)}{d_k}$ . Hence vectors, which characterize position of the points in systems of coordinates of the video cameras, may be written as follows:

$$\mathbf{r}_1 = [c_1^x z_1, c_1^y z_1, z_1, 1]^P, \quad \mathbf{r}_2 = [c_2^x z_2, c_2^y z_2, z_2, 1]^P. \quad (4)$$

Expression (1) may be written in the form of a system of linear equations (in the matrix form):

$$A_1 \mathbf{r}_1^P = A_2 \mathbf{r}_2^P. \quad (5)$$

System (5) is an overdetermined one. Having solved the system by means of the approximate method of the least squares, we will get vector  $\mathbf{z} = [z_1, z_2, e]^P$ , where  $e$  is the value of discrepancy. Then on the basis of expression (4) values of the rest components of vectors  $\mathbf{r}_1, \mathbf{r}_2$  are calculated, and using one of relations (1) vector  $\mathbf{r}_0$  is calculated, which determines coordinates of the point in the reference system of coordinates. So, if coordinates of conjugated points on two images  $(\tilde{o}_1^i, y_1^i), (\tilde{o}_2^i, y_2^i)$  and matrixes  $A_1, A_2$  are known, then it is easy to determine on the basis



Identification of butt joint line

Figure 2. Search of conjugated points

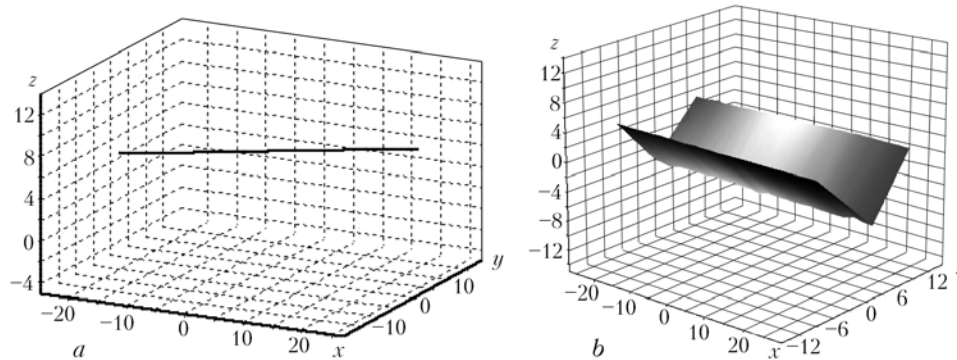


**Figure 3.** Results of stereoscopic measurement of spatial coordinates of joints: *a* — for butt joint with gap close to zero; *b* — for butt joint with V-grooves

of considered above relations spatial coordinates of the investigated point  $(x_0, y_0, z_0)$ .

Process of search of the conjugated points is illustrated in Figure 2 in case of the joint with a gap close to zero.

At initial stage identification of the joint line on the images, received from the sensor unit, is performed by means of the method described in [3]. On the joint line, identified on the first image, a point 1 is selected, for which epipolar line is constructed on the second image. Then a point 2 is determined, which is the result of intersection of the identified joint line on the second image with the found epipolar line. Points 1 and 2 represent a pair of conjugated points. In similar way the rest pairs of conjugated points are determined, whereby number of the pairs depends upon the required accuracy of the joint line determination.

For each pair of conjugated points a system of linear equations (5) is formed, and on the basis of equations (4) and (1) coordinates of the spatial point in the reference system of coordinates is calculated. Using found spatial points the joint line is constructed in 3D system of coordinates, which subsequently may be used for planning of the welding tool movement trajectory. In Figure 3, *a* the result of determining spatial position of the joint with a gap close to zero is shown. In this case orientation of the joint line with approximate length 50 mm is obtained within one stage, i.e. the joint coordinates have to be measured not very frequently even at maximum speeds of welding that significantly reduces requirements to calculation capacity of the stereoscopic system controller.

The developed algorithms also allow determining spatial coordinates of joints with V-grooves. For this purpose on each image identification of three lines, which correspond to two edges and root of the joint gap is performed. After determination of spatial orientation of each line, general geometry of the joint is formed in the reference system of coordinates. In Figure 3, *b* the result of stereoscopic measurement of spatial coordinates of the joint with V-grooves is shown. It is not difficult to construct by two lines of the gap the plane, which determines orientation of the structures being welded that may be used as the basis for directing the welding tool to the joint at right angle to the welding object plane when using robotic complexes.

The developed stereoscopic system has somewhat limited field of application. For example, in case of beveling of just one edge, one of the video cameras will not be able to «see» the root of gap, which will not allow determining coordinates of such joint. But at the same time development of stereoscopic means of technical vision represents a promising direction in the field of automation of welding processes, because stereoscopic systems allow getting the biggest volume of information on the object within one stage of measurement.

1. Moshkin, V.I., Petrov, A.A., Titov, V.S. et al. (1990) *Robot vision*. Ed. by Yu.G. Yakushenkov. Moscow: Mashinostroenie.
2. Kiselevsky, F.N., Kolyada, V.A. (2005) Calibration of triangular optical sensors. *The Paton Welding J.*, **5**, 48–49.
3. Kiselevsky, F.N., Butakov, G.A., Dolinenko, V.V. et al. (2003) Optical sensor for butt following at gap sizes close to zero. *Ibid.*, **2**, 48–50.



# SENSOR OF MOLTEN METAL POOL LEVEL IN ESW

Yu.N. LANKIN and E.N. BAJSHTRUK  
E.O. Paton Electric Welding Institute, NASU, Kiev, Ukraine

Inductive sensor of the molten metal pool level for ESW is described, which is characterized by increased sensitivity and stability.

**Keywords:** inductive sensor, eddy currents, molten metal pool level, electroslag welding

In electroslag welding (ESW) it is necessary that the molten metal pool level remained unchangeable relative the movable forming devices — slide blocks. It is possible, if at each instant of the time the condition

$$\sum_{i=1}^n S_{el}^i v_m^i = B(S + 2\Delta S)v_w$$

is observed, where  $n$  is the number of electrodes;  $S_{el}^i$  is the area of section of the  $i$ -th electrode;  $v_m^i$  is the melting rate of the  $i$ -th electrode;  $B$  is the welding gap width;  $S$  is the thickness of the metal being welded;  $\Delta S$  is the weld reinforcement;  $v_w$  is the welding speed (the speed of movement of the bogie and the slide blocks).

Stability of the level of the pool surface relative the movable mould (sliding block) exerts significant influence on quality of the weld surface, and significant change of its level can cause the emergency situation — spillage of the slag or metal pool.

Unfortunately, under real conditions the ESW process is affected by different disturbances, which cause significant fluctuations of  $v_m^i$ . In addition, width of the welding gap  $B$  does not remain constant over

the weld length because of insufficiently accurate assembly and presence of welding deformations. As a result in practice a welder has to correct  $v_w$  all the time or move the apparatus by pushing it at a high speed in order to maintain the slag pool level at least somewhat lower than upper edge of the sliding blocks. It is considered that in general it is practically impossible to perform ESW process without automatic stabilization of the metal pool level at the welding speed above 5 m/h. That's why the works connected with automatic adjustment of the metal pool level, were started even earlier than development of the welding current regulator [1]. In [2, 3] a big number of sensors of the molten metal pool level based on different physical principles — temperature, contact, radioactive and induction ones — were proposed. Nevertheless, they were not widely used.

In recent time interest to ESW again arose in connection with a certain revival of the industry. Spreading of high-speed ESW caused development of state-of-the-art welding equipment of new generation and recommencing of the work connected with automatic adjustment of the molten metal pool level.

A peculiar feature of the described sensor is increased sensitivity and stability of the readings due to application of new principles of the output signal processing. In recent developments of regulators of the metal pool level in the E.O. Paton EWI the eddy current sensors are used (Figure 1). The exciting coil 4 is installed on open-circuit I-like magnetic conductor 5, poles 2 of which are located in the groove 3 in the body of the water-cooled sliding block 1.

A simplified principle scheme of measurement of the metal pool level is presented in Figure 2. The circuit, consisting of the exciting coil L1 and capacitor C1, is included into one of the bridge arms (resistors R1–R3). The bridge is supplied by the sinusoidal 10 kHz voltage from the generator on the DD1, DD2, DD3, DS1, A1 and A2 microcircuits. On the DD1 and DD2 microcircuits the master oscillator of rectangular oscillations is assembled, frequency stability of which is ensured by the GB1 quartz resonator. These oscillations are fed to the input of the DD3 pulsation counter. Its output code serially addresses the DS1 read-only memory, in which the sinusoid current is recorded. The analogue-digital con-

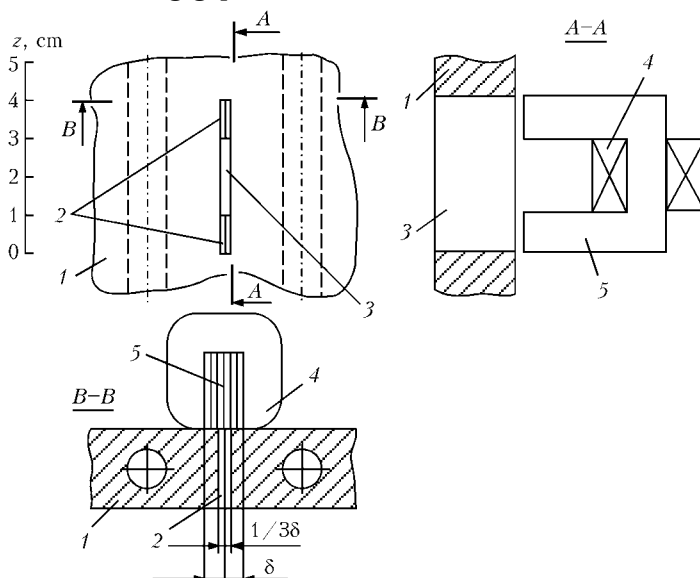


**Figure 1.** Scheme of location of surface level sensor of metal pool in slide block (for 1–5 see the text)

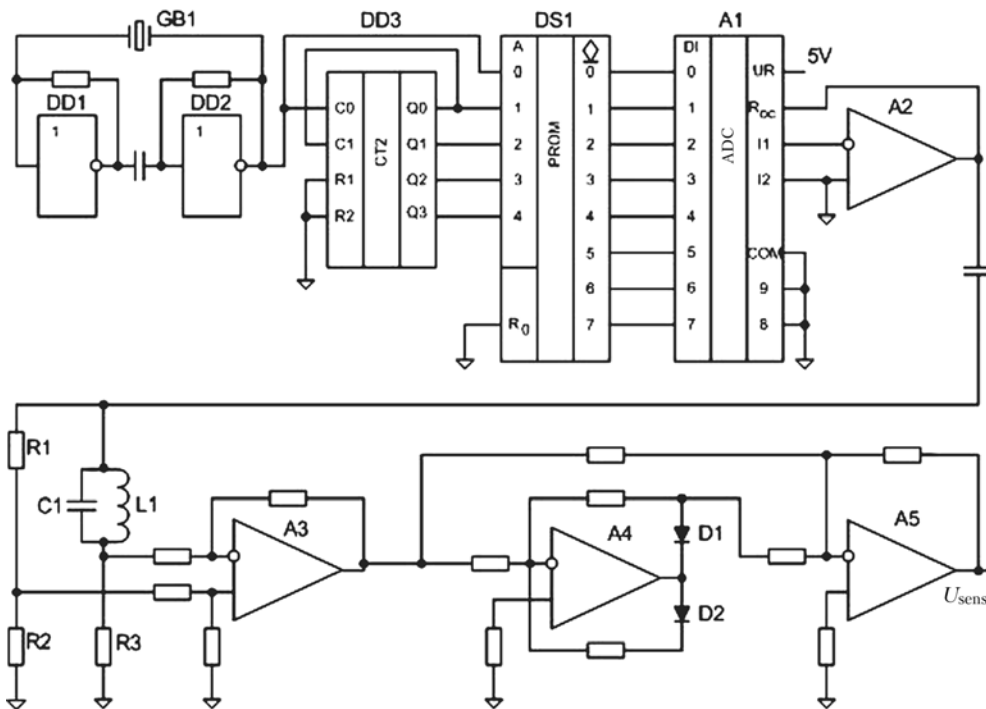


Figure 2. Principal scheme of the metal pool level sensor

verter (ADC) A1 and operation amplifier A2 convert this code into sinusoidal voltage of the measurement bridge power supply.

Circuit L1, C1 is adjusted to resonance with the power voltage frequency, when the metal pool level is below the lower pole of the level sensor magnetic conductor. In this position of the pool the bridge is adjusted at minimal (close to zero) signal in its diagonal. When the pool level increases relative lower pole of the magnetic conductor, excited in it eddy currents change active and inductive resistance of the circuit, whereby occurring voltage of the bridge unbalance is amplified by the A3 differential amplifier and rectified by the full-wave rectifier on A4 and A5 operational amplifiers and D1 and D2 diodes.

Application of the resonance significantly enhances sensitivity of the sensor, but establishes more strict requirements to stability of frequency and nonlinear distortions of the power sinusoidal voltage. Exactly because of this reason such a complex oscillator of the measurement bridge power voltage is used. In Figure 3 typical dependence of output voltage of the sensor  $U_{sens}$  upon the molten metal pool level is presented.

Within working range of change of the pool level transfer characteristic of the sensor is sufficiently linear for automatic stabilization of the pool level.

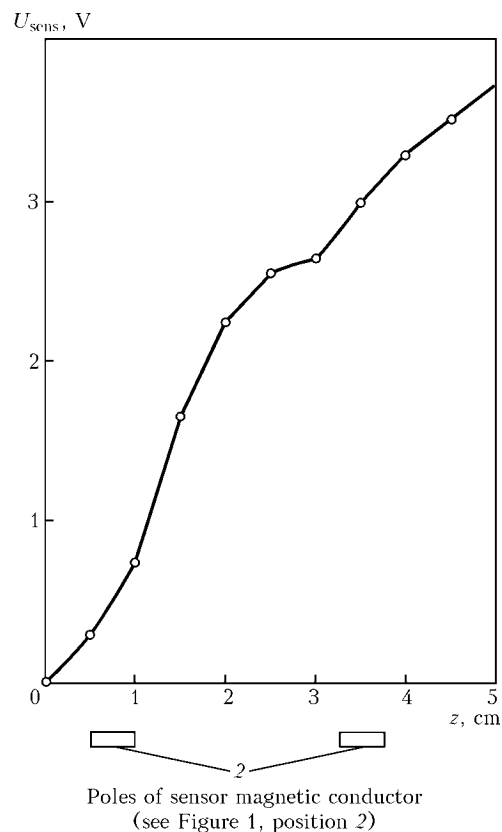


Figure 3. Output characteristic of the metal pool level sensor

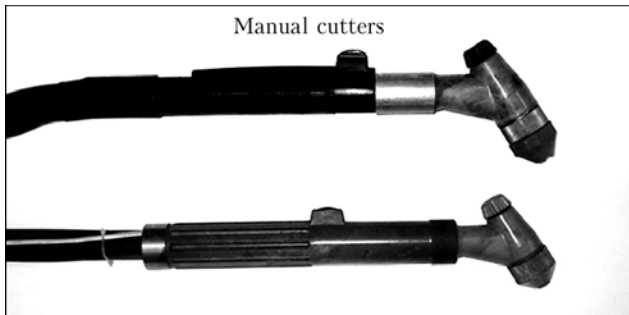
1. (1956) *Electroslag welding*. Ed. by B.E. Paton. Kiev: Mashgiz.
2. (1986) *Automation of welding processes*. Ed. by V.K. Lebedev, V.P. Chernysh. Kiev: Vyscha Shkola.

3. (1994) *Automatic control of electric welding processes and machines: Manual*. Ed. by V.K. Lebedev, V.P. Chernysh. Kiev: Vyscha Shkola.



## PROLONGATION OF OPERATIONAL LIFE OF THE APC INSTALLATION «KIEV-4»

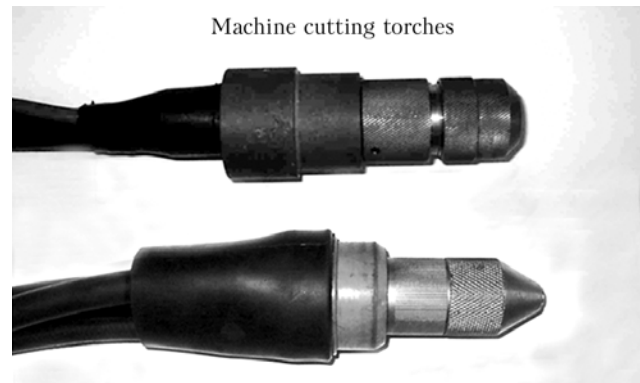
SIE «Plasmatron» is a traditional developer of the plasma installations. In addition to organization and development of the installations of new generation — universal ones for air-plasma cutting (APC) and electric arc welding of the «Duplex» type, economical and mobile installations «Kiev-5», «Kiev-8» and since the year 2007 «Dnepr-2», which ensure cutting of metals of up to 65 mm thickness by cutters with air cooling, the «Plasmatron» proposes modification of installations of «Kiev-4» and «Kiev-4M» type. The latter ones were produced in 1970–1980 of the previous century, but are still in operation at many enterprises of Ukraine and other CIS countries.



The retro installations, which were used for manual APC, are equipped with the manual VPR-11 cutter with a short operational life of the cathode-nozzle pair, failure of which frequently causes burning of the cathode unit and further unworthiness of the cutter as a whole. In case of using for manual cutting of the machine VPR-15 cutter with fully overlaid handles, although a more massive cathode-nozzle pair stipulates satisfactory term of operation, but big overall dimensions and mass of the cutter of such design impede its operation and maneuverability in cutting of the complex configuration components.

They relate to the class of powerful cutters, able to perform cutting of steels of up to 70 mm thickness at 300 A current. Their application for manual and machine cutting of metals of small and medium thicknesses (1–40 mm) at lower steps of the current (100

and 200 A) is problematic because of impossibility of ensuring satisfactory quality of cutting due to non-conformity of the cathode-nozzle chamber geometry of the cutters.



At discretion of the enterprises (on the basis of the results of investigation of the state of outdated installations and taking into account future production tasks) different options of the power supply scheme improvement of the installations, their equipment with the machine or manual cutters with air (for 100 and 150 A currents) or water (for 200–300 A currents) cooling are proposed, whereby satisfactory quality of cutting of small- and medium-thickness metals is ensured. Light and small-size manual water-cooled cutters using current up to 300 A, have the cathode-nozzle pair with long operational life and are equipped with the device, which significantly reduces harmful gas and dust release characteristic of cutting of the small- and medium-thickness metals. All plasma cutters are equipped with quickly replaceable cathode-nozzle units. Replacement of the outdated installations for new ones with a discount, depending upon state of the installation to be replaced, is possible.

The enterprise guarantees quick and quality solution of the customer's problems with free training of its specialists, transfer of technological recommendations, and subsequent supply of replaceable components and units.



## NKMZ GOT DOWN TO RENOVATION OF MILL IN HUNGARY

Novo-Kramatorsk Machine-Building Works (NKMZ), Kramatorsk, Donetsk oblast, finishes supply of equipment for the first stage of renovation of the three-high Lauta mill of the Dunaferri rolling plant, Budapest, Hungary. In parallel with implementation of this project, NKMZ got down to second stage of the mill renovation. The term of supply is the year 2007.

Introduction of the renovation measures, which will be performed by the NKMZ specialists, will allow the Dunaferri plant increasing the next year production of thick sheet from 120 to 200 thou t per year, having ensured high parameters of the produced products.

## NKMZ DREW CONTRACT ON RENOVATION OF MILL AT THE ILYICH MMW

NKMZ continues technical reequipment of the biggest enterprise in Ukraine --- the Ilyich Mariupol Metallurgical Works. After recent renovation and commissioning at this plant of two state-of-the-art slabbing machines for continuous casting of billets, NKMZ and MMW signed a new contract on fabrication and supply of the equipment for renovation of the hot rolling mill 1700. The main goal of the renovation is increase of the ready product competitiveness. To achieve this goal it is planned within the volume of this agreement

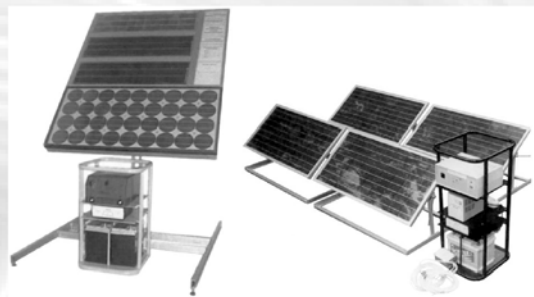
to install a complex of equipment of the universal four-high finishing stand No. 5A and two new reels with equipment for transportation and removal of coils. According to the contract, more than 4.5 thou t of high-technology equipment will be designed, fabricated and dispatched to the customer within 15 months. After its installation on the hot rolling mill 1700, productivity of the latter will be brought up to 4 mln t of rolled metal per year.

## MOBILE PHOTOVOLTAIC ELECTRIC WELDING SYSTEM

**Purpose.** The system is intended to perform welding operations in regions where the electric mains or other electric power sources are unavailable.

**Configuration.** The system consists of an electronic unit that includes a resonance welding converter, charging device, storage battery (StB) controller and StB. The solar battery is equipped with a position control system and consists of 10 modules.

**Functional capabilities.** Performance of electric welding operations under conditions of absence of the electric mains. Charging of StB from solar battery. Possibility of prompt selection of optimal orientation of solar battery. Charging of StB from other electric power sources (wind, diesel or hydraulic generator, etc.). Automatic mode of charging of StB, automatic protection from overcharging. Possibility of transportation using no transportation vehicles. Possibility of building up of StB capacity and solar battery power. Possibility of accelerated charging of StB. Protection of StB from sulphation. Possibility of utilisation of additional electric tools and electronic devices.



Contacts: Dr. Korotynsky A.E.  
E-mail: pwi\_otd55@paton.kiev.ua

## EXHIBITION

### «WELDING. ALLIED TECHNOLOGIES-2007» IN KIEV

Industrial exhibitions PATON EXPO that took place on April 16–19, 2007 at Expo Center KIEVEX-POPLAZA, combined such expositions as Welding. Allied Technologies-2007, Pipeline Transport-2007, Nondestructive Testing-2007, Industrial Painting and Corrosion Protection-2007, and Industrial Ecology-2007. They were organized by the Center of Technology Transfer of the E.O. Paton Electric Welding Institute of the NAS of Ukraine with the support of Welders' Society of Ukraine, company «Neftegaz Ukraine», OKO Association, Association of Industrial Reinforcement Construction of Ukraine, Association of Polymer Pipeline Manufacturers and Constructors of Ukraine.



Altogether 46 organizations, firms and companies from Ukraine, Russia, Poland, Turkey, Italy, Germany, Japan participated in the «Welding. Allied Technologies» Exhibition. The E.O. Paton Electric Welding Institute Technology Park, the Electric Welding Institute proper, its Design Office and pilot plants of Welding Consumables and Welding Equipment, STC SEPROZ, Inter-industry Training-At-

testation Center, well-known Ukrainian enterprises and companies --- KZESO, SELMA, Fronius-Ukraine, Kommunar, Binzel-Ukraine, SiMZ, DON-MET, NAV-KOTEX, ARKSEL, Artyom-Contact, ZONT, Interkhim-BTV, Linde Gas Ukraine, RUSO and others, Russian companies --- GRPZ, Mezghosmetiz, Plazma, Bulat --- were among the Exhibition participants. Products of the foreign countries outside the CIS were presented by Fronius Ukraine, Polysud, Ekkert, Panasonic companies, ESAB, Boehler, Tokyo Boeki Elme Messer Ukraine representative offices, Nelson company, Askainak, Mgm, EP Systems firms.

The Exhibition traditionally demonstrated the state-of-the-art and tendencies in design and manufacture of a wide range of equipment for different purposes --- from simple and available systems for manual arc welding to sophisticated developments of mechanized and automated equipment (semi-automatic and automatic welding machines, welding tractors), equipment with computer-assisted control.

The widest line of equipment for arc and plasma processes of welding and cutting was offered by KZESO, SELMA, Fronius-Ukraine, Kommunar and the PWI Pilot Plant of Welding Equipment, as well as SPC Plazma (Rostov-on-Don, Russia). Company SiMZ expanded the range of manufactured equipment. The Company's new product types include inverter welding installations of UDCh-201 UZ.1 Pulser type designed for manual MIG welding and TIG-D welding in continuous and pulse modes, inverter rectifiers of VDCh-201 Uz.1, VDCh-2001M UZ.1 type.

Japanese welding equipment of Denyo Company (Tokyo Voski Ltd.), namely a welding diesel-generators of DAW, TLW, DLW series with low fuel consumption, minimum noise level, high performance and minimum ecological impact, was displayed in Ukraine





for the first time. They are characterized by reliability, fatigue life, quality and cost-effectiveness.

Diversity of equipment for thermal, micro-plasma, gas-oxygen, plasma and hydro-abrasive cutting was demonstrated by ZONT (Ukraine), MKT, Mgm (Czechia), Ekkert (Germany) companies. The latter is one of the European leaders in manufacturing machines for profile thermal cutting, including manufacturing machines for laser cutting. Ekkert offers multifunctional machines for cutting, equipped with systems for drilling, marking, gas-oxygen and plasma cutting, and punching. V UpSupply Trading Company presents CNC machines for laser and plasma cutting from MiltiCam Company, USA, in Ukraine.

Welding consumable manufacturers were presented at the Exhibition on a much more modest scale. Only the expositions of ARKSEL, the PWI Pilot Plant of Welding Consumables, M.V. Frunze SMPO (Ukraine), Interkhim-BTV, ESAB representative office should be mentioned. Nevertheless, a vast range of consumables for different arc welding, cutting and surfacing processes was presented to Exhibition visitors, including those for performance of repair-reconditioning works.

Priority areas of Institute activities were presented in the E.O. Paton Electric Welding Institute booth, which were also reflected in the catalogue «Technologies. Materials. Equipment» (about 300 developments of the last 5–8 years) which was distributed at the Exhibition. The booth visitors were interested in the

new developments of the Institute and in a number of cases had concrete proposals on cooperation. Their attention was attracted by a new Ash 115M apparatus for electroslag welding that was successfully applied for position butt welding of the billets of oxygen converter supporting rings at OJSC Azovmash, micro-plasma welding system, as well as a system for non-destructive testing of quality and determination of the stress-strain state of structures by electron shearography and speckle-interferometry methods.

In conclusion it should be noted that the annual exhibition «Welding. Allied Technologies» has formed the image of the major profile exhibition in Ukraine. It attracted more than 3 thousand visitors during the four days of its running, including managers and representatives of technical services of industrial, state and commercial organizations, scientific staff of research institutes, designers, teachers and students of secondary and high schools, entrepreneurs and common interested persons from many regions of Ukraine, as well as Russia, Belarus, and Kazakhstan. Unfortunately, participation of companies from Russia and Belarus should be regarded as not representative enough. The latter, perhaps, can be due to a great number of exhibitions on welding in CIS, conducted in Moscow, St.-Petersburg, Kiev, Minsk, Nizhny Novgorod, Ufa, Sverdlovsk, Tomsk, Sochi and in other cities.

*V.N. Lipodaev, Dr. of Tech. Sci.*

## Prof. V.K. LEBEDEV is 85



6th of June 2007 is 85th anniversary of the known scientist in the field of welding technology and production, doctor of technical sciences, professor, honored figure of science and technology, Lenin prize, USSR, UkrSSR, Ukraine state prizes and Evgeny Paton prize winner, academician of National Academy of Sciences of Ukraine Vladimir K. Lebedev.

After graduation from Moscow Energy Institute in 1945 V.K. Lebedev actively included into investigations connected with development of new welding equipment, carried out in the Electric Welding Institute. Beginning of engineering and scientific activity of V. Lebedev coincided with complex and difficult period of restoration of destroyed by Great Patriotic war national economy. Continuously working in the E.O. Paton Electric Welding Institute for more than half century, V.K. Lebedev passed the way from a junior scientific researcher to the manager of a big research division and deputy director for scientific work. His first scientific researches were devoted to investigation of peculiarities and development of the methods of calculation of welding transformers with complex fields of dissipation, which was reflected in his candidate's thesis defended in 1948. In 1959 V.K. Lebedev was awarded degree of doctor of technical sciences for the work, which became a significant contribution into theory and practice of state-of-the-art transformer building.

V.K. Lebedev is one of leading specialists in the field of electrothermics and transformation of electric energy. The most significant works of the scientist are connected with investigation of the means of transformation of electric energy into the heat one, and development of dozen types of new sources of current for different kinds of arc, electroslog, resistance, electron beam and laser welding and special electrometallurgy. These sources of current are widely used in different branches of industry. Developments of V.K. Lebedev and his name are widely known not just in Ukraine, but far away from its borders.

In 1964 V.K. Lebedev was elected a corresponding member, and in 1972 --- academician of the NASU.

Results of investigations of V.K. Lebedev and his inventions became the basis for a new technology and original equipment for the resistance butt welding of items with big cross section of the components to be connected. This technology is, due to its high productivity, widely used in construction of railways, for which V.K. Lebedev in 1966 in composition of the team of authors was awarded Lenin prize. Subsequent development of investigations in this field caused development of technological complexes with intrapipe machines for resistance butt welding of big diameter pipes. V.K. Lebedev also made great contribution into development and introduction of the equipment for multiposition resistance welding of heads of the locomotive diesel blocks and heat exchangers of powerful transformers. These works were marked by the State prize of UkrSSR (1976).

In 1980s the scientist jointly with his co-workers carried out a cycle of investigations, which are of great significance for science and technology, including the field of resistance butt welding of power elements of missiles and apparatuses, marked in 1986 by the State prize of USSR.

V.K. Lebedev is author of many published scientific works, monographies, and inventions in the field of new methods of welding and welding equipment. Many his inventions are protected by patents of Ukraine, Russia, USA, and other countries.

V.K. Lebedev combines his intense creative work with ability not just to feel the needs of production, but to determine prospective priority ways of development of science and technology. Characteristic of creative work of V.K. Lebedev is wide range of scientific interests and deep interest in practical application of the results of the carried out investigations.

In 2001 V.K. Lebedev was awarded Evgeny Paton prize for a cycle of works in the field of welding and related technologies.

On the basis of idea of B.E. Paton the work in quite new for the welders field was carried out --- welding of soft tissues of animals and people. A creative team of workers of the E.O. Paton EWI and Institute of Surgery and Transplantation (Prof. Yu.A. Furmanov) of the AMSU was established. V.K. Lebedev coordinated activity of these teams. After multiple experiments on laboratory rats and rabbits positive results were obtained. It became possible to replace traditional methods of stitching soft tissues by threads or metal clamps by resistance welding with high frequency currents. The work of these teams interested American company CSMG, which assumed financing of the most expensive part of the investiga-



tions that ensured acceleration of the investigations and application thereof in clinical practice.

Development by V.K. Lebedev of theoretical basis for the process of connection of alive tissues allowed developing for the first time in the world practice of welding medical equipment and welding medical toolkit for performance of surgical operations for recovery of physiological functions of damaged human organs. New welding medical technology is successfully used in clinics of Kiev and other cities of Ukraine.

Leading surgeons of Kiev professors M.P. Zakh-rash, A.V. Makarov, S.E. Podpryatov and M.E. Nechitajlo made great contribution into development of the technique for welding of tissues and organs and development of the tools. In 2004 work in the field of welding of soft tissues of animals and people was awarded State prize of Ukraine.

At present V.K. Lebedev is adviser of the PWI board. He is actively engaged in scientific-organizational and public activity: deputy chief editor of «Avtomaticheskaya Svarka» journal, deputy chairman of a specialized council for defending of candidate's and doctor's theses, chairman of Ukrainian certification committee of welders.

V.K. Lebedev willingly and generously transfers his rich experience and knowledge to his disciples, colleagues, young scientists. 10 doctors and 42 candidates of technical sciences defended their theses under his guidance.

Long creative work of V.K. Lebedev is marked by state awards. All those, who work and communicate with V.K. Lebedev, unanimously mark his exclusive decency, good-heartedness, goodwill, and intelligence.

*We cordially congratulate the hero of the jubilee and wish him from the bottom of our hearts good health, personal happiness and great success in accomplishment of his creative plans.*

*E.O. Paton Electric Welding Institute  
of the NAS of Ukraine  
Ukrainian Welding Society  
Editorial boards of  
«Avtomaticheskaya Svarka» and  
«The Paton Welding Journal»*

## **RANGE OF KL-109, KL-110 AND KL-111 UNIVERSAL MACHINES FOR EBW OF LARGE AND HEAVY WORKPIECES**

- PC and programmable controllers are used.
- Electron beam parameters analysis and «black box» type self-diagnostics of machine by PC.
- Real-time seam tracking and monitoring of EBW process by RASTR system on the basis of the secondary electron emission.
- Gun power source with electron tube flashless system.

Mobile type 15, 30 or 60 kW electron beam gun at accelerating voltage of 60 kV.

### **Design**

The work chamber has two sliding doors. The workpiece table is moved out of the work chamber onto the runout platform of EBW process. The table accommodates rotators with horizontal and vertical axis, and also back centre. The electron gun 3-axis-manipulator has the travelling distance in X-direction up to 3000 mm, in Y-direction up to 730 mm and in Z-direction up to 1500 mm. Precision of the guidance and drive system equals that of precision machine tools operation with tolerances in the hundredth-of-a-millimeter range.

Contacts: Prof. Nazarenko O.K.  
E-mail: nazarenko@technobeam.com.ua

